

Shell formulas for instantons and gauge origami

Jiaqun Jiang

Department of Physics and Center for Field Theory & Particle Physics, Fudan University, 200005, Songhu Road, 200438 Shanghai, China

E-mail: jiangjiaqun@gmail.com

ABSTRACT: We introduce the shell formula—a framework capable of providing a unified description for various partition functions whose pole structures are classified by Young diagrams of arbitrary dimension. This formalism encompasses a wide range of physical systems, including instanton partition functions of 5d pure super Yang–Mills theory with classical gauge groups, as well as gauge origami configurations such as the magnificent four, tetrahedron instantons, Donaldson–Thomas invariants, and spiked instantons.

Contents

1	Introduction	1
2	Young diagrams and shell formula	2
2.1	Young diagram and poles	2
2.2	Shell formula and the \mathcal{J} -factor	3
3	Instanton of 5d pure SYM	6
3.1	5d pure $U(N)$ SYM	6
3.2	5d pure $SO(N)$ SYM	8
3.3	5d pure $Sp(2N)$ SYM	9
4	Gauge origami	12
4.1	Magnificent four	13
4.2	Tetrahedron instanton	16
4.3	Donaldson-Thomas counting	18
4.4	Spiked instanton	22
5	Discussion	24
A	Examples of charges of shellboxes	26
A.1	Labels of Young diagram and notations	26
A.2	Shell and \mathcal{J} -factor	27
B	Witten index and JK-residue	29
B.1	1d $\mathcal{N} = (0, 2)$ quiver and Witten index	29
B.2	Jeffery-Kirwan residue	29
C	Detail computations for various cases	31
C.1	5d $Sp(2)$ SYM	31
C.2	D0-D6 partition function	33
C.3	DT counting	35
C.4	D0-D8 partition function	38

1 Introduction

The study of supersymmetric gauge theories has unveiled intriguing interrelations among quantum field theory, algebraic geometry, and combinatorics. One of the striking manifestations of this interplay is the appearance of integer partitions (2d Young diagrams), or more generally, plane and solid partitions (3d and 4d Young diagrams), in the exact partition functions of supersymmetric systems. These Young diagrams naturally emerge in supersymmetric localization computations, instanton counting [1–5], and topological string amplitude calculations [6–10], encoding the BPS spectra of brane configurations.

The story began with supersymmetric localization techniques to directly compute the instanton partition function of $U(N)$ supersymmetric Yang-Mills (SYM) theory with 8 supercharges [1, 2,

[11], where each box of the 2d Young diagram corresponds to a fixed point of the torus action in the instanton moduli space. Nekrasov's calculations not only reproduced the Seiberg-Witten prepotential [12], but also connected with various frameworks such as the BPS/CFT correspondence [3, 13–18], topological vertex computations [6, 19, 20], and quantum algebras [15, 21–24].

Subsequently, developments in gauge origami and topological vertex techniques revealed that Young diagrams with asymptotic boundaries are intimately connected to a wide class of physical systems. In the Donaldson–Thomas (DT) framework [25–27], 3d Young diagrams with asymptotic 2d Young diagram boundaries describe D0–D2–D6 bound states on \mathbb{C}^3 . The intersecting D4-brane configurations further lead to spiked instantons [3, 28, 29] while D6-brane configurations give rise to tetrahedron instantons [5, 30, 31], which correspond to 2d and 3d Young diagrams growing along different directions, respectively. Moreover, the magnificent four [4, 32–34] is a physical realization of D0–D8 systems, where 4d Young diagrams label bound states. This construction provides a unifying framework that geometrically lifts lower-dimensional combinatorial structures into a single parent theory on \mathbb{C}^4 .

In this paper, we introduce a universal formula, referred to as the *shell formula*, which provides a compact and systematic representation of the Witten index for the classes of systems discussed above. The shell formula enables a unified treatment of several seemingly distinct problems. In particular, it allows us to express the instanton partition functions of 5d $\mathcal{N} = 1$ pure SYM theories with BCD-type gauge groups in the unrefined limit [10, 35]. It further provides a concise description of tetrahedron instantons and leads to natural recursion relations governing the addition of Young diagram boxes. Moreover, the shell formula yields a precise formulation of the partition function for DT counting, both before and after taking residues. Finally, it offers a description of the magnificent four system and its associated recursion relations, without introducing additional sign rules [34].

The structure of this paper is as follows. In Sec. 2, we review the definition of Young diagrams, define the shell of a Young diagram, the charge of each shellbox, and the core of the shell formula: the \mathcal{J} -factor that takes Young diagrams of arbitrary dimensions as input. We also briefly describe properties of the shell formula, such as its recursion relations and translation invariance. In Sec. 3, we briefly describe the instanton moduli space and instanton partition functions of 5d $\mathcal{N} = 1$ pure SYM theories with classical gauge groups, and express them using the shell formula. In Sec. 4, we use the shell formula to express the partition functions of the magnificent four, tetrahedron instantons, DT counting and spiked instantons. In Appendix A, we explain the notation used in this paper and provide several examples of \mathcal{J} -factor computations. In Appendix B, we briefly review the definition of the Witten index and the method for computing Jeffery-Kirwan residue (JK-residue). In Appendix C, we present detailed computational examples for several theories.

2 Young diagrams and shell formula

In this section, we will introduce the definition of Young diagrams in arbitrary dimensions, the construction of the shell formula, and derive some properties of the \mathcal{J} -factor for the shell formula.

2.1 Young diagram and poles

A Young diagram is a combinatorial object defined by very simple rules. For example, the different ways to partition a positive integer into a sum of non-increasing positive integers correspond to different 2-dimensional Young diagrams, also known as integer partitions. Naturally, this concept can be generalized to higher dimensions, such as 3d Young diagrams: plane partitions, and 4d Young diagrams: solid partitions, and so forth. Here, a Young diagram can be defined as:

Definition 2.1 (Young diagram). *A d -dimensional Young diagram is a finite subset $\mathbf{Y} \subseteq \mathbb{Z}^d$ for which there exists a point $\mathbf{z} = (z_1, \dots, z_d) \in \mathbb{Z}^d$, called the origin of \mathbf{Y} , such that the following*

monotonicity condition holds:

$$\begin{aligned} &\text{if } \mathbf{x} = (x_1, \dots, x_d) \in \mathbf{Y} \text{ and } z_i \leq y_i \leq x_i \text{ for all } i = 1, \dots, d, \\ &\text{then } \mathbf{y} = (y_1, \dots, y_d) \in \mathbf{Y}. \end{aligned}$$

In particular, the empty set \emptyset is also considered a Young diagram (with no origin specified).

Young diagrams can be used to express various partition functions discussed in Sec. 3 and Sec. 4. Specifically, the poles of the instanton partition function are in one-to-one correspondence with the coordinates of the boxes in the Young diagram. Given an instanton integral function $\mathcal{I}(\phi)$, with integration variables $\phi = (\phi_1, \dots, \phi_k)$, after applying the JK-residue as Appendix B.2, we can obtain the integral as:

$$\oint_{\text{JK}} \prod_{I=1}^k \frac{d\phi_I}{2\pi i} \mathcal{I}(\phi) = \sum_{\phi_*} \text{JK-Res}(\eta) \mathcal{I}(\phi) \quad (2.1)$$

In the scenarios we consider, the JK-residue selects a list of specific poles that corresponds to a configuration of Young diagram lists. The correspondence is as follows: for a Young diagram list: $\mathbf{Y} = (\mathbf{Y}_A, \mathbf{Y}_B, \dots)$, where the subscript $A \equiv (A, \alpha) = (a_1 a_2 \dots a_d, \alpha)$ of each d -dimensional Young diagram \mathbf{Y}_A represents its basis $\epsilon_A = (\epsilon_{a_1}, \dots, \epsilon_{a_d})$ and an additional label (color) α . Each box $\mathbf{x}_{A,i}$ in each Young diagram \mathbf{Y}_A has its corresponding coordinate. Then the pole at $\phi_* = (\phi_{1*}, \dots, \phi_{k*})$ is given by:

$$(\phi_{1*}, \dots, \phi_{k*}) = (\mathcal{X}_A(\mathbf{x}_{A,1}), \dots, \mathcal{X}_A(\mathbf{x}_{A,n_A}), \mathcal{X}_B(\mathbf{x}_{B,1}), \dots, \mathcal{X}_B(\mathbf{x}_{B,n_B}), \dots) \quad (2.2)$$

where $n_A = |\mathbf{Y}_A|$ is the number of boxes in \mathbf{Y}_A . The total number of box is $\sum_A n_A = k$. And with the Coulomb branch parameter v_A , the $\mathcal{X}_A(\mathbf{x})$ is defined as:

$$\mathcal{X}_A(\mathbf{x}) \equiv v_A + (\mathbf{x} - \mathbf{1}) \cdot \epsilon_A = v_A + \sum_{i=1}^d (x_i - 1) \epsilon_{a_i} \quad (2.3)$$

Note that all partition functions discussed below share a similar structure after integration, namely:

$$\text{JK-Res}(\eta) \mathcal{I}(\phi) \supset \frac{1}{\text{sh}(\phi_{i*} - \mathcal{X}_A(\mathbf{1}))} \prod_{\mathbf{y} \in \mathbf{Y}_A} \frac{\prod_{\mathbf{b} \in \mathbf{B}_{\text{even}}} \text{sh}(\phi_{i*} - \mathcal{X}_A(\mathbf{y}) - \mathbf{b} \cdot \epsilon_A)}{\prod_{\mathbf{b} \in \mathbf{B}_{\text{odd}}} \text{sh}(\phi_{i*} - \mathcal{X}_A(\mathbf{y}) - \mathbf{b} \cdot \epsilon_A)} \quad (2.4)$$

where $\text{sh}(x) = e^{x/2} - e^{-x/2}$. For a set of all d -tuples of binaries $\mathbf{B}_d = \{\mathbf{b} = (b_1, \dots, b_d) | b_i \in \{0, 1\}\}$, $\mathbf{B}_{\text{even}} \subset \mathbf{B}_d$ is the set of all binary tuples with $|\mathbf{b}| = \sum_i b_i \in 2\mathbb{Z}$, and \mathbf{B}_{odd} is with the elements $|\mathbf{b}| \in 2\mathbb{Z} + 1$. This common structure motivates us to define the shell of Young diagrams and the shell formula.

2.2 Shell formula and the \mathcal{J} -factor

To introduce the construction of the shell formula, it is necessary to first define the shell of a Young diagram (initially introduced in [36]) and the charge associated with each box within a shell.

Definition 2.2 (Shell of a Young diagram). *Given a d -dimensional Young diagram \mathbf{Y} , and the set of all d -tuples of binaries \mathbf{B}_d . The shell \mathcal{S} of \mathbf{Y} is defined as:*

$$\mathcal{S}(\mathbf{Y}) \equiv (\mathbf{Y} + \mathbf{B}_d) \setminus \mathbf{Y} \quad (2.5)$$

Definition 2.3 (Charge of shellbox). *For each $\mathbf{x} = (x_1, \dots, x_d)$ represents the location of a box in the shell $\mathcal{S}(\mathbf{Y})$, and $|\mathbf{b}| \equiv \sum_{i=1}^d b_i$ is the number of 1's in the binary tuples \mathbf{b} . The charge Q of each box \mathbf{x} is defined as:*

$$Q_{\mathbf{Y}}(\mathbf{x}) = \sum_{\substack{\mathbf{b} \in \mathbf{B}_d \\ \mathbf{x} - \mathbf{b} \in \mathbf{Y}}} (-1)^{|\mathbf{b}|} \quad (2.6)$$

We provide some examples for the charges and the shell of Young diagrams in Appendix A.2. For a generic d -dimensional Young diagram \mathbf{Y} , the charges of the shellboxes can take the value from $-d$ to d .

With these definitions in place, we can now define the central component of the shell formula:

Definition 2.4 (\mathcal{J} -factor). *Given a d -dimensional Young diagram $\mathbf{Y}_{\mathcal{A}}$ with label $\mathcal{A} = (A, \alpha) = (a_1 a_2 \dots a_d, \alpha)$. The \mathcal{J} -factor can be defined as:*

$$\begin{aligned}\mathcal{J}(x|\mathbf{Y}_{\mathcal{A}}) &\equiv \prod_{\mathbf{y} \in \mathcal{S}(\mathbf{Y}_{\mathcal{A}})} \text{sh}(x - \mathcal{X}_{\mathcal{A}}(\mathbf{y}))^{Q_{\mathbf{Y}_{\mathcal{A}}}(\mathbf{y})} \\ \mathcal{J}(x|\emptyset_{\mathcal{A}}) &\equiv \frac{1}{\text{sh}(x - \mathcal{X}_{\mathcal{A}}(\mathbf{1}))}\end{aligned}\quad (2.7)$$

To illustrate the \mathcal{J} -factor, we provide detailed calculations of several examples in the Appendix A.2.

We now present certain algebraic properties of the \mathcal{J} -factor, which will be utilized in subsequent derivations. This discussion is self-contained and can be skipped without loss of continuity:

- Expansion: $\mathcal{J}(x|\mathbf{Y}_{\mathcal{A}})$ can be expanded as a product of every box $\mathbf{y} \in \mathbf{Y}_{\mathcal{A}}$ as:

$$\mathcal{J}(x|\mathbf{Y}_{\mathcal{A}}) = \frac{1}{\text{sh}(x - \mathcal{X}_{\mathcal{A}}(\mathbf{1}))} \prod_{\mathbf{y} \in \mathbf{Y}_{\mathcal{A}}} \frac{\prod_{\mathbf{b} \in \mathbf{B}_{\text{even}}} \text{sh}(x - \mathcal{X}_{\mathcal{A}}(\mathbf{y}) - \mathbf{b} \cdot \boldsymbol{\epsilon}_A)}{\prod_{\mathbf{b} \in \mathbf{B}_{\text{odd}}} \text{sh}(x - \mathcal{X}_{\mathcal{A}}(\mathbf{y}) - \mathbf{b} \cdot \boldsymbol{\epsilon}_A)} \quad (2.8)$$

We note that this product expansion coincides exactly with the common structure (2.4) shared by all partition functions mentioned above, and provides the precise justification for the definition of the \mathcal{J} -factor.

As an example, for the 2d Young diagram $\lambda_{12,\alpha}$ with label $(12, \alpha)$, the \mathcal{J} -factor is:

$$\begin{aligned}\mathcal{J}(x|\lambda_{12,\alpha}) &= \frac{1}{\text{sh}(x - \mathcal{X}_{12,\alpha}(\mathbf{1}))} \prod_{\mathbf{y} \in \lambda_{12,\alpha}} \frac{\text{sh}(x - \mathcal{X}_{12,\alpha}(\mathbf{y}) - (0,0) \cdot \boldsymbol{\epsilon}_{12}) \text{sh}(x - \mathcal{X}_{12,\alpha}(\mathbf{y}) - (1,1) \cdot \boldsymbol{\epsilon}_{12})}{\text{sh}(x - \mathcal{X}_{12,\alpha}(\mathbf{y}) - (0,1) \cdot \boldsymbol{\epsilon}_{12}) \text{sh}(x - \mathcal{X}_{12,\alpha}(\mathbf{y}) - (1,0) \cdot \boldsymbol{\epsilon}_{12})} \\ &= \frac{1}{\text{sh}(x - v_{12,\alpha})} \prod_{\mathbf{y} \in \lambda_{12,\alpha}} \frac{\text{sh}(x - \mathcal{X}_{12,\alpha}(\mathbf{y})) \text{sh}(x - \mathcal{X}_{12,\alpha}(\mathbf{y}) - \boldsymbol{\epsilon}_{12})}{\text{sh}(x - \mathcal{X}_{12,\alpha}(\mathbf{y}) - \boldsymbol{\epsilon}_{1,2})}\end{aligned}\quad (2.9)$$

- Translation invariant: \mathcal{J} -factor only involves the difference between the coordinates of boxes, therefore:

$$\mathcal{J}(\mathcal{X}_{A,\alpha}(\mathbf{x})|\mathbf{Y}_{A,\beta}) = \mathcal{J}(\mathcal{X}_{A,\alpha}(\mathbf{x} + \mathbf{y})|\mathbf{Y}_{A,\beta} + \mathbf{y}) \quad (2.10)$$

Let \mathbf{y} be an arbitrary constant d -dimensional vector, so that $\mathbf{x} + \mathbf{y} = (x_1 + y_1, \dots, x_d + y_d)$. Then, $\mathbf{Y}_{A,\beta} + \mathbf{y}$ denotes shifting the coordinates of every box in $\mathbf{Y}_{A,\beta}$ by adding \mathbf{y} .

- Swapping property: For two d -dimensional Young diagrams $\mathbf{Y}_{A,\alpha}$ and $\mathbf{Y}_{A,\beta}$ with the same basis A , we swap the two Young diagrams as:

$$\begin{aligned}&\prod_{\mathbf{x} \in \mathbf{Y}_{A,\alpha}} \text{sh}(\mathcal{X}_{A,\alpha}(\mathbf{x}) - \mathcal{X}_{A,\beta}(\mathbf{1})) \mathcal{J}(\mathcal{X}_{A,\alpha}(\mathbf{x})|\mathbf{Y}_{A,\beta}) \\ &= \prod_{\mathbf{y} \in \mathbf{Y}_{A,\beta}} (\text{sh}(\mathcal{X}_{A,\beta}(\mathbf{y} + \mathbf{1}) - \mathcal{X}_{A,\alpha}(\mathbf{1})) \mathcal{J}(\mathcal{X}_{A,\beta}(\mathbf{y} + \mathbf{1})|\mathbf{Y}_{A,\alpha}))^{(-1)^d} \\ &= \prod_{\mathbf{y} \in \mathbf{Y}_{A,\beta} + \mathbf{1}} (\text{sh}(\mathcal{X}_{A,\beta}(\mathbf{y}) - \mathcal{X}_{A,\alpha}(\mathbf{1})) \mathcal{J}(\mathcal{X}_{A,\beta}(\mathbf{y})|\mathbf{Y}_{A,\alpha}))^{(-1)^d}\end{aligned}\quad (2.11)$$

For example, swapping the two 2d Young diagrams $\lambda_{12,1}$ and $\lambda_{12,2}$, we have:

$$\begin{aligned} & \prod_{\mathbf{x} \in \lambda_{12,1}} \text{sh}(\mathcal{X}_{12,1}(\mathbf{x}) - \mathcal{X}_{12,2}(\mathbf{1})) \mathcal{J}(\mathcal{X}_{12,1}(\mathbf{x}) | \lambda_{12,2}) \\ &= \prod_{\mathbf{y} \in \lambda_{12,2} + \mathbf{1}} \text{sh}(\mathcal{X}_{12,2}(\mathbf{y}) - \mathcal{X}_{12,1}(\mathbf{1})) \mathcal{J}(\mathcal{X}_{12,2}(\mathbf{y}) | \lambda_{12,1}) \end{aligned} \quad (2.12)$$

And for two 3d Young diagrams $\pi_{123,1}$ and $\pi_{123,2}$, we have:

$$\begin{aligned} & \prod_{\mathbf{x} \in \pi_{123,1}} \text{sh}(\mathcal{X}_{123,1}(\mathbf{x}) - \mathcal{X}_{123,2}(\mathbf{1})) \mathcal{J}(\mathcal{X}_{123,1}(\mathbf{x}) | \pi_{123,2}) \\ &= \prod_{\mathbf{y} \in \pi_{123,2} + \mathbf{1}} \frac{1}{\text{sh}(\mathcal{X}_{123,2}(\mathbf{y}) - \mathcal{X}_{123,1}(\mathbf{1})) \mathcal{J}(\mathcal{X}_{123,2}(\mathbf{y}) | \pi_{123,1})} \end{aligned} \quad (2.13)$$

- Recursion relation: Consider two d -dimensional Young diagrams $\mathbf{Y}_{\mathcal{A}}$ and $\mathbf{Y}'_{\mathcal{A}}$ with identical label \mathcal{A} . If the configuration of $\mathbf{Y}'_{\mathcal{A}} = \mathbf{Y}_{\mathcal{A}} \cup \mathbf{w}$ is obtained by adding one box \mathbf{w} to $\mathbf{Y}_{\mathcal{A}}$, then we can compute the ratio of the corresponding \mathcal{J} -factor for these two Young diagrams:

$$\begin{aligned} & \frac{\prod_{\mathbf{x} \in \mathbf{Y}_{\mathcal{A}} \cup \mathbf{w}} \mathcal{J}(\mathcal{X}_{\mathcal{A}}(\mathbf{x}) | \mathbf{Y}_{\mathcal{A}} \cup \mathbf{w})}{\prod_{\mathbf{x} \in \mathbf{Y}_{\mathcal{A}}} \mathcal{J}(\mathcal{X}_{\mathcal{A}}(\mathbf{x}) | \mathbf{Y}_{\mathcal{A}})} \\ &= \mathcal{J}(\mathcal{X}_{\mathcal{A}}(\mathbf{w}) | \mathbf{Y}_{\mathcal{A}} \cup \mathbf{w}) \frac{\prod_{\mathbf{x} \in \mathbf{Y}_{\mathcal{A}}} \mathcal{J}(\mathcal{X}_{\mathcal{A}}(\mathbf{x}) | \mathbf{Y}_{\mathcal{A}} \cup \mathbf{w})}{\prod_{\mathbf{x} \in \mathbf{Y}_{\mathcal{A}}} \mathcal{J}(\mathcal{X}_{\mathcal{A}}(\mathbf{x}) | \mathbf{Y}_{\mathcal{A}})} \\ &= \mathcal{J}(\mathcal{X}_{\mathcal{A}}(\mathbf{w}) | \mathbf{Y}_{\mathcal{A}} \cup \mathbf{w}) \frac{\prod_{\mathbf{x} \in \mathbf{Y}_{\mathcal{A}} \cup \mathbf{w}} (\text{sh}(\mathcal{X}_{\mathcal{A}}(\mathbf{x} + \mathbf{1}) - \mathcal{X}_{\mathcal{A}}(\mathbf{1})) \mathcal{J}(\mathcal{X}_{\mathcal{A}}(\mathbf{x} + \mathbf{1}) | \mathbf{Y}_{\mathcal{A}}))^{(-1)^d}}{\prod_{\mathbf{x} \in \mathbf{Y}_{\mathcal{A}}} \mathcal{J}(\mathcal{X}_{\mathcal{A}}(\mathbf{x}) | \mathbf{Y}_{\mathcal{A}}) \text{sh}(\mathcal{X}_{\mathcal{A}}(\mathbf{x}) - \mathcal{X}_{\mathcal{A}}(\mathbf{1}))} \\ &= \mathcal{J}(\mathcal{X}_{\mathcal{A}}(\mathbf{w}) | \mathbf{Y}_{\mathcal{A}} \cup \mathbf{w}) (\text{sh}(\mathcal{X}_{\mathcal{A}}(\mathbf{w}) - \mathcal{X}_{\mathcal{A}}(\mathbf{0})) \mathcal{J}(\mathcal{X}_{\mathcal{A}}(\mathbf{w} + \mathbf{1}) | \mathbf{Y}_{\mathcal{A}}))^{(-1)^d} \\ & \quad \times \frac{\prod_{\mathbf{x} \in \mathbf{Y}_{\mathcal{A}}} (\text{sh}(\mathcal{X}_{\mathcal{A}}(\mathbf{x}) - \mathcal{X}_{\mathcal{A}}(\mathbf{0})) \mathcal{J}(\mathcal{X}_{\mathcal{A}}(\mathbf{x} + \mathbf{1}) | \mathbf{Y}_{\mathcal{A}}))^{(-1)^d}}{\prod_{\mathbf{x} \in \mathbf{Y}_{\mathcal{A}}} \mathcal{J}(\mathcal{X}_{\mathcal{A}}(\mathbf{x}) | \mathbf{Y}_{\mathcal{A}}) \text{sh}(\mathcal{X}_{\mathcal{A}}(\mathbf{x}) - \mathcal{X}_{\mathcal{A}}(\mathbf{1}))} \\ &= \mathcal{J}(\mathcal{X}_{\mathcal{A}}(\mathbf{w}) | \mathbf{Y}_{\mathcal{A}} \cup \mathbf{w}) (\text{sh}(\mathcal{X}_{\mathcal{A}}(\mathbf{w}) - \mathcal{X}_{\mathcal{A}}(\mathbf{0})) \mathcal{J}(\mathcal{X}_{\mathcal{A}}(\mathbf{w} + \mathbf{1}) | \mathbf{Y}_{\mathcal{A}}))^{(-1)^d} \end{aligned} \quad (2.14)$$

where we use the swapping properties (2.11) in the last equality.

For example, for two 3d Young diagrams $\pi_{123,1}$ and $\pi_{123,1} \cup \mathbf{w}$, the recursion relation is:

$$\begin{aligned} & \frac{\prod_{\mathbf{x} \in \pi_{123,1} \cup \mathbf{w}} \mathcal{J}(\mathcal{X}_{123,1}(\mathbf{x}) | \pi_{123,1} \cup \mathbf{w})}{\prod_{\mathbf{x} \in \pi_{123,1}} \mathcal{J}(\mathcal{X}_{123,1}(\mathbf{x}) | \pi_{123,1})} \\ &= \frac{\mathcal{J}(\mathcal{X}_{123,1}(\mathbf{w}) | \pi_{123,1} \cup \mathbf{w})}{\mathcal{J}(\mathcal{X}_{123,1}(\mathbf{w} + \mathbf{1}) | \pi_{123,1}) \text{sh}(\mathcal{X}_{123,1}(\mathbf{w}) - \mathcal{X}_{123,1}(\mathbf{0}))} \end{aligned} \quad (2.15)$$

- Splitting property: Consider a d -dimensional Young diagram $\mathbf{Y}_{\mathcal{A}}$ with label \mathcal{A} , which can be partitioned into two d -dimensional Young diagrams $\mathbf{Y}'_{\mathcal{A}}$ and $\mathbf{Y}''_{\mathcal{A}}$:

$$\mathbf{Y}_{\mathcal{A}} = \mathbf{Y}'_{\mathcal{A}} \cup \mathbf{Y}''_{\mathcal{A}} \quad (2.16)$$

where the starting box of $\mathbf{Y}'_{\mathcal{A}}$ coincides with that of the original $\mathbf{Y}_{\mathcal{A}}$, while the starting box of $\mathbf{Y}''_{\mathcal{A}}$ is at $\mathbf{y} = (y_1, \dots, y_d) \in \mathbf{Y}_{\mathcal{A}}$. Then, by applying the properties of the \mathcal{J} -factor mentioned above, we can show that the \mathcal{J} -factor can be expressed as the product of the \mathcal{J} -factors corresponding to the Young diagrams $\mathbf{Y}'_{\mathcal{A}}$ and $\mathbf{Y}''_{\mathcal{A}}$:

$$\mathcal{J}(x | \mathbf{Y}_{\mathcal{A}}) = \mathcal{J}(x | \mathbf{Y}'_{\mathcal{A}}) \mathcal{J}(x | \mathbf{Y}''_{\mathcal{A}}) \text{sh}(x - \mathcal{X}_{\mathcal{A}}(\mathbf{y})) \quad (2.17)$$

For instance, $\{(1,1), (1,2)\} = \{(1,1)\} \cup \{(1,2)\}$ with $\{(1,2)\}$ being a single box Young diagram starting at $(1,2)$, therefore:

$$\mathcal{J}(x|\{(1,1), (1,2)\}_{12,1}) = \mathcal{J}(x|\{(1,1)\}_{12,1}) \mathcal{J}(x|\{(1,2)\}_{12,1}) \operatorname{sh}(x - \mathcal{X}_{12,1}(1,2)) \quad (2.18)$$

3 Instanton of 5d pure SYM

In this section, we employ the shell formula defined above to rewrite the instanton partition function for 5d $\mathcal{N} = 1$ pure SYM with classical gauge group [1, 37, 38]. Although these instanton partition functions can be expressed in terms of the Nekrasov factor, the shell formula representation makes the formulas more intuitive for visualizing the interactions between instantons and various D-branes. Note that in this section, since all space directions lie in $\mathbb{C}_1 \times \mathbb{C}_2 = (x^0, x^1, x^2, x^3)$, all the Young diagrams are oriented in the 1,2-direction, so we will temporarily omit the basis specification in the subsequent discussion.

3.1 5d pure $U(N)$ SYM

First, we consider the celebrated Nekrasov partition function. For $\mathcal{N} = 1$ SYM theory with eight supercharges on the spacetime $\mathbb{C}_1 \times \mathbb{C}_2 \times S^1$, we begin with the well-known case of pure $U(N)$ gauge theory for clarity. After topological twisting, the partition function can be supersymmetrically localized onto the moduli space of classical solutions to the equations of motion $F = *F$, namely the instanton moduli space $\mathcal{M}_{U(N),k}^{\text{inst}}$. $\mathcal{M}_{U(N),k}^{\text{inst}}$ is characterized by ADHM data [39], which for pure $U(N)$ theory can be expressed as a quiver diagram in Fig. 1.

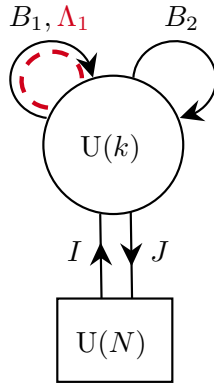


Figure 1. ADHM quiver diagram of D0-D4 system in the infinite adjoint mass limit as $\mathcal{N} = (0,2)$ SUSY QM. The black solid lines represent chiral multiplets, and the red dashed lines represent fermi multiplets. The circular nodes denote gauge groups, while the square nodes denote flavor groups. In this quiver, we have a $U(k)$ gauge group, a $U(N)$ flavor group, a fundamental chiral I , an anti-fundamental chiral J , two adjoint chirals $B_{1,2}$ respectively, and an adjoint fermi Λ_1 .

Then the moduli space can be expressed as:

$$\mathcal{M}_{U(N),k}^{\text{inst}} = \{(B_1, B_2, I, J) | \mu_{\mathbb{R}} = \mu_{\mathbb{C}} = 0\} / U(k) \quad (3.1)$$

where the ADHM equations are:

$$\begin{aligned} \mu_{\mathbb{R}} &= \sum_{i=1}^2 [B_i, B_i^\dagger] + II^\dagger - JJ^\dagger \\ \mu_{\mathbb{C}} &= [B_1, B_2] + IJ \end{aligned}$$

$\mathcal{M}_{U(N),k}^{\text{inst}}$ defined in this way is neither compact nor smooth. Therefore, we need to slightly modify the conditions of the ADHM construction (3.1) by changing $\mu_{\mathbb{R}} = 0$ to $\mu_{\mathbb{R}} = \zeta \cdot \mathbf{1}_k$, thereby avoiding singularities in the moduli space. Furthermore, we introduce the Ω -background to render the entire integral finite. The role of the Ω -background is as follows:

$$(B_1, B_2, I, J, \Lambda_1) \xrightarrow{U(1)_{\epsilon_1} \times U(1)_{\epsilon_2}} (q_1^{-1} B_1, q_2^{-1} B_2, I, q_{12}^{-1} J, q_{12}^{-1} \Lambda_1) \quad (3.2)$$

where $q_i \equiv e^{-\epsilon_i}$ and $q_{ij} = q_i q_j$.

The Ω -background effectively localizes 2 complex planes $\mathbb{C}_1 \times \mathbb{C}_2$ into a point. Thus the 5d SYM theory can now be viewed as a supersymmetric quantum mechanics (SUSY QM) on S^1 . Thus using the Losev–Moore–Nekrasov–Shatashvili (LMNS) formulism [40], we can write down the Nekrasov partition function as:

$$\mathcal{Z}_{\text{inst}}^{\text{U}(N)}(v_1, \dots, v_N) = \sum_{k=0}^{\infty} \mathfrak{q}^k \mathcal{Z}_{N,k}^{\text{U}}(v_1, \dots, v_N) \quad (3.3)$$

where k is the instanton number, and \mathcal{Z}_k is:

$$\begin{aligned} \mathcal{Z}_{N,k}^{\text{U}}(v_1, \dots, v_N) &= \oint_{\text{JK}} \prod_{i=1}^k \frac{d\phi_i}{2\pi i} \mathcal{I}_{N,k}^{\text{U}} \\ \mathcal{I}_{N,k}^{\text{U}} &= \frac{1}{k!} \prod_{i \neq j}^k \text{sh}(\phi_i - \phi_j) \prod_{i,j=1}^k \frac{\text{sh}(\phi_i - \phi_j - \epsilon_{12})}{\text{sh}(\phi_i - \phi_j - \epsilon_{1,2})} \prod_{i=1}^k \prod_{\alpha=1}^N \frac{1}{\text{sh}(\phi_i - v_{\alpha}) \text{sh}(v_{\alpha} - \epsilon_{12} - \phi_i)} \end{aligned} \quad (3.4)$$

where $\text{sh}(x - \epsilon_{1,2}) = \text{sh}(x - \epsilon_1) \text{sh}(x - \epsilon_2)$. The Coulomb branch parameters v_{α} effectively indicate the location of the α -th D4-brane along the complex planes $\mathbb{C}^2 = \mathbb{C}_1 \times \mathbb{C}_2$ as we soon generalize the notation in different directions. After applying the JK-residue, the poles can be classified by a set of N 2d Young diagrams $\vec{\lambda} = (\lambda_1, \dots, \lambda_N)$. For the α -th Young diagram, the box at position $\mathbf{x} = (i, j)$ contributes a pole at:

$$\mathcal{X}_{\alpha}(\mathbf{x}) = v_{\alpha} + (\mathbf{x} - \mathbf{1}) \cdot \epsilon_{12} = v_{\alpha} + i\epsilon_1 + j\epsilon_2 - \epsilon_{12} \quad (3.5)$$

To obtain the closed-form expression for the k -instanton partition function, we can further define the famous *Nekrasov factor* [1]:

$$N_{\alpha, \beta}^{\vec{\lambda}}(\mathbf{x}) \equiv v_{\alpha} - v_{\beta} + L_{\lambda_{\alpha}}(\mathbf{x})\epsilon_1 - A_{\lambda_{\beta}}(\mathbf{x})\epsilon_2 - \epsilon_{12} \quad (3.6)$$

where the $L_{\lambda_{\alpha}}(\mathbf{x})$ and $A_{\lambda_{\alpha}}(\mathbf{x})$ are the leg and arm of the box (\mathbf{x}) in λ_{α} respectively (Definitions of arm and leg will be given in the Appendix A). Therefore, the instanton partition function can be written as:

$$\mathcal{Z}_{N,k}^{\text{U}}(v_1, \dots, v_N) = \sum_{\|\vec{\lambda}\|=k} \mathcal{Z}^{\text{U}}(\vec{\lambda}) = \sum_{\|\vec{\lambda}\|=k} \prod_{\alpha=1}^N \prod_{\mathbf{x} \in \lambda_{\alpha}} \frac{1}{\text{sh}(-N_{\alpha, \beta}^{\vec{\lambda}}(\mathbf{x})) \text{sh}(N_{\alpha, \beta}^{\vec{\lambda}}(\mathbf{x}) + \epsilon_{12})} \quad (3.7)$$

where $\|\vec{\lambda}\| \equiv \sum_{\alpha} |\lambda_{\alpha}|$ is the number of total boxes in all Young diagrams.

While the Nekrasov factor provides a compact encoding of Young diagram data and yields a concise expression for the instanton partition function, it lacks straightforward generalization to higher-dimensional Young diagrams and makes the derivation of algebraic relations—such as recursion formulas—rather cumbersome. For this reason, we introduce the \mathcal{J} -factor defined in (2.7) and rewrite the instanton partition function as follows:

$$\mathcal{Z}_{N,k}^{\text{U}}(v_1, \dots, v_N) = \sum_{\|\vec{\lambda}\|=k} \prod_{\alpha=1}^N \prod_{\mathbf{x} \in \lambda_{\alpha}} \frac{\mathcal{J}(\mathcal{X}_{\alpha}(\mathbf{x}) | \lambda_{\beta})}{\text{sh}(-\mathcal{X}_{\alpha}(\mathbf{x}) + \mathcal{X}_{\beta}(\mathbf{0}))} \quad (3.8)$$

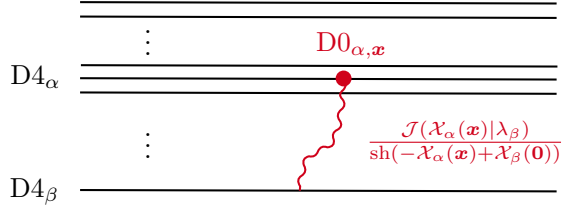


Figure 2. The instanton configuration of 5d pure $U(N)$ SYM can be constructed from type IIA D0-D4 brane system after integrating out the adjoint hypermultiplets. The D4-branes extend along two complex directions $\mathbb{C}_1, \mathbb{C}_2$, and the time direction x^0 . $D4_{\alpha}$ refers to the α -th D4-brane, while $D0_{\alpha, \mathbf{x}}$ denotes the D0-brane within $D4_{\alpha}$ corresponding to the instanton at coordinate \mathbf{x} in the Young diagram. The red wavy line represents strings connecting $D0_{\alpha, \mathbf{x}}$ and $D4_{\beta}$, and the contribution of these strings to the index is $\mathcal{J}(\mathcal{X}_{\alpha}|\lambda_{\beta})/\text{sh}(-\mathcal{X}_{\alpha} + \mathcal{X}_{\beta})$.

In this result, we can observe the contribution from the effective interaction of each instanton with the D4-branes. Here, v_{α} represents the position of each D4-brane at low energy, and $\mathcal{X}_{\alpha}(\mathbf{x})$ denotes the position of each D0-brane at low energy. Thus, schematically, as shown in Fig. 2, in each specific vacuum corresponding to the Young diagram λ_{β} , the contribution from the D0-D4 strings is given by:

$$\frac{\mathcal{J}(\mathcal{X}_{\alpha}(\mathbf{x})|\lambda_{\beta})}{\text{sh}(-\mathcal{X}_{\alpha}(\mathbf{x}) + \mathcal{X}_{\beta}(\mathbf{0}))} \quad (3.9)$$

Notice that in the case of a 2d Young diagram, the \mathcal{J} -factor and the Nekrasov factor are equivalent up to a sh :

$$\mathcal{J}(\mathcal{X}_{\alpha}(\mathbf{x})|\lambda_{\beta}) = \frac{\text{sh}(-\mathcal{X}_{\alpha}(\mathbf{x}) + \mathcal{X}_{\beta}(\mathbf{0}))}{\text{sh}(-N_{\alpha, \beta}^{\lambda}(\mathbf{x})) \text{sh}(N_{\alpha, \beta}^{\lambda}(\mathbf{x}) + \epsilon_{12})} \quad (3.10)$$

One can obtain the instanton partition function $\mathcal{Z}_{N,k}^{\text{SU}}$ of $SU(N)$ SYM by simply imposing the traceless condition $\sum_{\alpha=1}^N v_{\alpha} = 0$.

We can also use property (2.14) to derive recursion relations for the Nekrasov partition function. When adding the contribution of an instanton within a D4-brane, that is, the ratio of the partition function contribution from the Young diagram $\lambda_{\alpha} \cup \square$ to that from λ_{α} :

$$\begin{aligned} \frac{\mathcal{Z}^{\text{U}}(\lambda_{\alpha} \cup \square)}{\mathcal{Z}^{\text{U}}(\lambda_{\alpha})} &= \left(\prod_{\mathbf{x} \in \lambda_{\alpha} \cup \square} \frac{\mathcal{J}(\mathcal{X}_{\alpha}(\mathbf{x})|\lambda_{\alpha} \cup \square)}{\text{sh}(-\mathcal{X}_{\alpha}(\mathbf{x}) + \mathcal{X}_{\alpha}(\mathbf{0}))} \right) \Big/ \left(\prod_{\mathbf{y} \in \lambda_{\alpha}} \frac{\mathcal{J}(\mathcal{X}_{\alpha}(\mathbf{y})|\lambda_{\alpha})}{\text{sh}(-\mathcal{X}_{\alpha}(\mathbf{y}) + \mathcal{X}_{\alpha}(\mathbf{0}))} \right) \\ &= -\mathcal{J}(\mathcal{X}_{\alpha}(\square)|\lambda_{\alpha} \cup \square) \times \mathcal{J}(\mathcal{X}_{\alpha}(\square + \mathbf{1})|\lambda_{\alpha}) \end{aligned} \quad (3.11)$$

where \square in the equation represents its coordinate in the Young diagram. This recursion relation is connected to the quantum toroidal algebra and qq -characters [15, 16, 21, 22, 41, 42].

3.2 5d pure $SO(N)$ SYM

Next, we turn our attention to pure SYM theories for Lie groups of types B and D [38]. We can express the instanton moduli space via the ADHM construction. First, since $SO(N)$ involves a symmetric bilinear form, to ensure the moment maps $\mu_{\mathbb{R}}$ and $\mu_{\mathbb{C}}$ are invariant under the gauge group $SO(N)$, the quotient group must incorporate an antisymmetric bilinear form. That is, the quotient group is of type C: $Sp(2k) \subset U(2k)$ [37]. The resulting integral form of the instanton

partition function is then given by:

$$\begin{aligned} \mathcal{I}_{N,k}^{\text{SO}} = & \frac{1}{k! 2^k} \prod_{i \neq j}^k \text{sh}(\phi_i - \phi_j) \prod_{i,j=1}^k \frac{\text{sh}(\phi_i - \phi_j - \epsilon_{12})}{\text{sh}(\phi_i - \phi_j - \epsilon_{1,2})} \frac{\prod_{i \leq j}^k \text{sh}(\pm(\phi_i + \phi_j)) \text{sh}(\pm(\phi_i + \phi_j) - \epsilon_{12})}{\prod_{i < j}^k \text{sh}(\pm(\phi_i + \phi_j) - \epsilon_{1,2})} \\ & \times \prod_{i=1}^k \frac{1}{\prod_{\alpha=1}^n \text{sh}(\pm\phi_i \pm v_\alpha - \frac{1}{2}\epsilon_{12})} \left(\frac{1}{\text{sh}(\pm\phi_i - \frac{1}{2}\epsilon_{12})} \right)^\chi \end{aligned} \quad (3.12)$$

where $n = \lfloor \frac{N}{2} \rfloor$ is the rank of $\text{SO}(N)$, and $\chi = N \bmod 2$ labels the B and D type Lie group.

Classifying the poles of this integral has been a challenging problem. However, we can simplify the problem by considering the *unrefined limit* $\epsilon_2 = -\epsilon_1$. In this limit, the same as (3.5), the non-trivial poles simplify and can be classified by 2d Young diagrams [10]. Consequently, in the unrefined limit, we can express the partition function concisely using the shell formula:

$$\begin{aligned} \mathcal{Z}_{N=2n+\chi,k}^{\text{SO}}(v_1, \dots, v_n) = & \lim_{\epsilon_2 \rightarrow -\epsilon_1} \sum_{||\lambda||=k} \prod_{\alpha=1}^n \prod_{\mathbf{x} \in \lambda_\alpha} \frac{\text{sh}(2\mathcal{X}_\alpha(\mathbf{x}) + \epsilon_{1,2}) \text{sh}^2(2\mathcal{X}_\alpha(\mathbf{x}))}{\text{sh}^\chi(\pm\mathcal{X}_\alpha(\mathbf{x}))} \\ & \times \prod_{\beta=1}^n \frac{\mathcal{J}(\pm\mathcal{X}_\alpha(\mathbf{x})|\lambda_\beta)}{\text{sh}(\pm\mathcal{X}_\alpha(\mathbf{x}) + \mathcal{X}_\beta(\mathbf{0}))} \end{aligned} \quad (3.13)$$

We introduce the limit $\lim_{\epsilon_2 \rightarrow -\epsilon_1}$ to extract a specific coefficient from singular terms. This is necessary because, in the factor $\mathcal{J}(\pm\mathcal{X}_\alpha|\lambda_\beta)/\text{sh}(\pm\mathcal{X}_\alpha + \mathcal{X}_\beta)$, the condition $\alpha = \beta$ for diagonal boxes in λ_α produces terms like $\text{sh}(a\epsilon_{12})/\text{sh}(b\epsilon_{12})$. The limit yields the coefficient a/b , which plays a critical role in the subsequent analysis of $\text{Sp}(2N)$ SYM theory in Sec. 3.3.

In order to endow this shell formula with physical meaning, similar to that in Fig. 2, we first engineer this system using a 5-brane web in IIB theory [43–45]. The construction requires $\lfloor \frac{N}{2} \rfloor$ D5-branes, 2 NS5-branes, and an O5-plane, with their orientations given in Tab. 1.

	\mathbb{C}_1		\mathbb{C}_2		x^5	x^6	x^7	x^8	$\mathbb{R} \times \mathbb{S}^1$	
	1	2	3	4	5	6	7	8	9	0
D5	-	-	-	-	-	•	•	•	•	-
$\text{O}5^\pm, \widetilde{\text{O}5}^\pm$	-	-	-	-	-	•	•	•	•	-
NS5	-	-	-	-	•	-	•	•	•	-

Table 1. Brane configuration of 5d SO or Sp pure SYM. Consider D5-branes, NS5-branes, and O5-planes in type IIB string theory. The symbol $-$ denotes an extended direction of the D-branes, whereas \bullet denotes a point-like direction. The D5-branes and O5-planes extend along the directions \mathbb{C}_1 , \mathbb{C}_2 , x^5 , and x^0 , while the NS5-branes extend along \mathbb{C}_1 , \mathbb{C}_2 , x^6 , and x^0 . The non-Abelian gauge group is constructed from the D5-branes. The $\text{O}5^-$ -plane projects out the symmetric vector states to form SO gauge groups, while the $\text{O}5^+$ -plane projects out the antisymmetric vector states to form Sp gauge groups.

The presence of the O5-plane causes strings winding around it to undergo an orientation reversal. Hence, such strings contribute an additional negative sign: $\mathcal{X}_\alpha \rightarrow -\mathcal{X}_\alpha$ to the partition function, as shown in Fig. 3.

3.3 5d pure $\text{Sp}(2N)$ SYM

A scenario where the shell formula proves particularly useful is in explaining the *BPS jumping phenomenon* [10, 35]. Let us consider the case of $\text{Sp}(2N)$. According to the ADHM construction, the quotient group for the $\text{Sp}(2N)$ instanton moduli space for k instantons is the orthogonal group

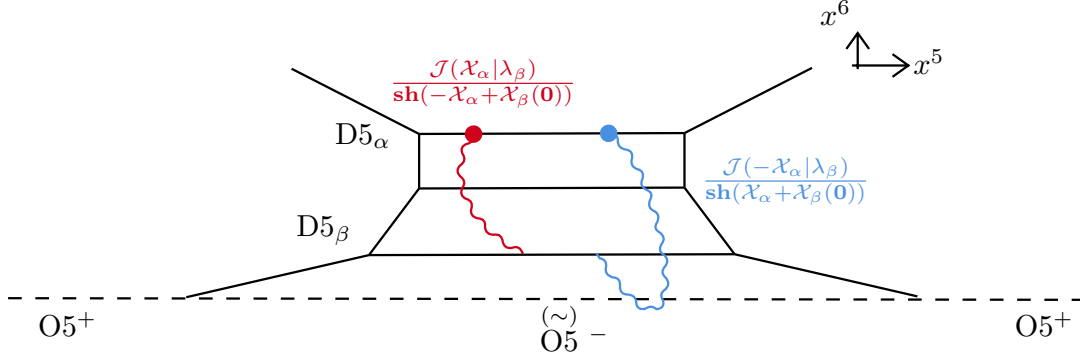


Figure 3. On the x^5 - x^6 plane, the horizontally extending lines represent D5-branes, while the vertical or slanted lines represent NS5-branes. For the SO gauge group, we need to use an $O5^-$ or $\widetilde{O5}^-$ orientifold at the bottom, where, when it crosses an NS5-brane, it becomes an $O5^+$. For the $SO(2n)$ gauge group, we require n D5-branes and an $O5^-$. For $SO(2n+1)$, we need n D5-branes and an $\widetilde{O5}^-$ [45]. The red wavy lines represent the effective contribution of strings connecting $D1_{\alpha,x}$ and $D5_\beta$, which is identical to that of the $U(N)$ gauge group given in (3.9). The blue wavy lines correspond to strings connecting $D1_{\alpha,x}$ and $D5_\beta$ whose orientation is reversed by the O-plane; their effective contribution matches the original one, subject to the replacement $X_\alpha \rightarrow -X_\alpha$.

$O(k)$. Furthermore, since we are considering 5d SYM and $\pi_4(\mathrm{Sp}(2N)) = \mathbb{Z}_2$, the 5d Sp SYM partition function naturally includes a discrete topological angle θ . We define this θ to take values 0 or π . This discrete angle precisely corresponds to the two distinct components of the O group. Therefore, based on the ADHM data, we can write down the two instanton partition functions for the Sp group:

$$\begin{aligned} \mathcal{Z}_{2N,k}^{\mathrm{Sp},\theta=0} &= \mathcal{Z}_{2N,k}^{\mathrm{Sp},+} + \mathcal{Z}_{2N,k}^{\mathrm{Sp},-} \\ \mathcal{Z}_{2N,k}^{\mathrm{Sp},\theta=\pi} &= \mathcal{Z}_{2N,k}^{\mathrm{Sp},+} - \mathcal{Z}_{2N,k}^{\mathrm{Sp},-} \end{aligned} \quad (3.14)$$

where the integrand of $\mathcal{Z}^{\mathrm{Sp},\pm}$ are as follow [37, 46, 47]:

$$\begin{aligned} \mathcal{I}_{2N,k}^{\mathrm{Sp},+} &= \frac{1}{l! 2^{l+\chi}} \prod_{i \neq j}^l \mathrm{sh}(\phi_i - \phi_j) \prod_{i,j=1}^l \frac{\mathrm{sh}(\phi_i - \phi_j - \epsilon_{12})}{\mathrm{sh}(\phi_i - \phi_j - \epsilon_{1,2})} \frac{\prod_{i < j}^l \mathrm{sh}(\pm(\phi_i + \phi_j)) \mathrm{sh}(\pm(\phi_i + \phi_j) - \epsilon_{12})}{\prod_{i \leq j}^l \mathrm{sh}(\pm(\phi_i + \phi_j) - \epsilon_{1,2})} \\ &\times \prod_{i=1}^l \frac{1}{\prod_{\alpha=1}^N \mathrm{sh}(\pm\phi_i \pm v_\alpha - \frac{1}{2}\epsilon_{12})} \left(\frac{1}{\mathrm{sh}(\epsilon_{1,2})} \frac{1}{\prod_{\alpha=1}^N \mathrm{sh}(\pm v_\alpha - \frac{1}{2}\epsilon_{12})} \prod_{i=1}^l \frac{\mathrm{sh}(\pm\phi_i) \mathrm{sh}(\pm\phi_i - \epsilon_{12})}{\mathrm{sh}(\pm\phi_i - \epsilon_{1,2})} \right)^\chi \end{aligned} \quad (3.15)$$

$$\begin{aligned} \mathcal{I}_{2N,k}^{\mathrm{Sp},-} &= \frac{1}{(l-1+\chi)! 2^{l+\chi}} \prod_{i \neq j}^l \mathrm{sh}(\phi_i - \phi_j) \prod_{i,j=1}^l \frac{\mathrm{sh}(\phi_i - \phi_j - \epsilon_{12})}{\mathrm{sh}(\phi_i - \phi_j - \epsilon_{1,2})} \frac{\prod_{i < j}^{l-1+\chi} \mathrm{sh}(\pm(\phi_i + \phi_j)) \mathrm{sh}(\pm(\phi_i + \phi_j) - \epsilon_{12})}{\prod_{i \leq j}^{l-1+\chi} \mathrm{sh}(\pm(\phi_i + \phi_j) - \epsilon_{1,2})} \\ &\times \prod_{i=1}^{l-1+\chi} \frac{1}{\prod_{\alpha=1}^N \mathrm{sh}(\pm\phi_i \pm v_\alpha - \frac{1}{2}\epsilon_{12})} \left(\frac{1}{\mathrm{sh}(\epsilon_{1,2})} \frac{1}{\prod_{\alpha=1}^N \mathrm{ch}(\pm v_\alpha - \frac{1}{2}\epsilon_{12})} \prod_{i=1}^{l-1+\chi} \frac{\mathrm{ch}(\pm\phi_i) \mathrm{ch}(\pm\phi_i - \epsilon_{12})}{\mathrm{ch}(\pm\phi_i - \epsilon_{1,2})} \right) \\ &\times \left(\frac{\mathrm{ch}(\epsilon_{12})}{\mathrm{sh}(2\epsilon_{1,2})} \frac{1}{\prod_{\alpha=1}^N \mathrm{sh}(\pm v_\alpha - \frac{1}{2}\epsilon_{12})} \prod_{i=1}^{l-1+\chi} \frac{\mathrm{sh}(\pm\phi_i) \mathrm{sh}(\pm\phi_i - \epsilon_{12})}{\mathrm{sh}(\pm\phi_i - \epsilon_{1,2})} \right)^{1-\chi} \end{aligned} \quad (3.16)$$

where $l = \lfloor \frac{k}{2} \rfloor$ and $\chi \equiv k \pmod{2}$. Note that in our simplified notation, the expression written as $\mathcal{I}_{2N,k}^{\mathrm{Sp},-}$ is not correct after applying the JK-residue when k is even. Fortunately, however, it is valid in the unrefined limit. Since the classification of poles remains unknown for the refined case, we exclusively focus on the unrefined limit.

In the unrefined limit, the poles are classified by $N+4$ Young diagrams [10]. Among these, the first N Young diagrams are labeled by the N coulomb branch parameters v_1, \dots, v_N in the partition function as (3.5). The additional four poles require distinct labeling according to the following Tab. 2.

	v_{N+1}	v_{N+2}	v_{N+3}	v_{N+4}
$+, k = \text{even}$	$\epsilon_1/2$	$\epsilon_1/2 + \pi i$	$\epsilon_{12}/2$	$\epsilon_{12}/2 + \pi i$
$+, k = \text{odd}$	$\epsilon_1/2$	$\epsilon_1/2 + \pi i$	ϵ_1	$\epsilon_{12}/2 + \pi i$
$-, k = \text{even}$	$\epsilon_1/2$	$\epsilon_1/2 + \pi i$	ϵ_1	$\epsilon_1 + \pi i$
$-, k = \text{odd}$	$\epsilon_1/2$	$\epsilon_1/2 + \pi i$	$\epsilon_{12}/2$	$\epsilon_1 + \pi i$

Table 2. The four additional poles required for the Sp instanton partition function.

Therefore, for the $\text{Sp}(2N)$ plus sector, we can write its closed-form expression as:

$$\mathcal{Z}_{2N,k=2l+\chi}^{\text{Sp},+}(v_1, \dots, v_N) = \lim_{\epsilon_2 \rightarrow -\epsilon_1} \sum_{||\vec{\lambda}||=l} \left(\prod_{\alpha=1}^{N+4} \prod_{\mathbf{x} \in \lambda_\alpha} \frac{\prod_{\beta=1}^{N+4} \mathcal{J}(\pm \mathcal{X}_\alpha(\mathbf{x}) | \lambda_\beta)}{\prod_{\beta=1}^N \text{sh}(\pm \mathcal{X}_\alpha(\mathbf{x}) + \mathcal{X}_\beta(\mathbf{0}))} \right) \left(\frac{\prod_{\alpha=1}^{N+4} \mathcal{J}(0 | \lambda_\alpha)}{\prod_{\alpha=1}^N \text{sh}(0 + \mathcal{X}_\alpha(\mathbf{0}))} \right)^\chi \quad (3.17)$$

where, as Tab. 2 shows, we need to identify $v_{N+1} = \frac{1}{2}\epsilon_1$, $v_{N+2} = \frac{1}{2}\epsilon_1 + \pi i$, $v_{N+3} = \chi \epsilon_1 + \frac{1}{2}(1-\chi) \epsilon_{12}$ and $v_{N+4} = \frac{1}{2}\epsilon_{12} + \pi i$.

We remark that without using the $\lim_{\epsilon_2 \rightarrow -\epsilon_1}$, the BPS jumping coefficients $C_{\vec{\lambda}, \mathbf{v}}^{\text{Sp}}$ must be manually included in each term of the summation:

$$\mathcal{Z}_{2N,k}^{\text{Sp},\pm} = \sum_{||\vec{\lambda}||=l} C_{\vec{\lambda}, \mathbf{v}}^{\text{Sp}} \mathcal{Z}^{\text{Sp},\pm}(\vec{\lambda}), \quad C_{\vec{\lambda}, \mathbf{v}}^{\text{Sp}} = \prod_{\alpha=N+1}^{N+4} C_{\lambda_\alpha, v_\alpha}^{\text{Sp}} \quad (3.18)$$

These coefficients $C_{\vec{\lambda}, \mathbf{v}}^{\text{Sp}}$ depend on the specific shapes of the Young diagrams $\vec{\lambda}$ and the corresponding Coulomb branch parameters \mathbf{v} : $C_{\emptyset, v_\alpha}^{\text{Sp}} = 1$, and

$$\begin{aligned} C_{\lambda_\alpha, v_\alpha=0, \pi i, \frac{\epsilon_1}{2}, \frac{\epsilon_1}{2} + \pi i}^{\text{Sp}} &= \frac{2^{2j-1}}{\binom{2j-1}{j-1}}, \quad \text{where } j \text{ is number of diagonal boxes } \mathbf{x} = (i, i) \text{ in } \lambda_\alpha, \\ C_{\lambda_\alpha, v_\alpha=\epsilon_1, \epsilon_1 + \pi i}^{\text{Sp}} &= \frac{2^{2j}}{\binom{2j+1}{j}}, \quad \text{where } j \text{ is number of superdiagonal boxes } \mathbf{x} = (i, i+1) \text{ in } \lambda_\alpha. \end{aligned} \quad (3.19)$$

Consequently, the introduction of these extra coefficients obstructs the computation of the topological vertex for the O^+ -plane [48] and the derivation of the algebraic properties of the partition functions. Fortunately, by employing the shell formula with the unrefined limit $\lim_{\epsilon_2 \rightarrow -\epsilon_1}$, these coefficients can be seamlessly absorbed into the limiting procedure. For clarity, we include detailed calculations in Appendix C.1 to demonstrate how these coefficients arise.

Similarly, the minus sector for $\text{Sp}(2N)$ can be expressed through analogous formulas:

$$\begin{aligned} \mathcal{Z}_{2N,k=2l+\chi}^{\text{Sp},-}(v_1, \dots, v_N) &= \lim_{\epsilon_2 \rightarrow -\epsilon_1} \sum_{||\vec{\lambda}||=l-1+\chi} \left(\prod_{\alpha=1}^{N+4} \prod_{\mathbf{x} \in \lambda_\alpha} \frac{\prod_{\beta=1}^{N+4} \mathcal{J}(\pm \mathcal{X}_\alpha(\mathbf{x}) | \lambda_\beta)}{\prod_{\beta=1}^N \text{sh}(\pm \mathcal{X}_\alpha(\mathbf{x}) + \mathcal{X}_\beta(\mathbf{0}))} \right) \\ &\quad \times \left(\frac{\prod_{\alpha=1}^{N+4} \mathcal{J}(\pi i | \lambda_\alpha)}{\prod_{\alpha=1}^N \text{sh}(-\pi i + \mathcal{X}_\alpha(\mathbf{0}))} \right) \left(\frac{\prod_{\alpha=1}^{N+4} \mathcal{J}(0 | \lambda_\alpha)}{\prod_{\alpha=1}^N \text{sh}(0 + \mathcal{X}_\alpha(\mathbf{0}))} \right)^{1-\chi} \end{aligned} \quad (3.20)$$

where we need to impose the extra poles conditions as Tab. 2, $v_{N+1} = \frac{1}{2}\epsilon_1$, $v_{N+2} = \frac{1}{2}\epsilon_1 + \pi i$, $v_{N+3} = (1 - \chi)\epsilon_1 + \frac{1}{2}\chi\epsilon_{12}$ and $v_{N+4} = \epsilon_1 + \pi i$.

To provide a physical interpretation for these four additional fixed Coulomb branch parameters v_{N+1} to v_{N+4} , we construct the Sp theory using a five-brane web and compare it with the SO theory. In the five-brane web construction, as illustrated in Tab. 1, the Sp theory can be realized with an O5-plane [35, 45]. Analysis based on RR charge and monodromy reveals that an $O5^+$ -plane is effectively equivalent to an $O5^-$ -plane plus 2^{p-4} Dp-branes. These Dp-branes are frozen near the orientifold plane and must acquire specific VEVs. Hence, an $O5^+$ -plane corresponds approximately to an $O5^-$ -plane together with two frozen D5-branes. Accordingly, as depicted in Fig. 4, we can transition from the $Sp(2N)$ theory to the $SO(2N+8)$ theory incorporating 4 D5-branes with specific VEVs.

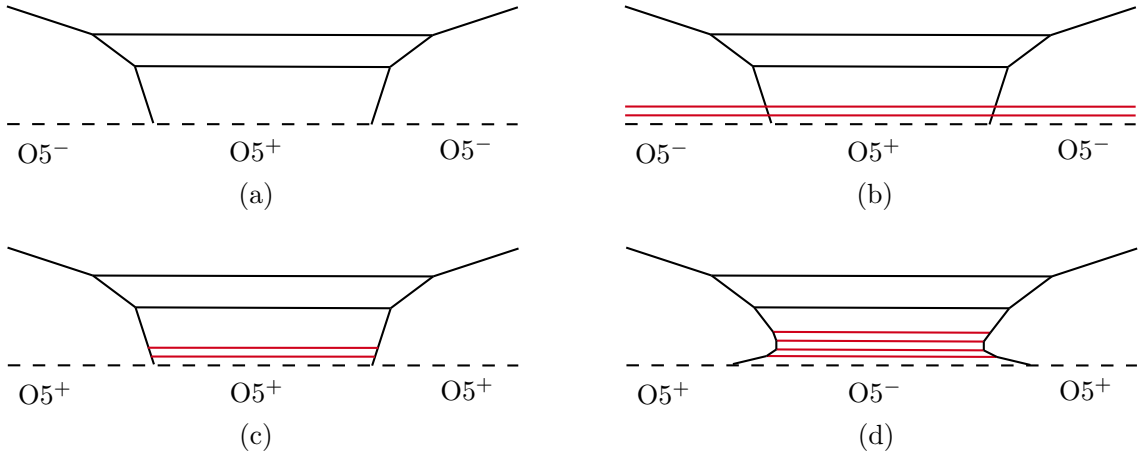


Figure 4. (a) The brane construction for the Sp gauge group is similar to Fig. 3. For the $Sp(2N)$ group, we require N D5-branes, an $O5^+$, and NS5-branes. Furthermore, we can transform this into the brane construction for $SO(2N+8)$. The transformation process is as follows: (b) We bring two D5-branes from infinity via Higgsing to the vicinity of the O-plane and freeze them. At this point, both the left and right sides at the bottom consist of $O5^-$ plus two D5-branes, while the central part at the bottom consists of $O5^+$ plus two D5-branes. (c) Using the equivalence $O5^- + 2 D5 \sim O5^+$, we can replace both sides of the bottom with $O5^+$. (d) Through the equivalence $O5^+ \sim O5^- + 2 D5$, the central part can be replaced with $O5^- + 4 D5$. Therefore, $Sp(2N)$ can be viewed as $SO(2N+8)$ with 4 Coulomb branch parameters v_{N+1}, \dots, v_{N+4} fixed as Tab. 2, corresponding to the frozen D5-branes.

Therefore, as shown in Fig. 5, we can conclude from the formula that the effective contribution of the strings connecting the D1-brane to the four frozen D5-branes to the partition function is $\mathcal{J}(\pm \mathcal{X}_\alpha | \lambda_\beta)$, which differs from the contribution coming from other strings.

We can check the Lie algebra-theoretic relations of instanton partition functions. The isomorphisms $Sp(2) \simeq SU(2)$ and $Sp(4) \simeq SO(5)$ of Lie algebras lead to the equality of the partition functions:

$$\begin{aligned} \mathcal{Z}_{2,k}^{\text{SU}}(v_1) &= \mathcal{Z}_{2,k}^{\text{Sp},\theta=0}(v_1) \\ \mathcal{Z}_{5,k}^{\text{SO}}(v_1 + v_2, v_1 - v_2) &= \mathcal{Z}_{4,k}^{\text{Sp},\theta=0}(v_1, v_2) \end{aligned} \quad (3.21)$$

4 Gauge origami

In this section, we consider a more general setup called gauge origami [16]. Gauge origami refers to gauge theories defined on intersecting D-branes, which provides a systematic method to generalize

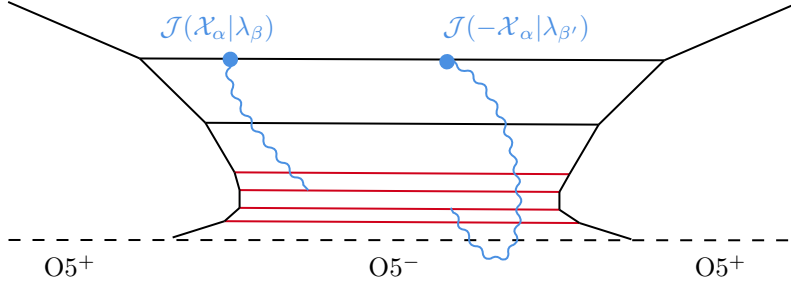


Figure 5. The brane construction of Sp gauge theory. The blue wavy lines represent the effective contribution of strings connecting the $D1_{\alpha,\omega}$ branes and the frozen $D5_\beta$ branes, where $\beta = N+1, \dots, N+4$. Unlike the string contributions connecting $D1$ and ordinary $D5$ branes mentioned above (3.9), the contribution of these strings is simply $J(X_\alpha | \lambda_\beta)$. For the contribution of strings that have been projected by the O-plane and connect $D1$ and the frozen $D5$ branes, we also need to replace X_β with $-X_\beta$.

instanton configurations. We will provide the shell formula for the gauge origami systems on $\mathbb{C}^4 \times \mathbb{R}^1 \times S^1$, including the D0-D8 system known as magnificent four [4, 32, 49], the D0-D6 system known as tetrahedron instantons [5, 30], the D0-D2-D6 system known as the Donaldson-Thomas counting [42, 50, 51], and the D0-D4 system known as spiked instantons [3, 15, 28].

4.1 Magnificent four

Nekrasov first introduced the D0-D8- $\bar{D}8$ system in type IIA theory and referred to it as the magnificent four [4]. To investigate the distribution of bound states in SUSY QM on D0-branes, we need to analyze the energy spectrum of this system. First, the brane configuration is as Tab. 3. D8-branes and anti-D8-branes wrap the directions $\mathbb{C}_{1,2,3,4}$ and are compactified on a circle S^1 along the x^0 direction.

	\mathbb{C}_1		\mathbb{C}_2		\mathbb{C}_3		\mathbb{C}_4		$\mathbb{R} \times S^1$	
	1	2	3	4	5	6	7	8	9	0
k D0	•	•	•	•	•	•	•	•	•	-
N D8	-	-	-	-	-	-	-	-	•	-
N $\bar{D}8$	-	-	-	-	-	-	-	-	•	-

Table 3. Brane configuration of the magnificent four. The symbol $-$ denotes an extended direction of the D-branes, whereas \bullet denotes a point-like direction. The D8-branes and anti-D8-branes extend along four complex directions $\mathbb{C}_{1,2,3,4}$ and the time direction x^0 , while the D0-branes, representing instanton probes, extend only along the time direction.

For simplicity, we first consider the case without anti-D8 branes. In the presence of a B-field [52], the energy spectrum of the D0-D8 system includes four complex adjoint chiral multiplets $B_{1,2,3,4}$ of 1d $\mathcal{N} = (0,2)$ SUSY QM arising from excitations of strings connecting D0-D0, and a fundamental chiral multiplet I arising from excitations of strings connecting D0-D8. The corresponding 1d $\mathcal{N} = (0,2)$ quiver diagram is given in Fig. 6.

The moduli space corresponding to this quiver provides the ADHM data for this D0-D8 system as:

$$\mathcal{M}_{N,k}^{\text{D0-D8}} = \{(\mathbf{B}, I) | \mu_{\mathbb{R}} - \zeta \cdot \mathbf{1}_k = \mu_{ab \in \underline{\mathbf{6}}} = 0\} / \text{U}(k) \quad (4.1)$$

where the moment maps are defined as:

$$\mu_{\mathbb{R}} = \sum_{a \in \underline{\mathbf{4}}} [B_a, B_a^\dagger] + I \cdot I^\dagger$$

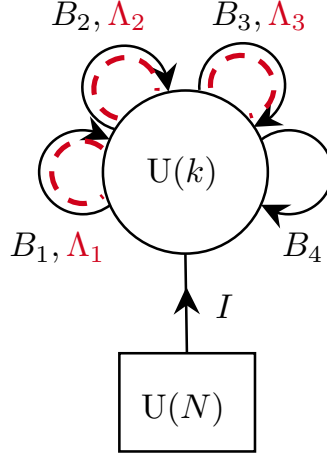


Figure 6. ADHM quiver diagram of D0-D8 system as $\mathcal{N} = (0, 2)$ SUSY QM. The black solid lines represent chiral multiplets, and the red dashed lines represent fermi multiplets. The circular nodes denote gauge groups, while the square nodes denote flavor groups. In this quiver, we have a $U(k)$ gauge group, a $U(N)$ flavor group, a fundamental chiral that contains I , four adjoint chirals that contain $B_{1,2,3,4}$ respectively, and three adjoint fermis that contain $\Lambda_{1,2,3}$ respectively.

$$\mu_{ab} = [B_a, B_b]$$

Similar to the case of pure SYM, where the D0-D4 system is placed in an Ω -background with $U(2)$ symmetry, we need to place the entire D0-D8 system in a background with $SU(4)$ symmetry. This is equivalent to considering the system in a spacetime with $SU(4)$ holonomy [53]. Consequently, the charges of the various fields under the $U(1)^3 \subset SU(4)$ transformation are respectively:

$$\begin{pmatrix} B_1, B_2, B_3, B_4 \\ I, \Lambda_1, \Lambda_2, \Lambda_3 \end{pmatrix} \xrightarrow{U(1)^3 \times U(1)^3 \times U(1)} \begin{pmatrix} q_1^{-1} B_1, q_2^{-1} B_2, q_3^{-1} B_3, q_{123} B_4 \\ I, q_{23} \Lambda_1, q_{13} \Lambda_2, q_{12} \Lambda_3 \end{pmatrix} \quad (4.2)$$

The D0-D8 partition function is:

$$\begin{aligned} \mathcal{Z}_{N,k}^{\text{D0-D8}}(v_{\underline{4},1}, \dots, v_{\underline{4},N}) &= \oint_{\text{JK}} \prod_{i=1}^k \frac{d\phi_i}{2\pi i} \mathcal{I}_{N,k}^{\text{D0-D8}} \\ \mathcal{I}_{N,k}^{\text{D0-D8}} &= \mathcal{I}_k^{\text{D0-D0}} \times \prod_{i=1}^k \prod_{\alpha=1}^N \frac{1}{\text{sh}(\phi_i - v_{\underline{4},\alpha})} \\ \mathcal{I}_k^{\text{D0-D0}} &= \frac{1}{k!} \prod_{i \neq j}^k \text{sh}(\phi_i - \phi_j) \prod_{i,j}^k \frac{\text{sh}(\phi_i - \phi_j - \epsilon_{1,2,3} - \epsilon_4)}{\text{sh}(\phi_i - \phi_j - \epsilon_{1,2,3,4})} \end{aligned} \quad (4.3)$$

where we impose the Calabi-Yau four-fold (CY4) condition $\epsilon_4 = -\epsilon_{123}$.

Similar to pure SYM theory, we can compute the JK-residue. The poles of the D0-D8 system can be classified by N 4d Young diagrams. Therefore, we can also write down a closed formula using the shell formula. However, it is important to note that this partition function (4.3) differs from the expansion of the \mathcal{J} -factor (2.8) under 4d Young diagrams $\rho_{\underline{4}}$:

$$\begin{aligned} \prod_{x \in \rho_{\underline{4}}} \mathcal{J}(\mathcal{X}_{\underline{4}}(x) | \rho_{\underline{4}}) &= \prod_{x \in \rho_{\underline{4}}} \frac{1}{\text{sh}(\mathcal{X}_{\underline{4}}(x) - \mathcal{X}_{\underline{4}}(1))} \\ &\times \prod_{y \in \rho_{\underline{4}}} \frac{\text{sh}(\mathcal{X}_{\underline{4}}(x) - \mathcal{X}_{\underline{4}}(y)) \text{sh}(\mathcal{X}_{\underline{4}}(x) - \mathcal{X}_{\underline{4}}(y) - \epsilon_{\underline{4}}) \prod_{ab \in \underline{6}} \text{sh}(\mathcal{X}_{\underline{4}}(x) - \mathcal{X}_{\underline{4}}(y) - \epsilon_{ab})}{\prod_{a \in \underline{4}} \text{sh}(\mathcal{X}_{\underline{4}}(x) - \mathcal{X}_{\underline{4}}(y) - \epsilon_a) \prod_{A \in \check{\underline{4}}} \text{sh}(\mathcal{X}_{\underline{4}}(x) - \mathcal{X}_{\underline{4}}(y) - \epsilon_A)} \end{aligned}$$

$$= \prod_{\mathbf{x} \in \rho_{\underline{4}}} \frac{1}{\text{sh}(\mathcal{X}_{\underline{4}}(\mathbf{x}) - \mathcal{X}_{\underline{4}}(\mathbf{1}))} \prod_{\mathbf{y} \in \rho_{\underline{4}}} \left(\frac{\text{sh}(\mathcal{X}_{\underline{4}}(\mathbf{x}) - \mathcal{X}_{\underline{4}}(\mathbf{y})) \text{sh}(\mathcal{X}_{\underline{4}}(\mathbf{x}) - \mathcal{X}_{\underline{4}}(\mathbf{y}) - \epsilon_{1,2,3} - \epsilon_4)}{\text{sh}(\mathcal{X}_{\underline{4}}(\mathbf{x}) - \mathcal{X}_{\underline{4}}(\mathbf{y}) - \epsilon_{1,2,3,4})} \right)^2 \quad (4.4)$$

This expression is essentially the square of the D0-D8 partition function. Therefore, if we use the original definition (2.7) to express the D0-D8 partition function, it is necessary to take the square root of the \mathcal{J} -factor, and each term in the summation will exhibit an ambiguous sign. Hence, in order to have a canonical sign choice and a well-defined formula, we define a modified \mathcal{J} -factor that takes roughly half of the shellboxes of the Young diagram, named \mathcal{J}_{\geq} :

$$\mathcal{J}_{\geq}(\mathcal{X}_{\mathcal{B}}(\mathbf{x}) | \rho_{\mathcal{A}}) \equiv \prod_{\substack{\mathbf{y} \in \mathcal{S}(\rho_{\mathcal{A}}) \\ x_d \geq y_d}} \text{sh}(\mathcal{X}_{\mathcal{B}}(\mathbf{x}) - \mathcal{X}_{\mathcal{A}}(\mathbf{y}))^{Q_{\rho_{\mathcal{A}}}(\mathbf{y})} \quad (4.5)$$

where we compare the last coordinates x_d and y_d of two boxes and only select the contribution from boxes where $x_d \geq y_d$. This definition precisely picks exactly the shellboxes we want, and yields the correct sign. Therefore, we can express the D0-D8 partition function as:

$$\mathcal{Z}_{N,k}^{\text{D0-D8}}(v_{\underline{4},1}, \dots, v_{\underline{4},N}) = \sum_{||\vec{\rho}||=k} \mathcal{Z}^{\text{D0-D8}}(\vec{\rho}) = \sum_{||\vec{\rho}||=k} \prod_{\alpha, \beta=1}^N \prod_{\mathbf{x} \in \rho_{\underline{4},\alpha}} \mathcal{J}_{\geq}(\mathcal{X}_{\underline{4},\alpha}(\mathbf{x}) | \rho_{\underline{4},\beta}) \quad (4.6)$$

where, $\vec{\rho}$ denotes an N -tuple of 4d Young diagrams with $||\vec{\rho}|| = k$. Therefore, similar to Fig. 2, the contribution from strings connecting D0-D8 can be effectively regarded simply as:

$$\mathcal{J}_{\geq}(\mathcal{X}_{\underline{4},\alpha}(\mathbf{x}) | \rho_{\underline{4},\beta}) \quad (4.7)$$

If we consider an equal number of anti-D8-branes, we need to replace the flavor group with $U(N|N)$ [54]. Effectively, this is equivalent to adding an equal number of Fermi multiplets to the SUSY QM. Therefore, at the level of the partition function, we only need to include the contribution from the corresponding Fermi multiplets, namely:

$$\begin{aligned} \mathcal{I}_{N,k}^{\text{D0-D8-}\overline{\text{D8}}} &= \mathcal{I}_{N,k}^{\text{D0-D8}} \times \prod_{i=1}^k \prod_{\alpha=1}^N \text{sh}(\phi_i - w_{\underline{4},\alpha}) \\ \mathcal{Z}_{N,k}^{\text{D0-D8-}\overline{\text{D8}}}(\{v_{\underline{4},\alpha}\}, \{w_{\underline{4},\alpha}\}) &= \sum_{||\vec{\rho}||=k} \prod_{\alpha, \beta=1}^N \prod_{\mathbf{x} \in \rho_{\underline{4},\alpha}} \text{sh}(-\mathcal{X}_{\underline{4},\alpha}(\mathbf{x}) + w_{\underline{4},\beta}) \mathcal{J}_{\geq}(\mathcal{X}_{\underline{4},\alpha}(\mathbf{x}) | \rho_{\underline{4},\beta}) \end{aligned} \quad (4.8)$$

The validity of this formula can be verified by computing the plethystic exponent (PE) expression [32]:

$$\mathcal{Z}_N^{\text{D0-D8-}\overline{\text{D8}}}(\{v_{\underline{4},\alpha}\}, \{w_{\underline{4},\alpha}\}) = \sum_{k=0}^{\infty} \mathfrak{q}^k \mathcal{Z}_{N,k}^{\text{D0-D8-}\overline{\text{D8}}} = \text{PE} \left(\frac{\text{sh}(\epsilon_{12,13,23})}{\text{sh}(\epsilon_{1,2,3,4})} \frac{\text{sh}(s)}{\text{sh}(p \pm \frac{1}{2}s)} \right) \quad (4.9)$$

where $s \equiv \sum_{i=1}^N (v_{\underline{4},i} - w_{\underline{4},i})$, and $\mathfrak{q} \equiv e^{-p}$. The PE operation is defined as:

$$\text{PE } f(x_1, \dots, x_r) \equiv \exp \sum_{m=1}^{\infty} \frac{1}{m} f(m x_1, \dots, m x_r) \quad (4.10)$$

We can also consider the recursion relation in the D0-D8 system, which is analogous to (3.11), describing the contribution from adding a 4d box \blacksquare to a 4d Young diagram $\rho_{\underline{4},\alpha}$. Therefore, the corresponding recursion relation can be written as:

$$\frac{\mathcal{Z}^{\text{D0-D8}}(\rho_{\underline{4},\alpha} \cup \blacksquare)}{\mathcal{Z}^{\text{D0-D8}}(\rho_{\underline{4},\alpha})} = \mathcal{J}_{\geq}(\mathcal{X}_{\underline{4},\alpha}(\blacksquare) | \rho_{\underline{4},\alpha} \cup \blacksquare) \mathcal{J}_{<}(\mathcal{X}_{\underline{4},\alpha}(\blacksquare) | \rho_{\underline{4},\alpha}) \quad (4.11)$$

Here, \blacksquare refers to the coordinate of the 4d box being added. The function $\mathcal{J}_{<}$ is defined analogously to \mathcal{J}_{\geq} in (4.5), but with the inequality $x_4 \geq y_4$ replaced by $x_4 < y_4$. Although this relation can be derived from the expansion (2.8), we dispense with the derivation as it is not needed for the subsequent discussion. To illustrate its validity, we provide examples in the Appendix C.4.

4.2 Tetrahedron instanton

We now consider a system whose fixed points are classified by 3d Young diagrams: the D0-D6 system, also known as tetrahedron instantons. This system was first studied in detail by Pomoni-Yan-Zhang [5, 30] in type IIB string theory using a D1-D7 system. After performing a T-duality transformation on x^9 on the D1-D7 system, the corresponding brane configuration is listed in Tab. 4. The ADHM data of this system can be represented by an $\mathcal{N} = (0, 2)$ SUSY QM quiver diagram.

	\mathbb{C}_1		\mathbb{C}_2		\mathbb{C}_3		\mathbb{C}_4		$\mathbb{R} \times \mathbb{S}^1$	
	1	2	3	4	5	6	7	8	9	0
k D0	•	•	•	•	•	•	•	•	•	-
$N_{\bar{4}}$ D6 ₄	-	-	-	-	-	-	•	•	•	-
$N_{\bar{3}}$ D6 ₃	-	-	-	-	•	•	-	-	•	-
$N_{\bar{2}}$ D6 ₂	-	-	•	•	-	-	-	-	•	-
$N_{\bar{1}}$ D6 ₁	•	•	-	-	-	-	-	-	•	-

Table 4. Brane configuration of tetrahedron instantons. $-$ represents the direction along which the D-branes extend, while \bullet represents the point-like directions of the D-branes. \bar{a} refers to the complement of a in $\{1, 2, 3, 4\}$. For example, the D6₄ brane refers to D6₁₂₃, i.e., the D6-brane extending along $\mathbb{C}_1, \mathbb{C}_2, \mathbb{C}_3$ and the time direction. The D0-brane extends only along the time direction. Here, we will need $N_{\bar{a}}$ of D6 _{\bar{a}} branes respectively.

It includes all adjoint fields $B_{1,2,3,4}$ from the magnificent four in Fig. 6 as well as $\Lambda_{1,2,3}$. It also contains four distinct fundamental chiral $I_{\bar{4},\bar{3},\bar{2},\bar{1}}$ and Fermi multiplets $\Lambda_{\bar{4},\bar{3},\bar{2},\bar{1}}$, corresponding to the four different D6-branes. The transformations of these fields under the $U(1)^3$ symmetries are listed as

$$\begin{pmatrix} I_{\bar{4}}, I_{\bar{3}}, I_{\bar{2}}, I_{\bar{1}} \\ \Lambda_{\bar{1}}, \Lambda_{\bar{2}}, \Lambda_{\bar{3}}, \Lambda_{\bar{4}} \end{pmatrix} \xrightarrow{U(1)_{\epsilon_1} \times U(1)_{\epsilon_2} \times U(1)_{\epsilon_3}} \begin{pmatrix} I_{\bar{4}}, I_{\bar{3}}, I_{\bar{2}}, I_{\bar{1}} \\ q_1^{-1} \Lambda_{\bar{1}}, q_2^{-1} \Lambda_{\bar{2}}, q_3^{-1} \Lambda_{\bar{3}}, q_{123} \Lambda_{\bar{4}} \end{pmatrix} \quad (4.12)$$

The ADHM equations of Tetrahedron instantons are:

$$\mathcal{M}_{N,k}^{\text{D0-D6}} = \{(\mathbf{B}, \mathbf{I}) | \mu_{\mathbb{R}} - \zeta \cdot \mathbf{1}_k = \mu_{ab \in \mathbf{6}} = \sigma_{\bar{a}} = 0\} / U(k) \quad (4.13)$$

where the moment maps are defined as:

$$\begin{aligned} \mu_{\mathbb{R}} &= \sum_{a \in \mathbf{4}} [B_a, B_a^\dagger] + I_{\bar{a}} I_{\bar{a}}^\dagger \\ \mu_{ab} &= [B_a, B_b] \\ \sigma_{\bar{a}} &= B_a I_{\bar{a}} \end{aligned} \quad (4.14)$$

Thus, the partition function is expressed as:

$$\mathcal{Z}_{N,k}^{\text{D0-D6}} = \oint_{\text{JK}} \prod_{i=1}^k \frac{d\phi_i}{2\pi i} \mathcal{I}_{N,k}^{\text{D0-D6}}, \quad \mathcal{I}_{N,k}^{\text{D0-D6}} = \mathcal{I}_k^{\text{D0-D0}} \times \prod_{i=1}^k \prod_{\mathcal{A}} \frac{\text{sh}(\phi_i - v_{\mathcal{A}} + \epsilon_{\mathcal{A}})}{\text{sh}(\phi_i - v_{\mathcal{A}})} \quad (4.15)$$

where $\mathcal{A} = (A, \alpha) \in \{(\bar{4}, 1), \dots, (\bar{4}, N_{\bar{4}}), (\bar{3}, 1), \dots, (\bar{1}, N_{\bar{1}})\}$ label each individual D6-brane, and $\mathbf{N} = (N_{\bar{4}}, N_{\bar{3}}, N_{\bar{2}}, N_{\bar{1}})$ denote the numbers of D6-branes in the four distinct orientations. $\mathcal{I}_k^{\text{D0-D0}}$ is the contribution from the D0-D0 strings in (4.3). After performing the JK-residue integral, the poles of this system can be classified by a set $\{\pi_{\mathcal{A}}\}$ of 3d Young diagrams in the four different directions. Using the shell formula, we can express the result after integration as:

$$\mathcal{Z}_{N,k}^{\text{D0-D6}} = \sum_{||\pi||=k} \left(\prod_{\mathcal{A}, \mathcal{B}} \prod_{\mathbf{x} \in \pi_{\mathcal{A}}} \text{sh}(\mathcal{X}_{\mathcal{A}}(\mathbf{x}) - \mathcal{X}_{\mathcal{B}}(\mathbf{0})) \mathcal{J}(\mathcal{X}_{\mathcal{A}}(\mathbf{x}) | \pi_{\mathcal{B}}) \right)$$

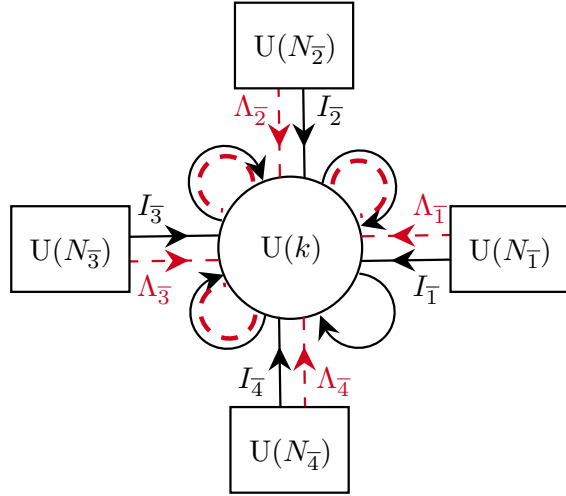


Figure 7. ADHM quiver diagram of D0-D6 system as $\mathcal{N} = (0, 2)$ SUSY QM. The black solid lines represent chiral multiplets, and the red dashed lines represent fermi multiplets. The circular nodes denote gauge groups, while the square nodes denote flavor groups. In this quiver, we have the $U(k)$ gauge group, four flavor groups $U(N_{\bar{1}, \bar{2}, \bar{3}, \bar{4}})$, four types of fundamental chiral multiplets $I_{\bar{1}, \bar{2}, \bar{3}, \bar{4}}$, four types of fundamental fermi multiplets $\Lambda_{\bar{1}, \bar{2}, \bar{3}, \bar{4}}$, four adjoint chiral multiplets $B_{1, 2, 3, 4}$, and three adjoint fermi multiplets $\Lambda_{1, 2, 3}$.

$$\times \left(\prod_{\mathcal{A}, \mathcal{B}} \prod_{\substack{\mathbf{x} \in \pi_{\mathcal{A}} \\ \mathbf{y} \in \pi_{\mathcal{B}}}} \frac{\text{sh}(\mathcal{X}_{\mathcal{A}}(\mathbf{x}) - \mathcal{X}_{\mathcal{B}}(\mathbf{y}) + \epsilon_B)}{\text{sh}(\mathcal{X}_{\mathcal{A}}(\mathbf{x}) - \mathcal{X}_{\mathcal{B}}(\mathbf{y}) + \epsilon_A)} \right) \left(\prod_{\substack{\mathcal{A}, \mathcal{B} \\ A < B}} \prod_{\substack{\mathbf{x} \in \pi_{\mathcal{A}} \\ \mathbf{y} \in \pi_{\mathcal{B}}}} \prod_{\substack{ab \in \mathbf{6} \\ \in A \\ \notin B}} \frac{\text{sh}(\mathcal{X}_{\mathcal{A}}(\mathbf{x}) - \mathcal{X}_{\mathcal{B}}(\mathbf{y}) + \epsilon_{ab})}{\text{sh}(\mathcal{X}_{\mathcal{A}}(\mathbf{x}) - \mathcal{X}_{\mathcal{B}}(\mathbf{y}) - \epsilon_{ab})} \right) \quad (4.16)$$

where the order $A < B$ is defined by the canonical ordering $123 < 124 < 134 < 234$. The equality in the second line can be interpreted as an additional contribution arising from the interaction between 3d Young diagrams in different directions.

Similarly, using the recursion relation of the \mathcal{J} -factor (2.14), we can directly derive the contribution from adding a D0-brane at location \square :

$$\frac{\mathcal{Z}^{\text{D0-D6}}(\pi_{\mathcal{A}} \cup \square)}{\mathcal{Z}^{\text{D0-D6}}(\pi_{\mathcal{A}})} = \frac{\mathcal{J}(\mathcal{X}_{\mathcal{A}}(\square) | \pi_{\mathcal{A}} \cup \square)}{\mathcal{J}(\mathcal{X}_{\mathcal{A}}(\square + \mathbf{1}) | \pi_{\mathcal{A}})} \quad (4.17)$$

We provide detailed calculations for several illustrative examples in the Appendix C.2.

Furthermore, we can directly observe from the partition function the similarity between the D0-D6 system (4.15) and the D0-D8- $\overline{\text{D8}}$ system (4.8). Indeed, D6-branes can simply arise from tachyon condensation between D8 and $\overline{\text{D8}}$ branes [4, 55, 56]. For instance, considering a system with only one pair of D8- $\overline{\text{D8}}$ -branes, its integrand is given by:

$$\mathcal{I}_{1,k}^{\text{D0-D8-}\overline{\text{D8}}} = \mathcal{I}_k^{\text{D0-D0}} \times \prod_{i=1}^k \frac{\text{sh}(\phi_i - w_{\underline{4},1})}{\text{sh}(\phi_i - v_{\underline{4},1})} \quad (4.18)$$

Once we identify $v_{\underline{4},1} = v_{123,1}$ and $w_{\underline{4},1} = v_{123,1} - \epsilon_{123}$, we can observe that this integrand is identical to that of a single D6-brane. This is because when we set $w_{\underline{4},1} = v_{123,1} - \epsilon_{123}$, we effectively bring the D8 and $\overline{\text{D8}}$ -branes close together. As shown in Fig. 8, the open strings connecting them develop a negative mass state: tachyon state, which renders the system unstable and causes it to

decay into a more stable vacuum configuration. In this case, the more stable vacuum configuration corresponds to a single D6-brane.

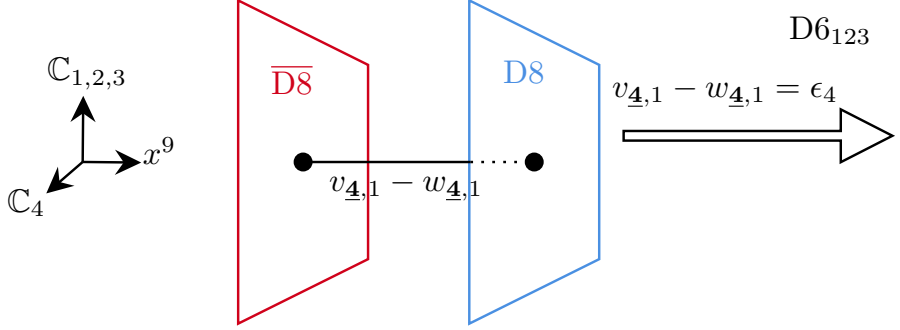


Figure 8. The D8- $\overline{\text{D8}}$ pair annihilates into a D6-brane through tachyon condensation. In the figure, the red brane represents the anti-D8-brane, with $w_{\underline{4},1}$ being its corresponding Coulomb branch parameter. The blue brane represents the D8-brane, with $v_{\underline{4},1}$ being its corresponding Coulomb branch parameter. When we adjust the moduli space coordinate to the place $v_{\underline{4},1} - w_{\underline{4},1} = \epsilon_4$, the D8- $\overline{\text{D8}}$ pair becomes equivalent to a single D6-brane oriented along $\mathbb{C}_{\bar{4}}$.

From the perspective of the shell formula, if the corresponding 4d Young diagram contains the box located at $(1, 1, 1, 2)$, then the contribution of the $\overline{\text{D8}}$ -brane becomes $\text{sh}(\epsilon_{1234})$ under the condition $w_{\underline{4},1} = v_{123,1} - \epsilon_{123}$ and $v_{\underline{4},1} = v_{123,1}$. Under the CY4 condition $\epsilon_{1234} = 0$, this term vanishes. This implies that the $\overline{\text{D8}}$ -brane contribution selects only those 4d Young diagrams that have exactly one layer in the fourth direction, i.e., 3d Young diagrams. In this case, the condition $x_4 \geq y_4$ in the \mathcal{J}_{\geq} -factor (4.5) becomes trivial.

It follows that the PE expression of the tetrahedron instanton [30, 32], derivable from that of the magnificent four (4.9), is manifestly independent of all the Coulomb branch parameters $\{v_{\mathcal{A}}\}$:

$$\mathcal{Z}_N^{\text{D0-D6}}(\{v_{\mathcal{A}}\}) = \sum_{k=0}^{\infty} \mathfrak{q}^k \mathcal{Z}_{N,k}^{\text{D0-D6}} = \text{PE} \left(\frac{\text{sh}(\epsilon_{12,13,23})}{\text{sh}(\epsilon_{1,2,3,4})} \frac{\text{sh}(s)}{\text{sh}(p \pm \frac{1}{2}s)} \right) \quad (4.19)$$

where the parameter $s \equiv \sum_{i=1}^N (v_{\underline{4},i} - w_{\underline{4},i})$ after tachyon condensation becomes:

$$\begin{aligned} s &= N_{\bar{4}} \epsilon_{123} + N_{\bar{3}} \epsilon_{124} + N_{\bar{2}} \epsilon_{134} + N_{\bar{1}} \epsilon_{234} \\ &= (N_{123} - N_{234}) \epsilon_1 + (N_{123} - N_{134}) \epsilon_2 + (N_{123} - N_{124}) \epsilon_3 \end{aligned} \quad (4.20)$$

We can briefly discuss the generalized tetrahedron instanton, namely the theory with the addition of anti-D6 branes [42, 57]. Similar to the anti-D8 case, the contribution of $\overline{\text{D6}}$ -brane to the index corresponds to the reciprocal of that of a D6-brane. Therefore, we can write its partition function as:

$$\mathcal{I}_{N,\mathcal{M},k}^{\text{D0-D6-}\overline{\text{D6}}} = \mathcal{I}_{N,k}^{\text{D0-D6}} \times \prod_{i=1}^k \prod_{\mathcal{B}} \frac{\text{sh}(-\phi_i + w_{\mathcal{B}})}{\text{sh}(-\phi_i + w_{\mathcal{B}} - \epsilon_{\mathcal{B}})} \quad (4.21)$$

where $w_{\mathcal{B}}$ is the fugacity for the $\overline{\text{D6}}$ -brane with $\mathcal{B} = (B, \beta) \in \{(\bar{4}, 1), \dots, (\bar{4}, M_{\bar{4}}), (\bar{3}, 1), \dots, (\bar{1}, M_{\bar{1}})\}$ label each $\overline{\text{D6}}$ -brane.

4.3 Donaldson-Thomas counting

Another interesting application of the shell formula is the DT counting [42, 50, 51, 57–59]. Mathematically, the DT invariants count the virtual Euler characteristics of moduli spaces of ideal sheaves

on a CY threefold, equivalently, the virtual counts of curve and point subschemes. Physically, the DT invariants count the bound states of D0-D2-D6 branes. Specifically, a single D2-brane corresponds to an infinitely long 3d Young diagram composed of individual boxes. Therefore, we can use the \mathcal{J} -factor to compute the partition function for the D0-D2-D6 system.

We consider the simplest DT invariant, corresponding to the system placed on the CY threefold \mathbb{C}^3 . For this configuration, the brane construction data are summarized in Tab. 5.

	\mathbb{C}_1		\mathbb{C}_2		\mathbb{C}_3		\mathbb{C}_4		$\mathbb{R} \times \mathbb{S}^1$	
	1	2	3	4	5	6	7	8	9	0
k D0	•	•	•	•	•	•	•	•	•	-
1 D6 ₁₂₃	-	-	-	-	-	-	•	•	•	-
N_1 D2 ₁	-	-	•	•	•	•	•	•	•	-
N_2 D2 ₂	•	•	-	-	•	•	•	•	•	-
N_3 D2 ₃	•	•	•	•	-	-	•	•	•	-

Table 5. Brane configuration of the DT counting. The symbol $-$ denotes an extended direction of the D-branes, whereas \bullet denotes a point-like direction. The D2-branes extend along one of the four complex directions $\mathbb{C}_{1,2,3,4}$ and also the time direction x^0 . And here we consider only 1 D6-brane extends on \mathbb{C}_{123}^3 .

The D6-brane extends over the full CY threefold \mathbb{C}_{123}^3 , with D2-branes on curve subschemes of \mathbb{C}_{123}^3 . Fixing the stable D2-branes configuration (the minimal plane partition/vacuum) allows us to count bound states on the world volume of the k D0-branes, i.e., to count placements of k boxes that preserve the 3d Young diagram. Analogously, the D0-D2-D6 framed quiver Fig. 9 can be drawn using the method of [59].

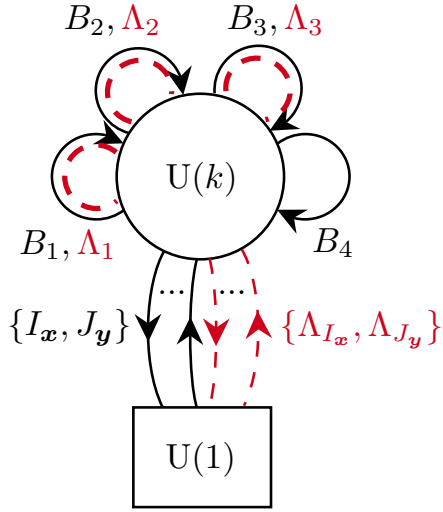


Figure 9. ADHM quiver diagram of D0-D2-D6 system as $\mathcal{N} = (0, 2)$ SUSY QM. The solid black lines represent chiral multiplets, including the adjoint chirals $B_{1,2,3,4}$, the fundamental chirals $\{I_x\}$, and the anti-fundamental chirals $\{J_y\}$. The red dashed lines denote Fermi multiplets, which consist of the adjoint fermis $\Lambda_{1,2,3}$, the fundamental fermis $\{\Lambda_{Ix}\}$, and the anti-fundamental fermis $\{\Lambda_{Jy}\}$. The precise numbers of the fields $\{I_x\}$, $\{J_y\}$, $\{\Lambda_{Ix}\}$, and $\{\Lambda_{Jy}\}$, as well as their respective $U(1)^3$ charges, are determined by the specific vacuum configuration of the D2-branes.

The vacuum configuration formed by the D2-branes can be viewed as the smallest infinite 3d Young diagram $\pi_{\lambda\mu\nu}$ (minimal plane partition) with three prescribed asymptotic boundary

conditions λ , μ , and ν that satisfy $|\lambda| = N_1$, $|\mu| = N_2$ and $|\nu| = N_3$. As illustrated in Fig. 10, its three asymptotic planes at infinity are precisely the given 2d Young diagrams λ , μ , and ν that serve as the boundary conditions. If all three asymptotic boundaries λ , μ , and ν are non-empty, this configuration is referred to as the 3-leg case. If exactly two of the boundaries are non-empty, it is called a 2-leg configuration. Finally, if only one boundary is non-empty, it is termed a 1-leg case.

From a given vacuum configuration, one can determine the numbers and $U(1)^3$ charges of the fields $\{I_x\}$, $\{J_y\}$, $\{\Lambda_{I_x}\}$, and $\{\Lambda_{J_y}\}$ via the corresponding framed quiver and its superpotential [51, 59] (the detailed algorithm for constructing the framed quiver and its superpotential are omitted in this work). This subsequently allows for the derivation of the integral expression for the partition function.

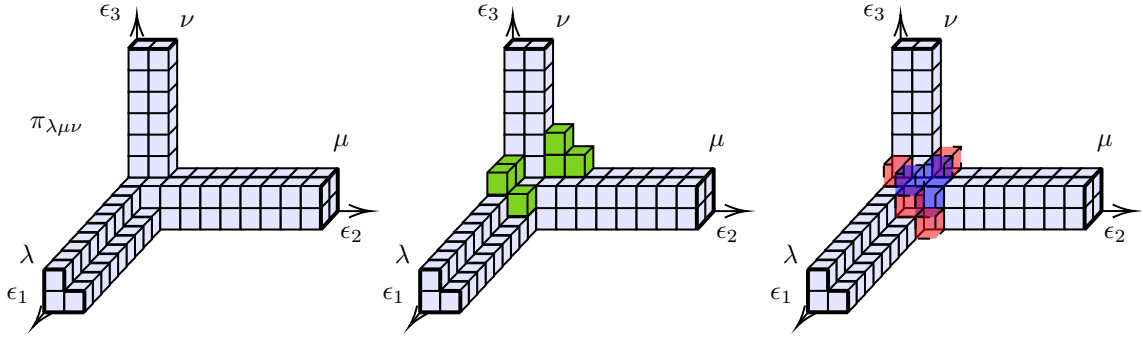


Figure 10. The left panel shows the minimal 3d Young diagram $\pi_{\lambda\mu\nu}$ (the minimal plane partition) for given asymptotic boundary conditions (λ, μ, ν) . It can be seen that the boundary condition in the 1-direction is the 2d Young diagram λ on the 23-plane, and so forth. The center panel displays a possible DT configuration given the vacuum $\pi_{\lambda\mu\nu}$. The green boxes correspond to D0-branes, and their number equals the instanton number k . The rule is that after placing the green boxes on the vacuum $\pi_{\lambda\mu\nu}$, the entire assembly must still form a valid 3d Young diagram. The right panel shows the shell boxes with non-zero charge for this vacuum diagram $\pi_{\lambda\mu\nu}$, where red boxes represent a charge of -1 and blue boxes represent a charge of $+1$.

However, by employing the shell formula and the recursion relation of 3d Young diagram (4.17), the partition function can be obtained directly from the minimal plane partition $\pi_{\lambda\mu\nu}$:

$$\mathcal{I}_{\lambda,\mu,\nu;k}^{\text{D0-D2-D6}} = \mathcal{I}_k^{\text{D0-D0}} \times \prod_{i=1}^k \frac{\mathcal{J}(\phi_i | \pi_{\lambda\mu\nu})}{\mathcal{J}_-(\phi_i + \epsilon_{123} | \pi_{\lambda\mu\nu})} \quad (4.22)$$

where the only label of the D6-brane: $(123, 1)$ under the 3d Young diagram $\pi_{\lambda\mu\nu}$ and the Coulomb branch parameter v are omitted for brevity. To maintain the proper $U(1)^3$ charges and representations of the multiplets, the definitions of \mathcal{J}_- and \mathcal{J} in (2.7) differ slightly. Specifically, \mathcal{J}_- is defined as:

$$\begin{aligned} \mathcal{J}_-(x | \mathbf{Y}_A) &\equiv \prod_{\mathbf{y} \in S(\mathbf{Y}_A)} -\text{sh}(\mathcal{X}_A(\mathbf{y}) - x)^{Q_{\mathbf{Y}_A}(\mathbf{y})} \\ \mathcal{J}_-(x | \emptyset_A) &\equiv \frac{-1}{\text{sh}(\mathcal{X}_A(\mathbf{1}) - x)} \end{aligned} \quad (4.23)$$

The \mathcal{J} -factor for $\pi_{\lambda\mu\nu}$ can be calculated using the following relation:

$$\mathcal{J}(x | \pi_{\lambda\mu\nu}) = \frac{\mathcal{J}(x | \pi_{\lambda\emptyset\emptyset}) \mathcal{J}(x | \pi_{\emptyset\mu\emptyset}) \mathcal{J}(x | \pi_{\emptyset\emptyset\nu}) \mathcal{J}(x | \pi_{\lambda\emptyset\emptyset} \cap \pi_{\emptyset\mu\emptyset} \cap \pi_{\emptyset\emptyset\nu})}{\mathcal{J}(x | \pi_{\lambda\emptyset\emptyset} \cap \pi_{\emptyset\mu\emptyset}) \mathcal{J}(x | \pi_{\lambda\emptyset\emptyset} \cap \pi_{\emptyset\emptyset\nu}) \mathcal{J}(x | \pi_{\emptyset\mu\emptyset} \cap \pi_{\emptyset\emptyset\nu})} \quad (4.24)$$

where, $\pi_{\lambda\emptyset\emptyset} \cap \pi_{\emptyset\mu\emptyset}$, $\pi_{\lambda\emptyset\emptyset} \cap \pi_{\emptyset\emptyset\nu}$, $\pi_{\emptyset\mu\emptyset} \cap \pi_{\emptyset\emptyset\nu}$, and $\pi_{\lambda\emptyset\emptyset} \cap \pi_{\emptyset\mu\emptyset} \cap \pi_{\emptyset\emptyset\nu}$ are all finite 3d Young diagrams, so we can directly compute their \mathcal{J} -factors by calculating the charges of their shellboxes. For the \mathcal{J} -factors of $\pi_{\lambda\emptyset\emptyset}$, $\pi_{\emptyset\mu\emptyset}$, and $\pi_{\emptyset\emptyset\nu}$ (the 1-leg cases), it can be shown recursively via (2.17)—as illustrated in Fig. 11—that the shellboxes with non-zero charge appear only at the two ends of the corresponding Young diagram. Moreover, without loss of generality, as illustrated in Fig. 11, the number of shell boxes with +1 charge at the infinite end of $\pi_{\emptyset\mu\emptyset}$ equals the number of those with -1 charge. Consequently, in this scenario, their net contribution to the \mathcal{J} -factor is:

$$\frac{\text{sh}(\infty\epsilon_2 + \dots)}{\text{sh}(\infty\epsilon_2 + \dots)} \frac{\text{sh}(\infty\epsilon_2 + \dots)}{\text{sh}(\infty\epsilon_2 + \dots)} \frac{\text{sh}(\infty\epsilon_2 + \dots)}{\text{sh}(\infty\epsilon_2 + \dots)} \times \dots = 1 \quad (4.25)$$

Therefore, since the total contribution from the shellboxes at the infinite end is exactly 1, to compute the \mathcal{J} -factor for such 1-leg Young diagrams, we only need to focus on the 2d Young diagram that defines the asymptotic boundary condition:

$$\begin{aligned} \mathcal{J}(x|\pi_{\lambda\emptyset\emptyset}) &= \mathcal{J}(x + v_{23,1} - v|\lambda_{23,1}) \\ \mathcal{J}(x|\pi_{\emptyset\mu\emptyset}) &= \mathcal{J}(x + v_{13,1} - v|\mu_{13,1}) \\ \mathcal{J}(x|\pi_{\emptyset\emptyset\nu}) &= \mathcal{J}(x + v_{12,1} - v|\nu_{12,1}) \end{aligned} \quad (4.26)$$

By applying the JK-residue, we obtain the refined DT invariant as:

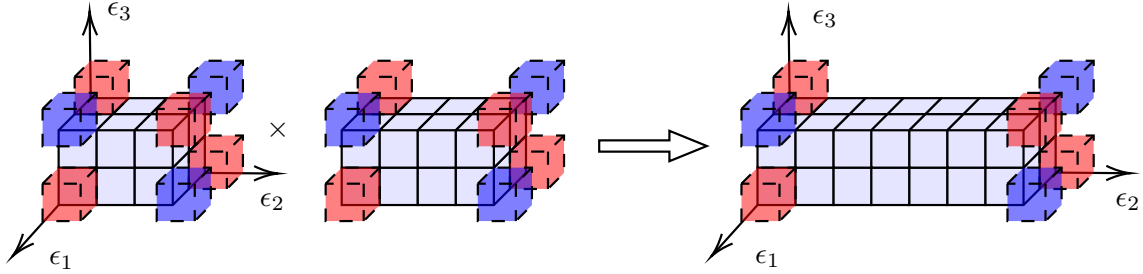


Figure 11. If we glue together two long legs with identical 2d Young diagram cross-sections, nontrivial shellboxes will only appear at the two ends of the combined leg. As shown in the figure, the cross-section is $\mu = \{(1, 1), (1, 2), (2, 1), (2, 2)\}$. It follows that for an infinitely long leg $\pi_{\emptyset\mu\emptyset}$ with cross-section μ , its nontrivial shellboxes are also confined to the starting end and the end at infinity. Furthermore, the contribution from the shellboxes at the infinite end to the \mathcal{J} -factor is exactly 1; i.e., their contribution can be disregarded.

$$\begin{aligned} \mathcal{Z}_{\lambda, \mu, \nu; k}^{\text{D0-D2-D6}} &= \oint_{\text{JK}} \prod_{i=1}^k \frac{d\phi_i}{2\pi i} \mathcal{I}_{\lambda, \mu, \nu; k}^{\text{D0-D2-D6}} \\ &= \sum_{|\tilde{\pi}_{\lambda\mu\nu}|=k} \prod_{\mathbf{x} \in \tilde{\pi}_{\lambda\mu\nu}} \frac{\mathcal{J}(\mathcal{X}(\mathbf{x})|\pi_{\lambda\mu\nu})}{\mathcal{J}_-(\mathcal{X}(\mathbf{x}) + \epsilon_{123}|\pi_{\lambda\mu\nu})} \prod_{\mathbf{y} \in \tilde{\pi}_{\lambda\mu\nu}} \text{sh}(\mathcal{X}(\mathbf{x}) - \mathcal{X}(\mathbf{y})) \mathcal{J}(\mathcal{X}(\mathbf{x})|\{\mathbf{y}\}) \end{aligned} \quad (4.27)$$

where let $\pi \supset \pi_{\lambda\mu\nu}$ be a infinite 3d Young diagram that contains the vacuum $\pi_{\lambda\mu\nu}$, then $\tilde{\pi}_{\lambda\mu\nu} \equiv \pi \setminus \pi_{\lambda\mu\nu}$. $\{\mathbf{x}\}$ represents a 3d Young diagram with exactly one box, originating not from $\mathbf{1}$ but from \mathbf{x} . The corresponding \mathcal{J} -factor can therefore be calculated via (2.10). Note that in the second line, although $\text{sh}(0)$ appears when $\mathbf{x} = \mathbf{y}$, the overall value remains finite.

If we consider the case where λ , μ , and ν are all empty sets \emptyset , i.e., $N_1 = N_2 = N_3 = 0$ and hence no D2-branes are present, the whole system reduces to the simplest sector of the tetrahedron

instanton in Sec. 4.2—namely, the D0–D6 system with a single D6-brane. In terms of the partition function, the DT invariant (4.27) for $\pi_{\emptyset\emptyset\emptyset} = \emptyset$ reads:

$$\begin{aligned}\mathcal{Z}_{\emptyset,\emptyset,\emptyset;k}^{\text{D0-D2-D6}} &= \sum_{|\pi|=k} \prod_{\mathbf{x} \in \pi} \frac{\text{sh}(\mathcal{X}(\mathbf{x}) - \mathcal{X}(\mathbf{0}))}{\text{sh}(\mathcal{X}(\mathbf{x}) - \mathcal{X}(\mathbf{1}))} \prod_{\mathbf{y} \in \pi} \text{sh}(\mathcal{X}(\mathbf{x}) - \mathcal{X}(\mathbf{y})) \mathcal{J}(\mathcal{X}(\mathbf{x})|\{\mathbf{y}\}) \\ &= \sum_{|\pi|=k} \prod_{\mathbf{x} \in \pi} \frac{\text{sh}(\mathcal{X}(\mathbf{x}) - \mathcal{X}(\mathbf{0}))}{\text{sh}(\mathcal{X}(\mathbf{x}) - \mathcal{X}(\mathbf{1}))} \prod_{\mathbf{y} \in \pi} \frac{\text{sh}(\mathcal{X}(\mathbf{x}) - \mathcal{X}(\mathbf{y})) \text{sh}(\mathcal{X}(\mathbf{x}) - \mathcal{X}(\mathbf{y}) - \epsilon_{12,13,23})}{\text{sh}((\mathcal{X}(\mathbf{x}) - \mathcal{X}(\mathbf{y}) - \epsilon_{1,2,3}) \text{sh}((\mathcal{X}(\mathbf{x}) - \mathcal{X}(\mathbf{y}) - \epsilon_{123}))} \\ &= \sum_{|\pi|=k} \prod_{\mathbf{x} \in \pi} \text{sh}(\mathcal{X}(\mathbf{x}) - \mathcal{X}(\mathbf{0})) \mathcal{J}(\mathcal{X}(\mathbf{x})|\pi)\end{aligned}\quad (4.28)$$

where in the first equality we have used the definition of the \mathcal{J} -factor: $\mathcal{J}(x|\emptyset) = 1/\text{sh}(x - \mathcal{X}(\mathbf{1}))$. For the second and third equalities, we employed the expansion formula (2.8) of the \mathcal{J} -factor. For the case $\lambda = \mu = \nu = \emptyset$, we have $\tilde{\pi}_{\emptyset\emptyset\emptyset} = \pi$. The last line of the equality is, as desired, equal to the partition function (4.16) of the tetrahedron instanton with a single D6-brane. Thus, we naturally obtain:

$$\mathcal{Z}_{\emptyset,\emptyset,\emptyset;k}^{\text{D0-D2-D6}} = \mathcal{Z}_{(1,0,0,0),k}^{\text{D0-D6}} \quad (4.29)$$

We provide detailed calculations for simple examples of the 1-leg and 3-leg configurations, as well as the derivation of (4.27) in the Appendix C.3.

4.4 Spiked instanton

The spiked instanton is also an interesting topic [3, 15, 28]. It can be obtained from the 5d $\mathcal{N} = 1$ theory introduced in Sec. 3.1 by incorporating D4-branes with different orientations and turning on the masses of the adjoint multiplets, or alternatively from the tetrahedron instanton discussed in Sec. 4.2 by introducing an equal number of anti-D6-branes through tachyon condensation. The corresponding brane configuration, as shown in Tab. 6, involves six types of D4-branes with distinct orientations. In the low-energy regime, D0-instantons can attach to any of these D4-branes in the form of 2d Young diagrams. With the ADHM quiver as $\mathcal{N} = (0, 2)$ SUSY QM as in Fig. 12, the

	C ₁		C ₂		C ₃		C ₄		R × S ¹	
	1	2	3	4	5	6	7	8	9	0
D0	•	•	•	•	•	•	•	•	•	-
D4 ₁₂	-	-	-	-	•	•	•	•	•	-
D4 ₁₃	-	-	•	•	-	-	•	•	•	-
D4 ₁₄	-	-	•	•	•	•	-	-	•	-
D4 ₂₃	•	•	-	-	-	-	•	•	•	-
D4 ₂₄	•	•	-	-	•	•	-	-	•	-
D4 ₃₄	•	•	•	•	-	-	-	-	•	-

Table 6. Brane configuration of spiked instantons. — represents the direction along which the D-branes extend, while • represents the point-like directions of the D-branes. In the spiked instanton, we consider six types of D4-branes, where the D4_{ab}₆-branes extend along C_{ab} and the time direction x⁰.

Instanton moduli space is defined as:

$$\mathcal{M}_{N,k}^{\text{D0-D4}} = \{(\mathbf{B}, \mathbf{I}, \mathbf{J}) | \mu_{\mathbb{R}} - \zeta \cdot \mathbf{1}_k = \mu_{ab} = \sigma_{a;bc} = \tilde{\sigma}_{a;bc} = 0\} / \text{U}(k) \quad (4.30)$$

where $a \in \underline{4}$, $ab, bc \in \underline{6}$. The moment maps in the spiked instantons cases are modified as:

$$\mu_{\mathbb{R}} = \sum_{a \in \underline{4}} [B_a, B_a^\dagger] + \sum_{ab \in \underline{6}} (I_{ab} I_{ab}^\dagger - J_{ab}^\dagger J_{ab})$$

$$\begin{aligned}
\mu_{ab} &= [B_a, B_b] + I_{ab} J_{ab} \\
\sigma_{a;bc} &= B_a I_{bc} \\
\tilde{\sigma}_{a;bc} &= J_{bc} B_a
\end{aligned} \tag{4.31}$$

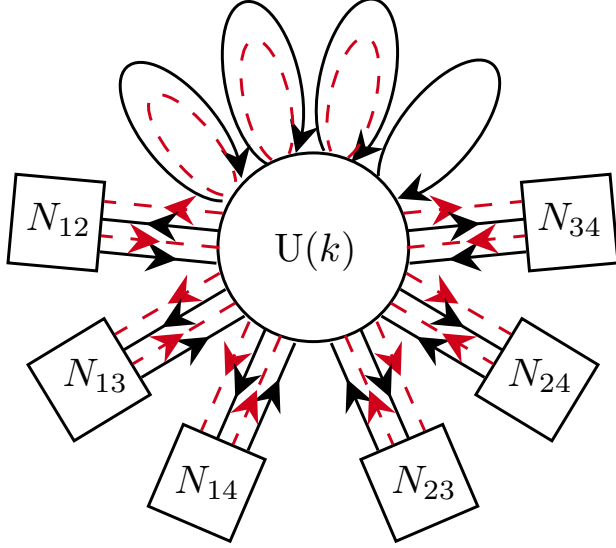


Figure 12. ADHM quiver diagram of D0-D4 system as $\mathcal{N} = (0, 2)$ SUSY QM. In this quiver, we have the $U(k)$ gauge group, six flavor groups $U(N_{ab \in \underline{\mathfrak{b}}})$, six types of fundamental chiral multiplets that contain $I_{ab \in \underline{\mathfrak{b}}}$, six types of anti-fundamental chirals that contain $J_{ab \in \underline{\mathfrak{b}}}$, twelve types of fermi multiplets $\Lambda_{I_{ab}}, \Lambda_{J_{ab}}$ correspond to I_{ab} and J_{ab} respectively, four adjoint chiral multiplets $B_{1,2,3,4}$, and three adjoint fermi multiplets $\Lambda_{1,2,3}$.

With all the data, we can express the spiked instanton partition function as:

$$\begin{aligned}
\mathcal{Z}_{N,k}^{\text{D0-D4}} &= \oint_{\text{JK}} \prod_{i=1}^k \frac{d\phi_i}{2\pi i} \mathcal{I}_{N,k}^{\text{D0-D4}} \\
\mathcal{I}_{N,k}^{\text{D0-D4}} &= \mathcal{I}_k^{\text{D0-D0}} \times \prod_{i=1}^k \prod_{\mathbf{ab}} \frac{\prod_{c \in \overline{\mathbf{ab}}} \text{sh}(\phi_i - v_{\mathbf{ab}} - \epsilon_c)}{\text{sh}(\phi_i - v_{\mathbf{ab}}) \text{sh}(-\phi_i + v_{\mathbf{ab}} - \epsilon_{ab})} \tag{4.32}
\end{aligned}$$

where $\mathbf{ab} = (ab, \alpha) \in \{(12, 1), \dots, (12, N_{12}), (13, 1), \dots, (34, N_{34})\}$ label each D4 brane, $\overline{\mathbf{ab}}$ denotes the complement of ab within $\underline{\mathfrak{4}}$, and $\mathbf{N} = (N_{12}, \dots, N_{34})$ corresponds to the numbers of D4-branes with different orientations. The poles of this residue integral can be classified by a set of 2d Young diagrams, hence, we can express it using the shell formula as follows:

$$\begin{aligned}
\mathcal{Z}_{N,k}^{\text{D4, } \mathbb{C}^4} &= \sum_{||\vec{\lambda}||=k} (-1)^k \prod_{\mathbf{ab}, \mathbf{ab}'} \left(\prod_{\mathbf{x} \in \lambda_{\mathbf{ab}}} \frac{\mathcal{J}(\mathcal{X}_{\mathbf{ab}}(\mathbf{x}) | \lambda_{\mathbf{ab}'})}{\text{sh}(-\mathcal{X}_{\mathbf{ab}}(\mathbf{x}) + \mathcal{X}_{\mathbf{ab}'}(\mathbf{0}))} \prod_{c \in \overline{\mathbf{ab}}} \text{sh}(\mathcal{X}_{\mathbf{ab}}(\mathbf{x}) - \mathcal{X}_{\mathbf{ab}'}(\mathbf{0}) + \epsilon_c) \right) \\
&\times \left(\prod_{\substack{\mathbf{x} \in \lambda_{\mathbf{ab}} \\ \mathbf{y} \in \lambda_{\mathbf{ab}'}}} \frac{\text{sh}(\mathcal{X}_{\mathbf{ab}}(\mathbf{x}) - \mathcal{X}_{\mathbf{ab}'}(\mathbf{y}) - \epsilon_{1,2,3} - \epsilon_4)}{\text{sh}(\mathcal{X}_{\mathbf{ab}}(\mathbf{x} + \mathbf{1}) - \mathcal{X}_{\mathbf{ab}'}(\mathbf{y})) \prod_{c \in \overline{\mathbf{ab}}} \text{sh}(\mathcal{X}_{\mathbf{ab}}(\mathbf{x}) - \mathcal{X}_{\mathbf{ab}'}(\mathbf{y}) + \epsilon_c)} \right) \tag{4.33}
\end{aligned}$$

From the perspective of tachyon condensation, this spiked instanton system can arise from a D6-anti-D6 system [42, 57]. For instance, on the integrand level, a D4₁₂-brane can be obtained from a D6₁₂₃- $\bar{D}6_{123}$ system by taking $v_{123,1} = v_{12,1}$, $w_{123,1} = v_{12,1} + \epsilon_3$, or from a D6₁₂₄- $\bar{D}6_{124}$ system by taking $v_{123,1} = v_{12,1}$, $w_{123,1} = v_{12,1} + \epsilon_4$ as in (4.21). Furthermore, if we consider only a single type of D4-brane, the resulting theory is precisely the 5d U(N) SYM theory with an additional adjoint hypermultiplet, where ϵ_3 can be interpreted as the mass fugacity for the adjoint hypermultiplet [35].

5 Discussion

In this work, the physical systems we discuss share two key features:

Their partition functions exhibit a universal structure, particularly in the D0-D0 sector. Specifically, the contributions from this sector all take the form of the expansion of the \mathcal{J} -factor (2.8):

- Sipked instanton and 5d SYM with classical gauge groups (for instance, on $\mathbb{C}_1 \times \mathbb{C}_2$):

$$\mathcal{Z}_k^{\text{D0-D4,U,SO,Sp}} \supset \prod_{i=1}^k \frac{\prod_{j \neq i}^k \text{sh}(\phi_i - \phi_j)}{\text{sh}(\phi_i - \mathcal{X}_\alpha(\mathbf{1}))} \prod_{i,j}^k \frac{\text{sh}(\phi_i - \phi_j - \epsilon_{12})}{\text{sh}(\phi_i - \phi_j - \epsilon_{1,2})} \quad (5.1)$$

- Tetrahedron instanton and DT counting (for instance, on $\mathbb{C}_1 \times \mathbb{C}_2 \times \mathbb{C}_3$):

$$\mathcal{Z}_k^{\text{D0-D6,D0-D2-D6}} \supset \prod_{i=1}^k \frac{\prod_{j \neq i}^k \text{sh}(\phi_i - \phi_j)}{\text{sh}(\phi_i - \mathcal{X}_\alpha(\mathbf{1}))} \prod_{i,j}^k \frac{\text{sh}(\phi_i - \phi_j - \epsilon_{12,13,23})}{\text{sh}(\phi_i - \phi_j - \epsilon_{1,2,3}) \text{sh}(\phi_i - \phi_j - \epsilon_{123})} \quad (5.2)$$

- Magnificent four:

$$\mathcal{Z}_k^{\text{D0-D8}} \supset \left(\prod_{i=1}^k \frac{1}{\text{sh}(\phi_i - \mathcal{X}_\alpha(\mathbf{1}))} \right) \left(\prod_{i \neq j}^k \text{sh}(\phi_i - \phi_j) \prod_{i,j}^k \frac{\text{sh}(\phi_i - \phi_j - \epsilon_{1234}) \prod_{ab \in \underline{\mathbf{6}}} \text{sh}(\phi_i - \phi_j - \epsilon_{ab})}{\text{sh}(\phi_i - \phi_j - \epsilon_{1,2,3,4}) \prod_{A \in \underline{\mathbf{4}}} \text{sh}(\phi_i - \phi_j - \epsilon_A)} \right)^{1/2} \quad (5.3)$$

Their BPS bound states can be classified by Young diagrams of different dimensions:

- For 5d SYM with classical gauge groups and spiked instantons, the poles are classified by tuples of 2d Young diagrams.
- For tetrahedron instantons and DT counting, the poles are classified by tuples of 3d Young diagrams.
- For magnificent four, the poles are classified by tuples of 4d Young diagrams.

Any physical system whose partition function satisfies the above two criteria can be described using the shell formula:

- Sipked instanton and 5d SYM with classical gauge groups:

$$\mathcal{Z}_k^{\text{D0-D4,U,SO,Sp}} \supset \prod_{\mathbf{x} \in \lambda} \frac{\mathcal{J}(\mathcal{X}(\mathbf{x}) | \lambda)}{\text{sh}(-\mathcal{X}(\mathbf{x}) + \mathcal{X}(\mathbf{0}))} \quad (5.4)$$

- Tetrahedron instanton:

$$\mathcal{Z}_k^{\text{D0-D6}} \supset \prod_{\mathbf{x} \in \pi} \text{sh}(\mathcal{X}(\mathbf{x}) - \mathcal{X}(\mathbf{0})) \mathcal{J}(\mathcal{X}(\mathbf{x}) | \pi) \quad (5.5)$$

- DT counting:

$$\mathcal{Z}_k^{\text{D0-D2-D6}} \supset \prod_{\substack{\mathcal{X} \in \mathcal{Z} \\ \mathcal{X} \in \pi_{\lambda\mu\nu}}} \frac{\mathcal{J}(\mathcal{X}(\mathbf{x}) | \pi_{\lambda\mu\nu})}{\mathcal{J}(\mathcal{X}(\mathbf{x}) + \epsilon_{123} | \pi_{\lambda\mu\nu})} \quad (5.6)$$

- Magnificent four:

$$\mathcal{Z}_k^{\text{D0-D8}} \supset \prod_{\mathbf{x} \in \rho} \mathcal{J}_{\geq}(\mathcal{X}(\mathbf{x}) | \rho) \quad (5.7)$$

The availability of these precise partition function expressions enables the systematic computation of additional properties, such as algebraic identities and recurrence relations.

A promising future direction is to employ the shell formula in any system meeting the above conditions, as well as to generalize its relationship to other known algebraic frameworks:

- We aim to clarify the precise relationship between the shell formula and the topological vertex. In particular, it would be valuable to derive an explicit expression for the O^+ -plane [9, 10, 48] vertex and understand how orientifold projections modify the combinatorial and representation-theoretic structure of the vertex.
- Another promising direction is to generalize the shell formula to SYM theories with matter fields in various representations. This includes both classical and exceptional Lie groups, where the structure of instanton moduli spaces becomes more general [35, 37, 60, 61]. Developing such generalizations may reveal how the shell formula encodes representation-dependent contributions and could potentially lead to new insights into exceptional gauge symmetries in non-perturbative string theory.
- Using the exact closed form of the magnificent four partition function, we can investigate its interplay with qq -characters and the representation theory of quantum algebras. This includes examining how the partition function furnishes generating functions for protected operators and how it realizes the action of quantum toroidal (or DIM-type) symmetries [15, 16, 21, 22, 41, 42].
- The configurations analyzed in this work involve D-branes extended along flat complex planes. A natural generalization is to place these branes on orbifolds or more general CY manifolds [59, 62], and to study how the corresponding moduli spaces and instanton sums are modified. One may also apply the same framework to the full 4G system of D0-D2-D4-D6-D8 branes [63], where additional couplings and defect sectors are expected to appear.
- The appendix focuses on the application of the shell formula to DT invariants of CY threefolds. This can be extended to physically broader settings, such as DT counting on CY fourfolds, where the enumerative theory involves self-dual obstruction bundles, as well as to Pandharipande-Thomas stable pair invariants [64–66]. Understanding how the shell formula adapts to these higher-dimensional or alternative enumerative theories may shed light on universal structures underlying BPS counting.

Acknowledgments

The author is grateful to Satoshi Nawata for his generous guidance and constant support throughout the development of this work. The author also warmly thanks Taro Kimura, Go Noshita, and Jiahao Zheng for many insightful conversations on gauge origami, DT counting, and for their thoughtful suggestions that greatly improved the presentation of this paper. This work is supported by the Shanghai Municipal Science and Technology Major Project (No.24ZR1403900).

A Examples of charges of shellboxes

In this appendix, we summarize notations necessary for the paper and present various examples of the definitions in Sec. 2.

A.1 Labels of Young diagram and notations

To concisely indicate the required ϵ_i parameter and the basis of Young diagrams, we adopt the following simplified notation:

- $\underline{4} = \{1, 2, 3, 4\}$, $a, b \in \underline{4}$.
- $\check{\underline{4}} = \{123, 124, 134, 234\} = \{\bar{4}, \bar{3}, \bar{2}, \bar{1}\}$, $A, B \in \check{\underline{4}}$.
- $\underline{6} = \{12, 13, 23, 14, 24, 34\}$, $ab \in \underline{6}$.

The Ω -background parameters $\epsilon_{1,2,3,4}$ are also denoted as:

$$q_i \equiv e^{-\epsilon_i}, \quad q_{i_1 \dots i_s} = q_{i_1} \dots q_{i_s} = e^{-(\epsilon_{i_1} + \dots + \epsilon_{i_s})} \quad (\text{A.1})$$

In this paper, we adopt the CY fourfold condition $\epsilon_4 = -\epsilon_{123}$ as a default assumption.

We employ \mathcal{A} , \mathcal{B} , \mathbf{ab} and \mathbf{ab}' to denote the label of each Young diagram, where $\mathcal{A} = \{234, 7\}$, for instance, $\mathbf{Y}_{\mathcal{A}}$ represents the 7-th Young diagram in the basis $\epsilon_2, \epsilon_3, \epsilon_4$.

The poles of all the integrands are denoted as:

$$\mathcal{X}_{\mathcal{A}}(\mathbf{x}) \equiv v_{\mathcal{A}} + (\mathbf{x} - \mathbf{1}) \cdot \boldsymbol{\epsilon}_{\mathcal{A}} = v_{\mathcal{A}} + \sum_{i=1}^d (x_i - 1) \epsilon_{a_i} \quad (\text{A.2})$$

Given a 2d Young diagram λ , we can define, for each box \mathbf{x} in λ , its leg $L_{\lambda}(\mathbf{x})$ and arm $A_{\lambda}(\mathbf{x})$ as illustrated in Fig. 13. The leg is the number of boxes in direction 1 from \mathbf{x} within λ , while the arm is the number of boxes in direction 2.

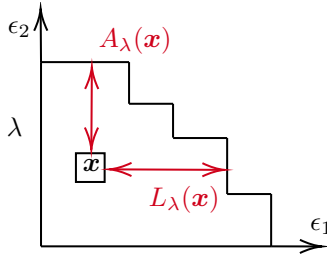


Figure 13. Leg length $L_{\lambda}(\mathbf{x})$ and arm length $A_{\lambda}(\mathbf{x})$ of a box \mathbf{x} in a Young diagram λ .

Given a tuple of Young diagrams $\vec{\mathbf{Y}} = (\mathbf{Y}_{\mathcal{A}}, \dots)$, the total number of boxes is defined as follows. For a single Young diagram $\mathbf{Y}_{\mathcal{A}}$, we denote its number of boxes by $|\mathbf{Y}_{\mathcal{A}}|$. Then, the total number of boxes for the tuple is defined as $||\vec{\mathbf{Y}}|| \equiv \sum_{\mathcal{A}} |\mathbf{Y}_{\mathcal{A}}|$.

Throughout this paper, the functions sh and ch that appear in all the partition functions are defined by:

$$\text{sh}(x) \equiv e^{x/2} - e^{-x/2}, \quad \text{ch}(x) \equiv e^{x/2} + e^{-x/2} \quad (\text{A.3})$$

And we denote the product for multiplicative parameters in the following expressions:

$$\begin{aligned} \text{sh}(\pm x \pm y) &= \text{sh}(x + y) \text{sh}(x - y) \text{sh}(-x + y) \text{sh}(-x - y) \\ \text{sh}(x + \epsilon_{12,13,\dots}) &= \text{sh}(x + \epsilon_{12}) \text{sh}(x + \epsilon_{13}) \times \dots \end{aligned} \quad (\text{A.4})$$

A.2 Shell and \mathcal{J} -factor

In this subsection, we will present several examples of Young diagrams along with their corresponding shells, and compute the corresponding \mathcal{J} -factor.

- For the simplest 2d Young diagram that consists of only one box: $\lambda_{12,1} = \{(1, 1)\}$, with the corresponding binaries tuples $\mathbf{B}_2 = \{(0, 0), (0, 1), (1, 0), (1, 1)\}$ as in the definition 2.5. The shell of $\lambda_{12,1}$ is then:

$$\begin{aligned} \mathcal{S}(\lambda_{12,1}) &= (\lambda_{12,1} + \mathbf{B}_2) \setminus \lambda_{12,1} \\ &= \{(1, 1), (1, 2), (2, 1), (2, 2)\} \setminus \{(1, 1)\} \\ &= \{(1, 2), (2, 1), (2, 2)\} \end{aligned} \quad (\text{A.5})$$

Therefore, the charge of each shellbox is defined as (2.6):

$$\begin{aligned} Q_{\lambda_{12,1}}(1, 2) &= (-1)^{|(0, 1)|} = -1 \\ Q_{\lambda_{12,1}}(2, 1) &= (-1)^{|(1, 0)|} = -1 \\ Q_{\lambda_{12,1}}(2, 2) &= (-1)^{|(1, 1)|} = 1 \end{aligned} \quad (\text{A.6})$$

So the \mathcal{J} -factor is:

$$\begin{aligned} \mathcal{J}(x | \lambda_{12,1}) &= \frac{\text{sh}(x - \mathcal{X}_{12,1}(2, 2))}{\text{sh}(x - \mathcal{X}_{12,1}(1, 2)) \text{sh}(x - \mathcal{X}_{12,1}(2, 1))} \\ &= \frac{\text{sh}(x - v_{12,1} - \epsilon_{12})}{\text{sh}(x - v_{12,1} - \epsilon_1) \text{sh}(x - v_{12,1} - \epsilon_2)} \end{aligned} \quad (\text{A.7})$$

We can see the Young diagram, the shell, and the corresponding charges in Fig. 14.

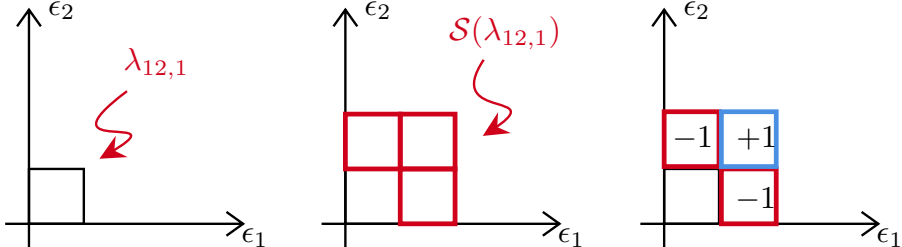


Figure 14. The leftmost diagram shows a 2d Young diagram $\lambda_{12,1}$ with only one box, labeled $\{(1, 1)\}$ indicating it is the first Young diagram in the 12-plane. In the middle diagram, the red boxes represent the shell $\mathcal{S}(\lambda_{12,1})$ of $\lambda_{12,1}$; for a 2d Young diagram with only one box, its shell $\mathcal{S}(\lambda_{12,1})$ consists of only 3 shellboxes. In the rightmost diagram, the charge of each shellbox is shown, where the $+1$ shellboxes are marked in blue and the -1 shellboxes are marked in red.

- We can consider a more general 2d Young diagram, as illustrated in Fig. 15. The left diagram shows the original Young diagram, the middle one displays its shell, and the right figure indicates the charge associated with each shellbox. We use blue boxes to represent $+1$ charge and red boxes to represent -1 charge.

Note that for any 2d Young diagram, a new box can be placed on any shellbox with -1 charge. After this placement, the entire configuration remains a valid 2d Young diagram. Therefore, the shellboxes with -1 charge correspond to the *addable boxes* \mathfrak{A} of the Young diagram. Similarly, each shellbox with $+1$ charge at position (i, j) corresponds to a *removable*

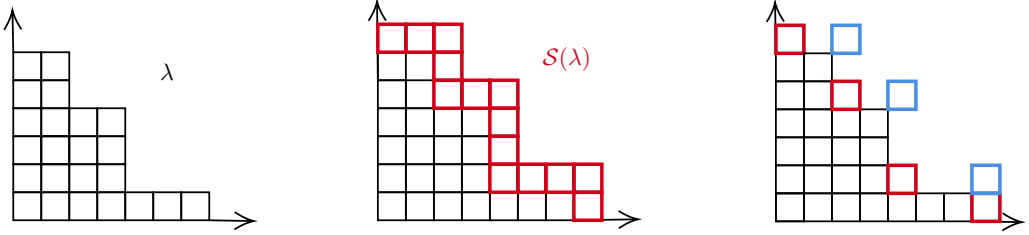


Figure 15. As shown in the leftmost figure, for a more general 2d Young diagram λ , its shellboxes $S(\lambda)$ are marked in red in the middle figure. In the rightmost figure, the charges of various shellboxes are indicated: red boxes have -1 charge, blue boxes have $+1$ charge, and other unmarked shellboxes have 0 charge.

box \mathfrak{R} at position $(i-1, j-1)$. Hence, in the case of 2d Young diagrams, the \mathcal{J} -factor can be expressed as:

$$\mathcal{J}(x|\lambda_{\mathbf{ab}}) = \frac{\prod_{\mathbf{y} \in \mathfrak{R}} \text{sh}(x - \mathcal{X}_{\mathbf{ab}}(\mathbf{y} + \mathbf{1}))}{\prod_{\mathbf{y} \in \mathfrak{A}} \text{sh}(x - \mathcal{X}_{\mathbf{ab}}(\mathbf{y}))} \quad (\text{A.8})$$

- As illustrated in Fig. 16, for any given 3d Young diagram, one can compute the charge associated with each shell box. However, unlike the case of 2d Young diagrams, these charges cannot be put into a one-to-one correspondence with addable and removable boxes. Consequently, the \mathcal{J} -factor for a 3d Young diagram cannot be expressed in the same form as (A.8).

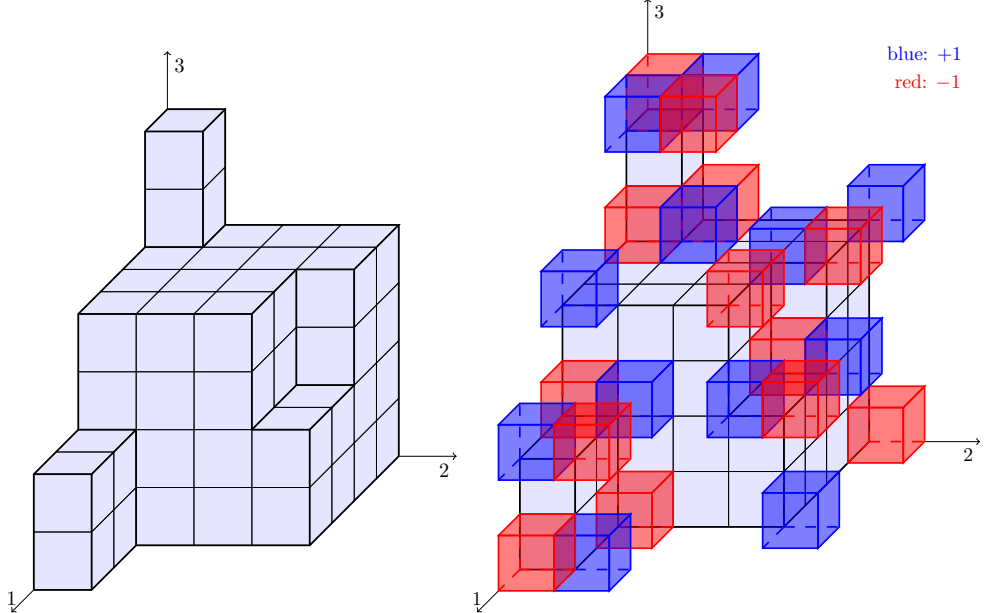


Figure 16. As shown in the left figure, for an arbitrary 3d Young diagram, we can compute the charges of its shellboxes. The result is shown in the right figure, where the red boxes have a charge of -1 and the blue boxes have a charge of $+1$.

- For a d -dimensional Young diagram, the charge of the shellbox can take any integer value from $-d$ to d .

B Witten index and JK-residue

B.1 1d $\mathcal{N} = (0, 2)$ quiver and Witten index

Given a SUSY QM, the definition of the Witten index is:

$$\mathcal{I} = \text{Tr}_{\mathcal{H}}(-1)^F e^{-\beta H - \sum_i T_i u_i} \quad (\text{B.1})$$

where F is the fermion number operator, $\{u_i\}$ are the chemical potentials of the flavor symmetries, $\{T_i\}$ are the Cartan generators of the flavor symmetries, and β denotes the size of the time circle \mathbb{S}^1 .

Given a supersymmetric field theory, we can use a quiver to describe the gauge symmetry, flavor symmetry, and all fields that transform non-trivially under these symmetries. For 1d $\mathcal{N} = (0, 2)$ SUSY QM, the quiver and its corresponding contributions to the Witten index are as follows:

- A circular node represents a gauge group, and each gauge group carries the contribution of the vector multiplet. In our cases, we only focus on the $U(k)$ gauge group:

$$\text{U}(k) \qquad \qquad \qquad \Rightarrow \qquad \qquad \left(\prod_{i=1}^k \frac{d\phi_i}{2\pi i} \right) \prod_{i \neq j}^k \text{sh}(\phi_i - \phi_j)$$

- a square node represents flavor symmetry. A black solid line with arrows connecting two square nodes represents a bifundamental chiral multiplet Φ_α^β . Under the flavor node pointed to by the arrow, they transform in the fundamental representation, while under the flavor node at the other end, they transform in the anti-fundamental representation. For such a chiral multiplet, with additional $U(1)$ flavor charges $q(\Phi_\alpha^\beta)$, its contribution to the index is:

$$\text{U}(N_a) \xrightarrow{\quad \leftarrow \quad} \text{U}(N_b) \qquad \Rightarrow \qquad \prod_{\alpha=1}^{N_a} \prod_{\beta=1}^{N_b} \frac{1}{\text{sh}(a_\alpha - b_\beta + q(\Phi_\alpha^\beta))}$$

- The red dashed lines represent fermi multiplets Ψ_α^β . Under the flavor node pointed to by the arrow, they transform in the fundamental representation, while under the flavor node at the other end, they transform in the anti-fundamental representation. Their contribution with additional $U(1)$ flavor charges $q(\Psi_\alpha^\beta)$ to the index is:

$$\text{U}(N_a) \xrightarrow{\quad \text{---} \quad \leftarrow \quad \text{---} \quad} \text{U}(N_b) \qquad \Rightarrow \qquad \prod_{\alpha=1}^{N_a} \prod_{\beta=1}^{N_b} \text{sh}(a_\alpha - b_\beta + q(\Psi_\alpha^\beta))$$

In our context, all $U(1)$ flavor symmetries are contained in the CY4 holonomy $U(1)^3 = U(1)_{\epsilon_1} \times U(1)_{\epsilon_2} \times U(1)_{\epsilon_3}$. For example, for the adjoint chiral B_1 , its $U(1)^3$ charges are $(-1, 0, 0)$, and thus its contribution to the index is:

$$\mathcal{I}(B_1) = \prod_{i,j}^k \frac{1}{\text{sh}(\phi_i - \phi_j - \epsilon_1)} \quad (\text{B.2})$$

B.2 Jeffery-Kirwan residue

The computation of the Witten index requires explicit evaluation of contour integrals. The JK-residue prescription [67–71] provides the correct method for performing these integrals. Here we review this JK-residue approach.

We consider a gauge theory with rank- k gauge group, which is $U(k)$ in our context. The Witten index is expressed as an integral of a meromorphic k -form over a specific cycle:

$$\mathcal{Z} = \oint_{JK} \prod_{I=1}^k \frac{d\phi_I}{2\pi i} \mathcal{I}(\phi) = \oint_{\text{specific cycles}} \mathcal{I}(\phi) d\phi_1 \wedge \cdots \wedge d\phi_k, \quad (\text{B.3})$$

where $\phi = (\phi_1, \dots, \phi_k)$ denotes the complexified gauge variables. The integrand $\mathcal{Z}(\phi)$ is periodic in each ϕ_I :

$$\mathcal{I}(\dots, \phi_I, \dots) = \mathcal{I}(\dots, \phi_I + 2\pi i, \dots). \quad (\text{B.4})$$

The poles of the integrand arise from the denominator, which takes the schematic form:

$$\mathcal{I}(\phi) \propto \prod_a \frac{1}{\text{sh} \left(\sum_{I=1}^k Q_a^I \phi_I + m_a \right)^{N_a}}, \quad (\text{B.5})$$

where $Q_a^I \in \mathbb{Q}$ are charge vectors and m_a are masses or equivariant parameters. The poles of \mathcal{I} are thus located at solutions of the equations

$$\sum_{I=1}^k Q_a^I \phi_I + m_a = 2\pi i n_a, \quad n_a \in \mathbb{Z}, \quad a = 1, \dots, k. \quad (\text{B.6})$$

The periodicity leads to multiple copies of poles shifted by $2\pi i$, and the allowed values of n_a can be parametrized by an invertible matrix Q_{ai} as

$$\begin{pmatrix} n_1 \\ \vdots \\ n_k \end{pmatrix} = \frac{Q}{|\det Q|} \cdot \begin{pmatrix} l_1 \\ \vdots \\ l_k \end{pmatrix}, \quad l_I \in 0, 1, \dots, |\det Q| - 1. \quad (\text{B.7})$$

Given a specific pole ϕ_* satisfying (B.6), the JK-residue is evaluated through the following steps

- Given a pole ϕ_* , we identify an associated set of charge vectors $Q_* = \{Q_1, \dots, Q_r\}$ with $r \geq k$, such that $Q_\ell \cdot \phi_* + m_\ell = n_\ell 2\pi i$ for any $Q_\ell \in Q_*$. We can construct a flag F from any k -sequence of linearly independent charge vectors $\{Q_{a_1}, \dots, Q_{a_k}\} \subset Q_*$ that satisfies:

$$\{0\} \subset F_1 \subset \dots \subset F_k = \mathbb{R}^k, \quad F_\ell = \text{span}\{Q_{a_1}, \dots, Q_{a_\ell}\} \quad (\text{B.8})$$

The sequence $\{Q_{a_1}, \dots, Q_{a_k}\}$ is called a basis $\mathcal{B}(F, Q_*)$ of F in Q_* .

- From each flag F and its basis $\mathcal{B}(F, Q_*)$, a sequence of vectors is constructed:

$$\kappa(F, Q_*) \equiv (\kappa_1, \dots, \kappa_k), \quad \text{where } \kappa_\ell = \sum_{\substack{Q \in Q_* \\ Q \in F_\ell}} Q \quad (\text{B.9})$$

Note that there are generally different flags F and different $\kappa(F, Q_*)$ for a given Q_* . If there exist different flags F, F' corresponding to the same $\kappa(F, Q_*) = \kappa(F', Q_*)$, we can arbitrarily pick one of them.

- We need to choose a reference vector $\eta = (\eta_1, \dots, \eta_k) \in (\mathbb{R}^k)^*$. And we only pick the sequence of vectors $\kappa(F, Q_*)$ that satisfies:

$$\kappa(F, Q_*)^T \cdot \lambda = \eta, \quad \text{where } \lambda = (\lambda_1, \dots, \lambda_k) \in \mathbb{R}_+^k \quad (\text{B.10})$$

For this purpose, one can define a delta function:

$$\delta(F, \eta) = \begin{cases} 1, & \kappa(F, Q_*) \text{ satisfies (B.10)} \\ 0, & \text{else} \end{cases} \quad (\text{B.11})$$

With these objects defined, the JK-residue of the given pole ϕ_* is:

$$\text{JK-Res}_{\phi=\phi_*}(\eta)\mathcal{I} = \sum_F \delta(F, \eta) \frac{\text{sgn} \det \kappa(F, Q_*)}{\det \mathcal{B}(F, Q_*)} \underset{\varepsilon_k=0}{\text{Res}} \dots \underset{\varepsilon_1=0}{\text{Res}} \mathcal{I} \Big|_{\substack{Q_{a_1} \phi_* + m_{a_1} + \varepsilon_1 = n_{a_1} 2\pi i \\ \vdots \\ Q_{a_k} \phi_* + m_{a_k} + \varepsilon_k = n_{a_k} 2\pi i}} \quad (\text{B.12})$$

where the sum is over all flags constructed from Q_* associated to ϕ_* . The $\varepsilon_1, \dots, \varepsilon_k$ represent the order of integral induced by the chosen flag F .

Finally, given a generic η , the JK-residue can be computed as follows:

$$\oint_{\text{JK}} \prod_{I=1}^k \frac{d\phi_I}{2\pi i} \mathcal{I}(\phi) = \sum_{\phi_*} \text{JK-Res}_{\phi=\phi_*}(\eta) \mathcal{I}(\phi) \quad (\text{B.13})$$

Note that in most cases, the results of the JK-residue are independent of the choice of the reference vector η . However, in our problems, the results sometimes depend on the choice of η . Thus, we should take the standard choice $\eta = (1, \dots, 1)$.

C Detail computations for various cases

In this appendix, we illustrate the underlying mechanisms through a series of low-instanton calculations, presented in order of increasing dimension of Young diagrams. Beginning with low-instanton examples in 5d Sp(2) SYM, we show how the BPS jumping coefficients arise in the instanton partition function. We then proceed to low-instanton computations in the D0-D6 system to elucidate how charges are generally assigned to shellboxes. After that, we compute simple examples of DT counting for the 1-leg and 3-leg cases, and briefly derive the integrand for the DT invariant. Finally, low-instanton examples for the magnificent four are analyzed to demonstrate the computation of \mathcal{J}_{\geq} -factor and the origin of the sign rule mentioned in [32].

C.1 5d Sp(2) SYM

- First, we can compute the instanton partition function for Sp(2) with $k = 1$. This partition function is trivial since the corresponding auxiliary gauge group has rank 0 at level $k = 1$. Therefore, we can directly write down its partition function according to (3.17) and (3.20):

$$\begin{aligned} \mathcal{Z}_{2,k=1}^{\text{Sp},+} &= \lim_{\epsilon_2 \rightarrow -\epsilon_1} \frac{\prod_{\alpha=1}^5 \mathcal{I}(0|\emptyset_\alpha)}{\text{sh}(0 + v_1 - \epsilon_{12})} \\ &= \lim_{\epsilon_2 \rightarrow -\epsilon_1} \frac{1}{\text{sh}(v_1 - \epsilon_{12}) \prod_{\alpha=1}^5 \text{sh}(-v_\alpha)} \\ &= \lim_{\epsilon_2 \rightarrow -\epsilon_1} \frac{-1}{\text{sh}(\frac{\epsilon_1}{2}) \text{sh}(\frac{\epsilon_1}{2} + \pi i) \text{sh}(\epsilon_1) \text{sh}(\frac{\epsilon_{12}}{2} + \pi i) \text{sh}(v_1) \text{sh}(v_1 - \epsilon_{12})} \\ &= \frac{1}{2 \text{sh}(v_1)^2 \text{sh}(\epsilon_1)^2} \\ \mathcal{Z}_{2,k=1}^{\text{Sp},-} &= \lim_{\epsilon_2 \rightarrow -\epsilon_1} \frac{\prod_{\alpha=1}^5 \mathcal{I}(\pi i|\emptyset_\alpha)}{\text{sh}(-\pi i + v_1 - \epsilon_{12})} \\ &= \lim_{\epsilon_2 \rightarrow -\epsilon_1} \frac{-1}{\text{sh}(\frac{\epsilon_1}{2}) \text{sh}(\frac{\epsilon_1}{2} + \pi i) \text{sh}(\epsilon_1) \text{sh}(\frac{\epsilon_{12}}{2} + \pi i) \text{sh}(v_1 + \pi i) \text{sh}(v_1 - \epsilon_{12} + \pi i)} \\ &= -\frac{\text{sh}(v_1)^2}{2 \text{sh}(2v_1)^2 \text{sh}(\epsilon_1)^2} \end{aligned} \quad (\text{C.1})$$

where we substituted the specific values of the frozen branes v_2, v_3, v_4 , and v_5 as Tab. 2, and we used the identity $\text{sh}(x + \pi i) = i \text{sh}(2x) / \text{sh}(x)$. Therefore, using another identity of the hyperbolic function $\text{sh}(x + \pi i)^2 + \text{sh}(x)^2 = -4$, we know the full partition function of Sp(2) when $k = 1$ is:

$$\mathcal{Z}_{2,k=1}^{\text{Sp}} = \mathcal{Z}_{2,k=1}^{\text{Sp},+} + \mathcal{Z}_{2,k=1}^{\text{Sp},-} = \frac{2}{\text{sh}(2v_1)^2 \text{sh}(\epsilon_1)^2} \quad (\text{C.2})$$

where, as expected, is exactly equal to the instanton partition function of the $SU(2)$ case at the unrefined limit.

- Next, we consider a more non-trivial case: $k = 2$. For the minus sector, the case of $k = 2$ still admits no non-trivial Young diagrams. Therefore, we can directly write down the result for the minus sector:

$$\begin{aligned} \mathcal{Z}_{2,k=2}^{\text{Sp},-} &= \lim_{\epsilon_2 \rightarrow -\epsilon_1} \frac{\prod_{\alpha=1}^5 \mathcal{J}(0|\emptyset_\alpha)}{\text{sh}(0+v_1-\epsilon_{12})} \frac{\prod_{\alpha=1}^5 \mathcal{J}(\pi i|\emptyset_\alpha)}{\text{sh}(-\pi i+v_1-\epsilon_{12})} \\ &= \frac{-1}{\text{sh}(2v_1)^2 \text{sh}(\epsilon_1)^2 \text{sh}(2\epsilon_1)^2} \end{aligned} \quad (\text{C.3})$$

However, the plus sector at level $k = 2$ possesses one degree of freedom corresponding to a single box. This box can be placed on any of the five empty Young diagrams, resulting in a total of five distinct Young diagram configurations $\vec{\lambda}$:

$$\begin{aligned} &(\{(1,1)\}_1, \emptyset_2, \emptyset_3, \emptyset_4, \emptyset_5), \quad (\emptyset_1, \{(1,1)\}_2, \emptyset_3, \emptyset_4, \emptyset_5), \quad (\emptyset_1, \emptyset_2, \{(1,1)\}_3, \emptyset_4, \emptyset_5) \\ &(\emptyset_1, \emptyset_2, \emptyset_3, \{(1,1)\}_4, \emptyset_5), \quad (\emptyset_1, \emptyset_2, \emptyset_3, \emptyset_4, \{(1,1)\}_5) \end{aligned} \quad (\text{C.4})$$

We also know the \mathcal{J} -factor for one box in 2d as (A.7). Therefore, the plus sector partition function is:

$$\begin{aligned} \mathcal{Z}_{2,k=2}^{\text{Sp},+} &= \lim_{\epsilon_2 \rightarrow -\epsilon_1} \sum_{i=1}^5 \frac{\mathcal{J}(\pm v_i | \{(1,1)\}_i)}{\text{sh}(v_i \pm v_i - \epsilon_{12}) \prod_{j \neq i}^5 \text{sh}(\pm v_i - v_j)} \\ &= \lim_{\epsilon_2 \rightarrow -\epsilon_1} \left(-\frac{1}{\text{sh}(2v_1 \pm \epsilon_1) \text{sh}(2v_1 + \epsilon_{12}) \text{sh}(\epsilon_{12}) \text{sh}(2v_1 - \epsilon_{12})^2} \right. \\ &\quad + \frac{1}{2 \text{sh}(v_1 \pm \frac{\epsilon_1}{2}) \text{sh}(v_1 - \epsilon_{12} \pm \frac{\epsilon_1}{2}) \text{sh}(2\epsilon_1)^2 \text{sh}(\epsilon_2)^2} \\ &\quad + \frac{\text{sh}(v_1 \pm \frac{\epsilon_1}{2}) \text{sh}(v_1 - \epsilon_{12} \pm \frac{\epsilon_1}{2})}{2 \text{sh}(2v_1 \pm \epsilon_1) \text{sh}(2v_1 - 2\epsilon_{12} \pm \epsilon_1) \text{sh}(2\epsilon_1)^2 \text{sh}(\epsilon_2)^2} \\ &\quad - \frac{\text{sh}(\epsilon_{12}^2)}{2 \text{sh}(v_1 \pm \frac{\epsilon_{12}}{2}) \text{sh}(v_1 - \epsilon_{12} \pm \frac{\epsilon_{12}}{2}) \text{sh}(\epsilon_1) \text{sh}(\epsilon_2)^2 \text{sh}(2\epsilon_1 + \epsilon_2)^2 \text{sh}(\epsilon_1 + 2\epsilon_2)} \\ &\quad - \frac{\text{sh}(\epsilon_{12})^2 \text{sh}(v_1 \pm \frac{\epsilon_{12}}{2}) \text{sh}(v_1 - \epsilon_{12} \pm \frac{\epsilon_{12}}{2})}{2 \text{sh}(2v_1 \pm \epsilon_{12}) \text{sh}(2v_1 - 2\epsilon_{12} \pm \epsilon_{12}) \text{sh}(\epsilon_1) \text{sh}(\epsilon_2)^2 \text{sh}(\epsilon_1 + 2\epsilon_2) \text{sh}(2\epsilon_1 + \epsilon_2)^2} \Big) \\ &= \frac{1}{\text{sh}(2v_1)^2 \text{sh}(2v_1 \pm \epsilon_1)^2 \text{sh}(\epsilon_1)^2} + \frac{1}{2 \text{sh}(v_1 \pm \frac{\epsilon_1}{2})^2 \text{sh}(\epsilon_1)^2 \text{sh}(2\epsilon_1)^2} + \frac{\text{sh}(v_1 \pm \frac{\epsilon_1}{2})^2}{2 \text{sh}(2v_1 \pm \epsilon_1)^2 \text{sh}(\epsilon_1)^2 \text{sh}(2\epsilon_1)^2} \end{aligned} \quad (\text{C.5})$$

Here, at the first equality, we have used $\mathcal{J}(x|\emptyset_\alpha) = 1/\text{sh}(x - v_\alpha)$. At the second equality, we substituted the specific values of the frozen branes as Tab. 2. Therefore, the complete partition function for the $\text{Sp}(2)$ $k = 2$ theory is given by:

$$\begin{aligned} \mathcal{Z}_{2,k=2}^{\text{Sp}} &= \frac{1}{\text{sh}(2v_1)^2 \text{sh}(2v_1 \pm \epsilon_1)^2 \text{sh}(\epsilon_1)^2} + \frac{1}{2 \text{sh}(v_1 \pm \frac{\epsilon_1}{2})^2 \text{sh}(\epsilon_1)^2 \text{sh}(2\epsilon_1)^2} \\ &\quad + \frac{\text{sh}(v_1 \pm \frac{\epsilon_1}{2})^2}{2 \text{sh}(2v_1 \pm \epsilon_1)^2 \text{sh}(\epsilon_1)^2 \text{sh}(2\epsilon_1)^2} - \frac{1}{\text{sh}(2v_1)^2 \text{sh}(\epsilon_1)^2 \text{sh}(2\epsilon_1)^2} \end{aligned} \quad (\text{C.6})$$

- To illustrate the emergence of BPS jumping coefficients (3.18), we consider the first non-trivial Young diagram configuration as $\vec{\lambda} = (\emptyset_1, \lambda_2, \emptyset_3, \emptyset_4, \emptyset_5)$, where the only non-empty Young diagram λ_2 is:

$$\lambda_2 = \{(1,1), (1,2), (1,3), (2,1), (3,1), (2,2)\} \quad (\text{C.7})$$

The corresponding \mathcal{J} -factor is given by:

$$\mathcal{J}(x|\lambda_2) = \frac{\operatorname{sh}(x - v_2 - \epsilon_1 - 3\epsilon_2) \operatorname{sh}(x - v_2 - 2\epsilon_{12}) \operatorname{sh}(x - v_2 - 3\epsilon_1 - \epsilon_2)}{\operatorname{sh}(x - v_2 - 3\epsilon_{1,2}) \operatorname{sh}(x - v_2 - \epsilon_1 - 2\epsilon_2) \operatorname{sh}(x - v_2 - 2\epsilon_1 - \epsilon_2)} \quad (\text{C.8})$$

The corresponding contribution of $\vec{\lambda}$ is then:

$$\mathcal{Z}^{\text{Sp},+}(\vec{\lambda}) \propto \lim_{\epsilon_2 \rightarrow -\epsilon_1} \frac{\operatorname{sh}(\epsilon_{12})^3}{2 \operatorname{sh}(2\epsilon_{12})^2 \operatorname{sh}(3\epsilon_{12})} = \frac{1}{24} \quad (\text{C.9})$$

Therefore, the term in $\mathcal{Z}^{\text{Sp},+}$ corresponds to $\vec{\lambda}$ at unrefined limit contains an extra coefficient $\frac{1}{24}$. Indeed, the exact result is:

$$\begin{aligned} \mathcal{Z}^{\text{Sp},+}(\vec{\lambda}) &= \frac{1}{24 \operatorname{sh}(\epsilon_1)^2 \operatorname{sh}(2\epsilon_1)^4 \operatorname{sh}(3\epsilon_1)^6 \operatorname{sh}(4\epsilon_1)^6 \operatorname{sh}(5\epsilon_1)^5 \operatorname{sh}(6\epsilon_1)^2} \\ &\times \frac{1}{\operatorname{sh}(v_1 \pm \frac{5}{2}\epsilon_1)^2 \operatorname{sh}(v_1 \pm \frac{3}{2}\epsilon_1)^4 \operatorname{sh}(v_1 \pm \frac{1}{2}\epsilon_1)^6} \end{aligned} \quad (\text{C.10})$$

By comparing the Eq.(2.12) of [10], the expression for the $\text{Sp}(2)$ plus sector with the configuration $\vec{\lambda} = (\emptyset_1, \lambda_2, \emptyset_3, \emptyset_4, \emptyset_5)$, is given by:

$$\begin{aligned} \mathcal{Z}^{\text{Sp},+}(\vec{\lambda}) &= C_{\vec{\lambda}, \mathbf{v}}^{\text{Sp}} \times \frac{1}{64 \operatorname{sh}(\epsilon_1)^2 \operatorname{sh}(2\epsilon_1)^4 \operatorname{sh}(3\epsilon_1)^6 \operatorname{sh}(4\epsilon_1)^6 \operatorname{sh}(5\epsilon_1)^5 \operatorname{sh}(6\epsilon_1)^2} \\ &\times \frac{1}{\operatorname{sh}(v_1 \pm \frac{5}{2}\epsilon_1)^2 \operatorname{sh}(v_1 \pm \frac{3}{2}\epsilon_1)^4 \operatorname{sh}(v_1 \pm \frac{1}{2}\epsilon_1)^6} \end{aligned} \quad (\text{C.11})$$

In this configuration, the number of diagonal boxes in λ_2 is $j = 2$. Hence, by (3.18), the coefficient $C_{\vec{\lambda}, \mathbf{v}}^{\text{Sp}}$ reads:

$$C_{\vec{\lambda}, \mathbf{v}}^{\text{Sp}} = C_{\emptyset, \frac{\epsilon_1}{2}}^{\text{Sp}} C_{\lambda_2, \frac{\epsilon_1}{2} + \pi i}^{\text{Sp}} C_{\emptyset, 0}^{\text{Sp}} C_{\emptyset, \pi i}^{\text{Sp}} = \frac{2^{2j-1}}{\binom{2j-1}{j-1}} = \frac{8}{3} \quad (\text{C.12})$$

Thus, the factor $\frac{1}{64}$ contained in (C.11), combined with the prefactor $C_{\vec{\lambda}, \mathbf{v}}^{\text{Sp}} = \frac{8}{3}$, yields the complete coefficient $\frac{1}{24}$, which matches exactly the result in (C.10). This example demonstrates that, through careful implementation of the limiting procedure $\lim_{\epsilon_2 \rightarrow -\epsilon_1}$, the coefficient $C_{\vec{\lambda}, \mathbf{v}}^{\text{Sp}}$ can be fully absorbed into the shell formula.

C.2 D0-D6 partition function

For brevity, in this appendix, we will consider a system containing only a single D6-brane and compute the explicit values of the first two instanton contributions as well as their ratio.

- For a D0-D6 $_{\bar{4}}$ system at the level $k = 1$, the partition function (4.15) involves only a first-order contour integral. In the case of a single D6-brane, we need only consider the unique 3d Young diagram configuration $\vec{\pi} = (\{(1, 1, 1)\})$. We begin by computing its corresponding shellboxes and their associated charges as Tab. 7.

Q = +1	(1, 2, 2)	(2, 1, 2)	(2, 2, 1)
Q = -1	(1, 1, 2)	(1, 2, 1)	(2, 1, 1)

Table 7. The charges of the shellboxes of the 3d Young diagram $\{(1, 1, 1)\}$. The second column displays the coordinates of each shellbox.

Therefore the \mathcal{J} -factor of $\{(1, 1, 1)\}$ is:

$$\mathcal{J}(x|\{(1, 1, 1)\}_{\bar{4}, 1}) = \frac{\operatorname{sh}(x - v_{\bar{4}, 1} - \epsilon_{12}) \operatorname{sh}(x - v_{\bar{4}, 1} - \epsilon_{13}) \operatorname{sh}(x - v_{\bar{4}, 1} - \epsilon_{23})}{\operatorname{sh}(x - v_{\bar{4}, 1} - \epsilon_{1, 2, 3}) \operatorname{sh}(x - v_{\bar{4}, 1} - \epsilon_{123})} \quad (\text{C.13})$$

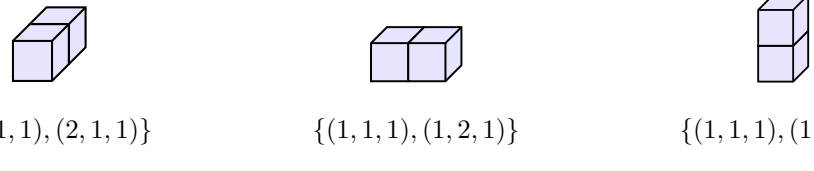
The partition function (4.16) becomes:

$$\begin{aligned} \mathcal{Z}_{(1, 0, 0, 0), k=1}^{\text{D0-D6}} &= \operatorname{sh}(\mathcal{X}_{\bar{4}, 1}(1, 1, 1) - \mathcal{X}_{\bar{4}, 1}(0, 0, 0)) \mathcal{J}(\mathcal{X}_{\bar{4}, 1}(1, 1, 1) | \{(1, 1, 1)\}_{\bar{4}, 1}) \\ &= -\frac{\operatorname{sh}(\epsilon_{12}) \operatorname{sh}(\epsilon_{13}) \operatorname{sh}(\epsilon_{23})}{\operatorname{sh}(\epsilon_1) \operatorname{sh}(\epsilon_2) \operatorname{sh}(\epsilon_3)} \end{aligned} \quad (\text{C.14})$$

We can also impose the CY threefold condition $\epsilon_{123} = 0$ [72]. Under this condition, the $k = 1$ partition function reduces to 1, which corresponds precisely to the MacMahon function at first order of \mathbf{q} :

$$\prod_{k=1}^{\infty} \frac{1}{(1 - \mathbf{q}^k)^k} = 1 + \mathbf{q} + 3\mathbf{q}^2 + 6\mathbf{q}^3 + 13\mathbf{q}^4 + \dots \quad (\text{C.15})$$

- At the level $k = 2$, there are 3 3d Young diagram configurations:



Let us focus on the configuration $\{(1, 1, 1), (1, 1, 2)\}$, the charges of the shellboxes are listed in Tab. 8.

$Q = +1$	$(1, 2, 3)$	$(2, 1, 3)$	$(2, 2, 1)$	
$Q = -1$	$(1, 1, 3)$	$(1, 2, 1)$	$(2, 1, 1)$	$(2, 2, 3)$

Table 8. The charges of the shellboxes of the 3d Young diagram $\{(1, 1, 1), (1, 1, 2)\}$. The second column displays the coordinates of each shellbox.

Therefore the corresponding \mathcal{J} -factor is:

$$\mathcal{J}(x|\{(1, 1, 1), (1, 1, 2)\}_{\bar{4}, 1}) = \frac{\operatorname{sh}(x - v_{\bar{4}, 1} - \epsilon_{12}) \operatorname{sh}(x - v_{\bar{4}, 1} - \epsilon_1 - 2\epsilon_3) \operatorname{sh}(x - v_{\bar{4}, 1} - \epsilon_2 - 2\epsilon_3)}{\operatorname{sh}(x - v_{\bar{4}, 1} - \epsilon_{1, 2}) \operatorname{sh}(x - v_{\bar{4}, 1} - 2\epsilon_3) \operatorname{sh}(x - v_{\bar{4}, 1} - \epsilon_{12} - 2\epsilon_3)} \quad (\text{C.16})$$

And the contribution from $\{(1, 1, 1), (1, 1, 2)\}$ is:

$$\mathcal{Z}_{(1, 0, 0, 0)}^{\text{D0-D6}}(\{(1, 1, 1), (1, 1, 2)\}_{\bar{4}, 1}) = \frac{\operatorname{sh}(\epsilon_{12}) \operatorname{sh}(\epsilon_{13}) \operatorname{sh}(\epsilon_{23}) \operatorname{sh}(\epsilon_{12} - \epsilon_3) \operatorname{sh}(\epsilon_1 + 2\epsilon_3) \operatorname{sh}(\epsilon_2 + 2\epsilon_3)}{\operatorname{sh}(\epsilon_1) \operatorname{sh}(\epsilon_2) \operatorname{sh}(\epsilon_3) \operatorname{sh}(2\epsilon_3) \operatorname{sh}(\epsilon_1 - \epsilon_3) \operatorname{sh}(\epsilon_2 - \epsilon_3)} \quad (\text{C.17})$$

Here, we can use the symmetry among ϵ_1 , ϵ_2 , and ϵ_3 to directly obtain the contributions from the other two Young diagram configurations $\{(1, 1, 1), (2, 1, 1)\}$ and $\{(1, 1, 1), (1, 2, 1)\}$. When the CY3 condition $\epsilon_{123} = 0$ is imposed, each term reduces to 1, resulting in a total contribution of $\mathcal{Z}_{(1, 0, 0, 0), k=2}^{\text{D0-D6}} = 3$, which matches the second-order coefficient of the MacMahon function (C.15).

- We can compare the contribution ratio between the $\{(1, 1, 1)\}$ and $\{(1, 1, 1), (1, 1, 2)\}$ configurations:

$$\frac{\mathcal{Z}^{\text{D0-D6}}(\{(1, 1, 1), (1, 1, 2)\}_{\bar{4}, 1})}{\mathcal{Z}^{\text{D0-D6}}(\{(1, 1, 1)\}_{\bar{4}, 1})} = -\frac{\text{sh}(\epsilon_{12} - \epsilon_3) \text{sh}(\epsilon_1 + 2\epsilon_3) \text{sh}(\epsilon_2 + 2\epsilon_3)}{\text{sh}(\epsilon_1 - \epsilon_3) \text{sh}(\epsilon_2 - \epsilon_3) \text{sh}(2\epsilon_3)} \quad (\text{C.18})$$

And we can computationally verify the recursion relation (4.17):

$$\begin{aligned} \mathcal{J}(\mathcal{X}_{\bar{4}, 1}(1, 1, 2) | \{(1, 1, 1), (1, 1, 2)\}_{\bar{4}, 1}) &= -\frac{\text{sh}(\epsilon_{13}) \text{sh}(\epsilon_{23}) \text{sh}(\epsilon_{12} - \epsilon_3)}{\text{sh}(\epsilon_3) \text{sh}(\epsilon_{123}) \text{sh}(\epsilon_1 - \epsilon_3) \text{sh}(\epsilon_2 - \epsilon_3)} \\ \mathcal{J}(\mathcal{X}_{\bar{4}, 1}(2, 2, 3) | \{(1, 1, 1)\}_{\bar{4}, 1}) &= \frac{\text{sh}(2\epsilon_3) \text{sh}(\epsilon_{13}) \text{sh}(\epsilon_{23})}{\text{sh}(\epsilon_3) \text{sh}(\epsilon_{123}) \text{sh}(\epsilon_1 + 2\epsilon_3) \text{sh}(\epsilon_2 + 2\epsilon_3)} \end{aligned} \quad (\text{C.19})$$

Thus, one can simply check:

$$\frac{\mathcal{Z}^{\text{D0-D6}}(\{(1, 1, 1), (1, 1, 2)\}_{\bar{4}, 1})}{\mathcal{Z}^{\text{D0-D6}}(\{(1, 1, 1)\}_{\bar{4}, 1})} = \frac{\mathcal{J}(\mathcal{X}_{\bar{4}, 1}(1, 1, 2) | \{(1, 1, 1), (1, 1, 2)\}_{\bar{4}, 1})}{\mathcal{J}(\mathcal{X}_{\bar{4}, 1}(2, 2, 3) | \{(1, 1, 1)\}_{\bar{4}, 1})} \quad (\text{C.20})$$

C.3 DT counting

In this appendix, we present example calculations for DT counting, including the 1-leg case with a derivation of the partition function (4.27), as well as an example for the 3-leg case. Consistent with the main text, since there is only a single D6-brane, we omit the Young diagram label $(123, 1)$.

- First, we can consider the partition function of three D2₁-branes inside a D6₁₂₃-brane. The vacuum configuration for this system, as shown in Fig. 17, corresponds to a minimal 3d Young diagram $\pi_{\lambda \emptyset \emptyset}$ extending infinitely in the \mathbb{C}_1 direction with boundary condition being a 2d Young diagram $\lambda_{23, 1} = \{(1, 1), (1, 2), (2, 1)\}$. The charges of the shellboxes of $\pi_{\lambda \emptyset \emptyset}$ is listed

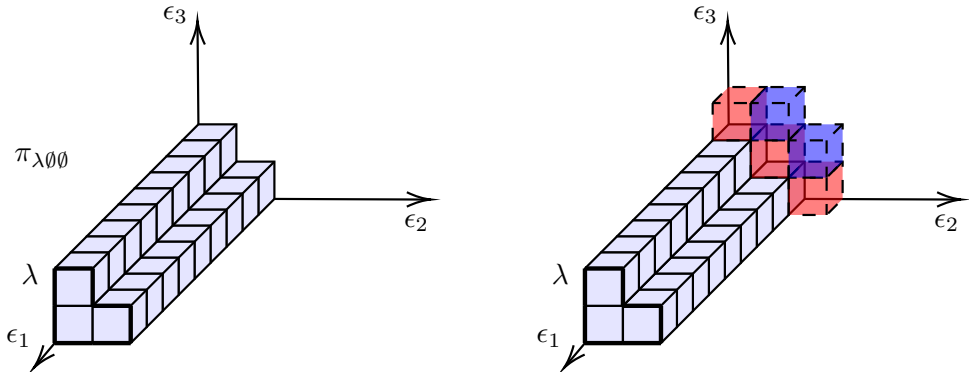


Figure 17. The left figure shows a one-leg 3d Young diagram $\pi_{\lambda \emptyset \emptyset}$ with boundaries, where the boundary in the ϵ_1 direction is a 2d Young diagram λ in the 23-plane, and the boundaries in the other two directions are empty sets \emptyset . The right figure shows the shellboxes with non-zero charges for $\pi_{\lambda \emptyset \emptyset}$, where red represents -1 charge and blue represents $+1$ charge. Note that the contributions from all shellboxes at the infinite boundary are canceled out; therefore, only the finite-distance shellboxes provide non-trivial contributions to the partition function.

in Tab. 9.

As (4.25) mentioned, the contribution to the \mathcal{J} -factor from the shellboxes at the infinite end reads:

$$\frac{\text{sh}(x - \infty\epsilon_1 - 2\epsilon_3) \text{sh}(x - \infty\epsilon_1 - \epsilon_{23}) \text{sh}(x - \infty\epsilon_1 - 2\epsilon_2)}{\text{sh}(x - \infty\epsilon_1) \text{sh}(x - \infty\epsilon_1 - \epsilon_2 - 2\epsilon_3) \text{sh}(x - \infty\epsilon_1 - 2\epsilon_2 - \epsilon_3)} = 1 \quad (\text{C.21})$$

Q = +1	(1, 2, 3)	(1, 3, 2)	(∞ , 1, 3)	(∞ , 2, 2)	(∞ , 3, 1)
Q = -1	(1, 1, 3)	(1, 2, 2)	(1, 3, 1)	(∞ , 1, 1)	(∞ , 2, 3)

Table 9. The charges of the shellboxes of the 3d Young diagram $\pi_{\lambda\emptyset\emptyset}$.

Therefore, the complete \mathcal{J} -factor as (4.26) is:

$$\begin{aligned}\mathcal{J}(x|\pi_{\lambda\emptyset\emptyset}) &= \frac{\text{sh}(x-v-\epsilon_2-2\epsilon_3)\text{sh}(x-v-2\epsilon_2-\epsilon_3)}{\text{sh}(x-v-2\epsilon_2)\text{sh}(x-v-2\epsilon_3)\text{sh}(x-v-\epsilon_{23})} \\ &= \mathcal{J}(x+v_{23,1}-v|\lambda_{23,1})\end{aligned}\quad (\text{C.22})$$

The partition function before integration reads:

$$\mathcal{I}_{\lambda,\emptyset,\emptyset;k}^{\text{D0-D2-D6}} = (-1)^k \mathcal{I}_k^{\text{D0-D0}} \times \prod_{i=1}^k \frac{\text{sh}(\phi_i-v-\epsilon_{234})}{\text{sh}(\phi_i-v-\epsilon_{23})} \frac{\text{sh}(\phi_i-v-2\epsilon_{2,3}-\epsilon_4)}{\text{sh}(\phi_i-v-2\epsilon_{2,3})} \frac{\text{sh}(-\phi_i+v+\epsilon_{2,3}-\epsilon_{14})}{\text{sh}(-\phi_i+v+\epsilon_{2,3}-\epsilon_1)} \quad (\text{C.23})$$

For the vacuum configuration $\pi_{\lambda\emptyset\emptyset}$ at $k=1$, there are three poles, which correspond to three distinct box locations:

$$\tilde{\pi}_{\lambda\emptyset\emptyset} = \pi \setminus \pi_{\lambda\emptyset\emptyset} = \{(1, 2, 2)\}, \quad \{(1, 3, 1)\}, \text{ and } \{(1, 1, 3)\} \quad (\text{C.24})$$

where $|\tilde{\pi}_{\lambda\emptyset\emptyset}| = k = 1$. Using (4.27), the partition functions read:

$$\begin{aligned}\mathcal{Z}_{\lambda,\emptyset,\emptyset}^{\text{D0-D2-D6}}(1, 2, 2) &= \frac{\text{sh}(\epsilon_{23})\text{sh}(\epsilon_1+2\epsilon_{2,3})}{\text{sh}(\epsilon_1)\text{sh}(\epsilon_2-\epsilon_3)^2} \\ \mathcal{Z}_{\lambda,\emptyset,\emptyset}^{\text{D0-D2-D6}}(1, 3, 1) &= \frac{\text{sh}(\epsilon_{13})\text{sh}(\epsilon_{23})\text{sh}(\epsilon_1+2\epsilon_2)\text{sh}(\epsilon_2-2\epsilon_3)\text{sh}(\epsilon_1+3\epsilon_2-\epsilon_3)}{\text{sh}(\epsilon_{1,2})\text{sh}(\epsilon_2-\epsilon_3)\text{sh}(2\epsilon_2-2\epsilon_3)\text{sh}(\epsilon_1+2\epsilon_2-\epsilon_3)} \\ \mathcal{Z}_{\lambda,\emptyset,\emptyset}^{\text{D0-D2-D6}}(1, 1, 3) &= -\frac{\text{sh}(\epsilon_{12})\text{sh}(\epsilon_{23})\text{sh}(2\epsilon_2-\epsilon_3)\text{sh}(\epsilon_1+2\epsilon_3)\text{sh}(\epsilon_1-\epsilon_2+3\epsilon_3)}{\text{sh}(\epsilon_{1,3})\text{sh}(\epsilon_2-\epsilon_3)\text{sh}(2\epsilon_2-2\epsilon_3)\text{sh}(\epsilon_1-\epsilon_2+2\epsilon_3)} \\ \mathcal{Z}_{\lambda,\emptyset,\emptyset;k=1}^{\text{D0-D2-D6}} &= \mathcal{Z}_{\lambda,\emptyset,\emptyset}^{\text{D0-D2-D6}}(1, 2, 2) + \mathcal{Z}_{\lambda,\emptyset,\emptyset}^{\text{D0-D2-D6}}(1, 3, 1) + \mathcal{Z}_{\lambda,\emptyset,\emptyset}^{\text{D0-D2-D6}}(1, 1, 3)\end{aligned}\quad (\text{C.25})$$

- An equivalent derivation follows by identifying the D2-brane with an infinite row of D0-branes. Interpreted as the placement of additional boxes on a prescribed vacuum 3d Young diagram $\pi_{\lambda\emptyset\emptyset}$ with $\lambda = \{(1, 1), (1, 2), (2, 1)\}$, DT invariant allows us to apply the D0-D6 recursion relation (4.17):

$$\begin{aligned}\mathcal{Z}_{\lambda,\emptyset,\emptyset}^{\text{D0-D2-D6}}(1, 2, 2) &= \frac{\mathcal{J}(\mathcal{X}(1, 2, 2)|\pi_{\lambda\emptyset\emptyset} \cup \{(1, 2, 2)\})}{\mathcal{J}(\mathcal{X}(1, 2, 2) + \epsilon_{123}|\pi_{\lambda\emptyset\emptyset})} \\ &= \frac{\mathcal{J}(\mathcal{X}(1, 2, 2)|\pi_{\lambda\emptyset\emptyset})}{\mathcal{J}(\mathcal{X}(1, 2, 2) + \epsilon_{123}|\pi_{\lambda\emptyset\emptyset})} \text{sh}(0) \mathcal{J}(\mathcal{X}(1, 2, 2)|\{(1, 2, 2)\}) \\ &= \frac{\text{sh}(\epsilon_{23})\text{sh}(\epsilon_1+2\epsilon_{2,3})}{\text{sh}(\epsilon_1)\text{sh}(\epsilon_2-\epsilon_3)^2}\end{aligned}\quad (\text{C.26})$$

where the second equality is obtained by applying (2.17). The contributions $\mathcal{Z}_{\lambda,\emptyset,\emptyset}^{\text{D0-D2-D6}}(1, 1, 3)$ and $\mathcal{Z}_{\lambda,\emptyset,\emptyset}^{\text{D0-D2-D6}}(1, 3, 1)$ from the other two poles can be derived similarly.

We may consider more general values of k . For a given pole, it corresponds to a set $\tilde{\pi}_{\lambda\emptyset\emptyset} = \{\mathbf{x}_1, \dots, \mathbf{x}_k\}$. Assuming these boxes are arranged in an order such that each step $\pi_{\lambda\emptyset\emptyset} \cup \{\mathbf{x}_1\}$, $\pi_{\lambda\emptyset\emptyset} \cup \{\mathbf{x}_1\} \cup \{\mathbf{x}_2\}, \dots$ remains a valid 3d Young diagram, the DT invariant at each step can be computed using the recursion relation:

$$\mathcal{Z}_{\lambda,\emptyset,\emptyset}^{\text{D0-D2-D6}}(x_1, x_2, \dots, x_k) = \frac{\mathcal{J}(\mathcal{X}(x_1)|\pi_{\lambda\emptyset\emptyset} \cup \{x_1\})}{\mathcal{J}(\mathcal{X}(x_1) + \epsilon_{123}|\pi_{\lambda\emptyset\emptyset})} \frac{\mathcal{J}(\mathcal{X}(x_2)|\pi_{\lambda\emptyset\emptyset} \cup \{x_1\} \cup \{x_2\})}{\mathcal{J}(\mathcal{X}(x_2) + \epsilon_{123}|\pi_{\lambda\emptyset\emptyset} \cup \{x_1\})} \times \dots$$

$$\begin{aligned}
&= \left(\prod_{i=1}^k \frac{\mathcal{J}(\mathcal{X}(\mathbf{x}_i) | \pi_{\lambda \emptyset \emptyset})}{\mathcal{J}(\mathcal{X}(\mathbf{x}_i) + \epsilon_{123} | \pi_{\lambda \emptyset \emptyset})} \right) \left(\prod_{i,j}^k \text{sh}(\mathcal{X}(\mathbf{x}_i) - \mathcal{X}(\mathbf{x}_j)) \mathcal{J}(\mathcal{X}(\mathbf{x}_i) | \mathbf{x}_j) \right) \\
&= \left(\prod_{i=1}^k \frac{\mathcal{J}(\mathcal{X}(\mathbf{x}_i) | \pi_{\lambda \emptyset \emptyset})}{\mathcal{J}(\mathcal{X}(\mathbf{x}_i) + \epsilon_{123} | \pi_{\lambda \emptyset \emptyset})} \right) \\
&\quad \times \left(\prod_{i,j}^k \frac{\text{sh}(\mathcal{X}(\mathbf{x}_i) - \mathcal{X}(\mathbf{x}_j)) \text{sh}(\mathcal{X}(\mathbf{x}_i) - \mathcal{X}(\mathbf{x}_j) - \epsilon_{12,13,23})}{\text{sh}(\mathcal{X}(\mathbf{x}_i) - \mathcal{X}(\mathbf{x}_j) - \epsilon_{1,2,3}) \text{sh}(\mathcal{X}(\mathbf{x}_i) - \mathcal{X}(\mathbf{x}_j) - \epsilon_{123})} \right) \quad (\text{C.27})
\end{aligned}$$

where in the second line, we have used the splitting (2.17) and swapping (2.11) properties. Note that in the second line, although $\text{sh}(0)$ appears when $i = j$, the overall value remains finite.

Thus, by substituting the integration variables ϕ_i back for $\mathcal{X}(\mathbf{x}_i)$ and, in order to obtain the correct pole structure, replacing the \mathcal{J} -factor in the denominator with \mathcal{J}_- , we arrive at the integral form of the DT invariant given in (4.27).

- We now consider the simplest 3-leg case: $\pi_{\lambda \lambda \lambda}$ as shown in Fig. 18, where λ is a Young diagram containing only one box, i.e., $\lambda = \{(1, 1)\}$. Using (4.24), we obtain the corresponding \mathcal{J} -factor:

$$\begin{aligned}
\mathcal{J}(x | \pi_{\lambda \lambda \lambda}) &= \frac{\mathcal{J}(x | \pi_{\lambda \emptyset \emptyset}) \mathcal{J}(x | \pi_{\emptyset \lambda \emptyset}) \mathcal{J}(x | \pi_{\emptyset \emptyset \lambda}) \mathcal{J}(x | \pi_{\lambda \emptyset \emptyset} \cap \pi_{\emptyset \lambda \emptyset} \cap \pi_{\emptyset \emptyset \lambda})}{\mathcal{J}(x | \pi_{\lambda \emptyset \emptyset} \cap \pi_{\emptyset \lambda \emptyset}) \mathcal{J}(x | \pi_{\lambda \emptyset \emptyset} \cap \pi_{\emptyset \emptyset \lambda}) \mathcal{J}(x | \pi_{\emptyset \lambda \emptyset} \cap \pi_{\emptyset \emptyset \lambda})} \\
&= \frac{\text{sh}(x - v - \epsilon_{123})^2}{\text{sh}(x - v - \epsilon_{12}) \text{sh}(x - v - \epsilon_{13}) \text{sh}(x - v - \epsilon_{23})} \quad (\text{C.28})
\end{aligned}$$

where in this configuration:

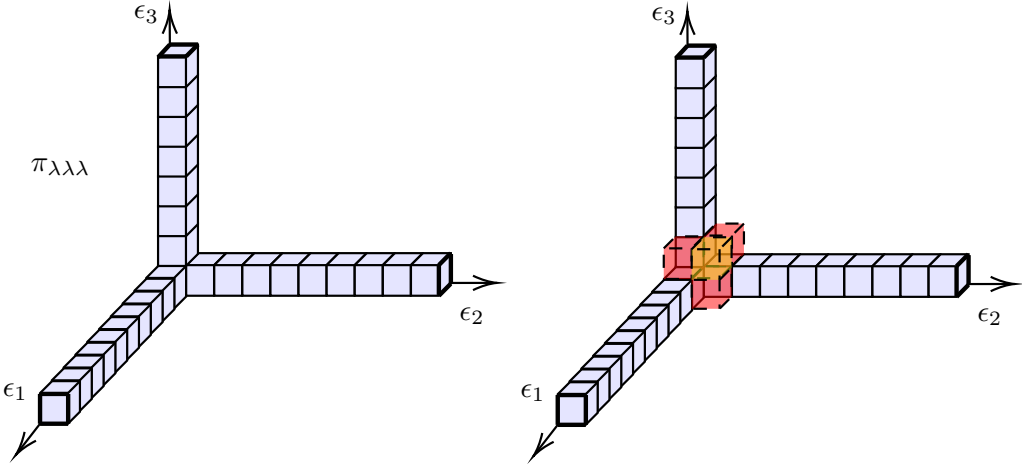


Figure 18. The left image shows the 3d Young diagram $\pi_{\lambda \lambda \lambda}$ corresponding to the vacuum configuration $(\lambda, \lambda, \lambda)$, where $\lambda = \{(1, 1)\}$ is a 2d Young diagram with a single box. The right image displays the shellboxes with non-trivial charges: red boxes carry charge -1 , and yellow boxes carry charge $+2$.

$$\pi_{\lambda \emptyset \emptyset} \cap \pi_{\emptyset \lambda \emptyset} \cap \pi_{\emptyset \emptyset \lambda} = \pi_{\lambda \emptyset \emptyset} \cap \pi_{\emptyset \emptyset \lambda} = \pi_{\lambda \emptyset \emptyset} \cap \pi_{\emptyset \lambda \emptyset} = \pi_{\emptyset \lambda \emptyset} \cap \pi_{\emptyset \emptyset \lambda} = \pi_{\emptyset \emptyset \lambda} \cap \pi_{\emptyset \lambda \emptyset} = \{(1, 1, 1)\} \quad (\text{C.29})$$

Therefore the integrand is:

$$\mathcal{I}_{\lambda, \lambda, \lambda; k}^{\text{D0-D2-D6}} = (-1)^k \mathcal{I}_k^{\text{D0-D0}} \times \prod_{i=1}^k \frac{\text{sh}(v - \epsilon_{1,2,3} - \phi_i) \text{sh}(\phi_i - v - \epsilon_{123})^2}{\text{sh}(\phi_i - v - \epsilon_{12,13,23}) \text{sh}(v - \phi_i)^2} \quad (\text{C.30})$$

After applying the JK-residue, the integral possesses three poles $\mathcal{X}(1, 2, 2)$, $\mathcal{X}(2, 1, 2)$, and $\mathcal{X}(2, 2, 1)$, whose corresponding evaluation yields:

$$\begin{aligned}\mathcal{Z}_{\lambda, \lambda, \lambda}^{\text{D0-D2-D6}}(1, 2, 2) &= - \frac{\text{sh}(\epsilon_1) \text{sh}(\epsilon_{12}) \text{sh}(\epsilon_{13}) \text{sh}(2\epsilon_2 + \epsilon_3) \text{sh}(\epsilon_2 + 2\epsilon_3)}{\text{sh}(\epsilon_{2,3}) \text{sh}(\epsilon_{23}) \text{sh}(\epsilon_1 - \epsilon_2) \text{sh}(\epsilon_1 - \epsilon_3)} \\ \mathcal{Z}_{\lambda, \lambda, \lambda}^{\text{D0-D2-D6}}(2, 1, 2) &= \frac{\text{sh}(\epsilon_2) \text{sh}(\epsilon_{12}) \text{sh}(\epsilon_{23}) \text{sh}(2\epsilon_1 + \epsilon_3) \text{sh}(\epsilon_1 + 2\epsilon_3)}{\text{sh}(\epsilon_{1,3}) \text{sh}(\epsilon_{13}) \text{sh}(\epsilon_1 - \epsilon_2) \text{sh}(\epsilon_2 - \epsilon_3)} \\ \mathcal{Z}_{\lambda, \lambda, \lambda}^{\text{D0-D2-D6}}(2, 2, 1) &= - \frac{\text{sh}(\epsilon_3) \text{sh}(\epsilon_{13}) \text{sh}(\epsilon_{23}) \text{sh}(2\epsilon_1 + \epsilon_2) \text{sh}(\epsilon_1 + 2\epsilon_2)}{\text{sh}(\epsilon_{1,2}) \text{sh}(\epsilon_{12}) \text{sh}(\epsilon_1 - \epsilon_3) \text{sh}(\epsilon_2 - \epsilon_3)}\end{aligned}\quad (\text{C.31})$$

For the 2-leg case, it suffices to note that its computation proceeds analogously to the 1-leg and 3-leg cases. Its \mathcal{J} -factor is given by:

$$\begin{aligned}\mathcal{J}(x|\pi_{\lambda\mu\emptyset}) &= \frac{\mathcal{J}(x|\pi_{\lambda\emptyset\emptyset})\mathcal{J}(x|\pi_{\emptyset\mu\emptyset})\mathcal{J}(x|\pi_{\lambda\emptyset\emptyset} \cap \pi_{\emptyset\mu\emptyset} \cap \pi_{\emptyset\emptyset\emptyset})}{\mathcal{J}(x|\pi_{\lambda\emptyset\emptyset} \cap \pi_{\emptyset\mu\emptyset})\mathcal{J}(x|\pi_{\lambda\emptyset\emptyset} \cap \pi_{\emptyset\emptyset\emptyset})\mathcal{J}(x|\pi_{\emptyset\mu\emptyset} \cap \pi_{\emptyset\emptyset\emptyset})} \\ &= \frac{\mathcal{J}(x|\pi_{\lambda\emptyset\emptyset})\mathcal{J}(x|\pi_{\emptyset\mu\emptyset})}{\mathcal{J}(x|\pi_{\lambda\emptyset\emptyset} \cap \pi_{\emptyset\mu\emptyset})}\end{aligned}\quad (\text{C.32})$$

C.4 D0-D8 partition function

In this appendix, we compute the one and two D0-branes contributions in the presence of a single D8-brane to explicitly demonstrate the computational procedure of the modified \mathcal{J} -factor (4.5). And, by considering the $k = 2$ case, elucidate the origin of the sign rule introduced in [32].

- For $N = 1$, the charges and shellboxes corresponds to 4d Young diagram with one box: $\{(1, 1, 1, 1)\}$ is listed in Tab. 10.

$Q = +1$	(1, 1, 2, 2)	(1, 2, 1, 2)	(1, 2, 2, 1)	(2, 1, 1, 2)
	(2, 1, 2, 1)	(2, 2, 1, 1)	(2, 2, 2, 2)	
$Q = -1$	(1, 1, 1, 2)	(1, 1, 2, 1)	(1, 2, 1, 1)	(1, 2, 2, 2)
	(2, 1, 1, 1)	(2, 1, 2, 2)	(2, 2, 1, 2)	(2, 2, 2, 1)

Table 10. The charges of the shellboxes of the 4d Young diagram $\{(1, 1, 1, 1)\}$. The second column displays the coordinates of each shellbox.

By the definition of \mathcal{J}_{\geq} (4.5), if the input is $\mathcal{X}_{\underline{4},1}(1, 1, 1, 1)$, then we only pick the shellboxes with the last coordinates $x_4 \leq 1$. Therefore, the shellboxes reduce to:

$Q = +1$	(1, 2, 2, 1)	(2, 1, 2, 1)	(2, 2, 1, 1)
$Q = -1$	(1, 1, 2, 1)	(1, 2, 1, 1)	(2, 1, 1, 1)

Table 11. The charges of the shellboxes of the 4d Young diagram $\{(1, 1, 1, 1)\}$ when the input of \mathcal{J}_{\geq} is $\mathcal{X}_{\underline{4},\alpha}(x_1, x_2, x_3, 1)$. The second column displays the coordinates of each shellbox.

Thus, we have:

$$\begin{aligned}\mathcal{Z}_{N=1, k=1}^{\text{D0-D8}} &= \mathcal{Z}^{\text{D0-D8}}(\{(1, 1, 1, 1)\}) = \mathcal{J}_{\geq}(\mathcal{X}_{\underline{4},1}(1, 1, 1, 1) | \{(1, 1, 1, 1)\}_{\underline{4},1}) \\ &= - \frac{\text{sh}(\epsilon_{12}) \text{sh}(\epsilon_{13}) \text{sh}(\epsilon_{23})}{\text{sh}(\epsilon_{1,2,3}) \text{sh}(\epsilon_{123})}\end{aligned}\quad (\text{C.33})$$

- Consider the partition function $\mathcal{Z}^{\text{D0-D8}}(\rho_{\underline{4},1})$ corresponds to $\rho_{\underline{4},1} = \{(1, 1, 1, 1), (2, 1, 1, 1)\}_{\underline{4},1}$, since the fourth coordinates of all the boxes are 1, we only need to consider the shellboxes with $x_4 \leq 1$ as Tab. 12.

Q = +1	(1, 2, 2, 1)	(3, 1, 2, 1)	(3, 2, 1, 1)
Q = -1	(1, 1, 2, 1)	(1, 2, 1, 1)	(3, 1, 1, 1) (3, 2, 2, 1)

Table 12. The charges of the shellboxes of the 4d Young diagram $\{(1, 1, 1, 1), (2, 1, 1, 1)\}$ when the input of \mathcal{J}_\geq is $\mathcal{X}_{\underline{4},\alpha}(x_1, x_2, x_3, 1)$. The second column displays the coordinates of each shellbox.

Therefore, we have:

$$\begin{aligned} \mathcal{Z}^{\text{D0-D8}}(\{(1, 1, 1, 1), (2, 1, 1, 1)\}_{\underline{4},1}) &= - \frac{\text{sh}(2\epsilon_1 + \epsilon_2) \text{sh}(2\epsilon_1 + \epsilon_3) \text{sh}(\epsilon_{23})}{\text{sh}(2\epsilon_1) \text{sh}(\epsilon_2) \text{sh}(\epsilon_3) \text{sh}(2\epsilon_1 + \epsilon_{23})} \\ &\quad \times \frac{\text{sh}(\epsilon_{12}) \text{sh}(\epsilon_1 - \epsilon_{23}) \text{sh}(\epsilon_{13})}{\text{sh}(\epsilon_1) \text{sh}(\epsilon_1 - \epsilon_2) \text{sh}(\epsilon_1 - \epsilon_3) \text{sh}(\epsilon_{123})} \end{aligned} \quad (\text{C.34})$$

For the other two Young diagrams $\{(1, 1, 1, 1), (1, 2, 1, 1)\}$ and $\{(1, 1, 1, 1), (1, 1, 2, 1)\}$, we can directly obtain the corresponding contributions by utilizing the symmetry of $\epsilon_1, \epsilon_2, \epsilon_3$. However, for $\{(1, 1, 1, 1), (1, 1, 1, 2)\}$, the full charges of the shellboxes are listed in Tab. 13.

Q = +1	(1, 1, 2, 3)	(1, 2, 1, 3)	(1, 2, 2, 1)	(2, 1, 1, 3)
	(2, 1, 2, 1)	(2, 2, 1, 1)	(2, 2, 2, 3)	
Q = -1	(1, 1, 1, 3)	(1, 1, 2, 1)	(1, 2, 1, 1)	(1, 2, 2, 3)
	(2, 1, 1, 1)	(2, 1, 2, 3)	(2, 2, 1, 3)	(2, 2, 2, 1)

Table 13. The charges of the shellboxes of the 4d Young diagram $\{(1, 1, 1, 1), (1, 1, 1, 2)\}$. The second column displays the coordinates of each shellbox.

Fortunately, for both inputs $\mathcal{X}_{\underline{4},\alpha}(1, 1, 1, 1)$ and $\mathcal{X}_{\underline{4},\alpha}(1, 1, 1, 2)$, the last coordinate of both boxes is less than 3. Therefore, the shellboxes actually required are the same as those shown in Tab. 11. Thus, the contribution of this Young diagram is:

$$\mathcal{Z}^{\text{D0-D8}}(\{(1, 1, 1, 1), (1, 1, 1, 2)\}_{\underline{4},1}) = \frac{\text{sh}(\epsilon_{12}) \text{sh}(\epsilon_{13}) \text{sh}(\epsilon_{23}) \text{sh}(\epsilon_{12} - \epsilon_4) \text{sh}(\epsilon_{13} - \epsilon_4) \text{sh}(\epsilon_{23} - \epsilon_4)}{\text{sh}(\epsilon_{1,2,3}) \text{sh}(\epsilon_{123})} \frac{\text{sh}(\epsilon_{1,2,3} - \epsilon_4) \text{sh}(\epsilon_{123} - \epsilon_4)}{(\text{C.35})}$$

- Next, we can verify the recursion relation (4.11) for 4d Young diagrams. For example, by comparing the contribution of $\{(1, 1, 1, 1)\}$ (C.33) with that of $\{(1, 1, 1, 1), (2, 1, 1, 1)\}$ (C.34), we have:

$$\frac{\mathcal{Z}^{\text{D0-D8}}(\{(1, 1, 1, 1), (2, 1, 1, 1)\}_{\underline{4},1})}{\mathcal{Z}^{\text{D0-D8}}(\{(1, 1, 1, 1)\}_{\underline{4},1})} = \frac{\text{sh}(2\epsilon_1 + \epsilon_2) \text{sh}(\epsilon_1 - \epsilon_2 - \epsilon_3) \text{sh}(2\epsilon_1 + \epsilon_3)}{\text{sh}(2\epsilon_1) \text{sh}(\epsilon_1 - \epsilon_2) \text{sh}(\epsilon_1 - \epsilon_3) \text{sh}(2\epsilon_1 + \epsilon_2 + \epsilon_3)} \quad (\text{C.36})$$

According to (4.11), we can obtain the $\mathcal{J}_\geq(\mathcal{X}_{\underline{4},1}(2, 1, 1, 1) | \{(1, 1, 1, 1), (2, 1, 1, 1)\}_{\underline{4},1})$ using the charges Tab. 12, and obtain the $\mathcal{J}_<(\mathcal{X}_{\underline{4},1}(2, 1, 1, 1) | \{(1, 1, 1, 1)\}_{\underline{4},1})$ using the boxes with coordinates greater than 1 in Tab. 10:

$$\begin{aligned} \mathcal{J}_\geq(\mathcal{X}_{\underline{4},1}(2, 1, 1, 1) | \{(1, 1, 1, 1), (2, 1, 1, 1)\}_{\underline{4},1}) &= \frac{\text{sh}(\epsilon_{12}) \text{sh}(\epsilon_1 - \epsilon_{23}) \text{sh}(\epsilon_{13})}{\text{sh}(\epsilon_1) \text{sh}(\epsilon_1 - \epsilon_{2,3}) \text{sh}(\epsilon_{123})} \\ \mathcal{J}_<(\mathcal{X}_{\underline{4},1}(2, 1, 1, 1) | \{(1, 1, 1, 1)\}_{\underline{4},1}) &= \frac{\text{sh}(\epsilon_1 - \epsilon_{24}) \text{sh}(\epsilon_1 - \epsilon_{34}) \text{sh}(\epsilon_4) \text{sh}(\epsilon_{234})}{\text{sh}(\epsilon_1 - \epsilon_4) \text{sh}(\epsilon_1 - \epsilon_{234}) \text{sh}(\epsilon_{24}) \text{sh}(\epsilon_{34})} \end{aligned} \quad (\text{C.37})$$

Therefore, by multiplying the two expressions and applying the CY4 condition $\epsilon_{1234} = 0$, we can verify the recursion relation of D0-D8 partition function (4.11):

$$\begin{aligned} \frac{\mathcal{Z}^{\text{D0-D8}}(\{(1, 1, 1, 1), (2, 1, 1, 1)\}_{\underline{4},1})}{\mathcal{Z}^{\text{D0-D8}}(\{(1, 1, 1, 1)\}_{\underline{4},1})} &= \mathcal{J}_\geq(\mathcal{X}_{\underline{4},1}(2, 1, 1, 1) | \{(1, 1, 1, 1), (2, 1, 1, 1)\}_{\underline{4},1}) \\ &\quad \times \mathcal{J}_<(\mathcal{X}_{\underline{4},1}(2, 1, 1, 1) | \{(1, 1, 1, 1)\}_{\underline{4},1}) \end{aligned} \quad (\text{C.38})$$

Now, using the $N = 1, k = 2$ calculation as an example, we explain the origin of the sign rule. For simplicity, we omit the label $(\underline{4}, 1)$.

- The D0-D0 sector $\tilde{\mathcal{I}}_k^{\text{D0-D0}}$ of the magnificent four partition function used in [32] differs from the $\mathcal{I}_k^{\text{D0-D0}}$ in (4.3) and is given by:

$$\tilde{\mathcal{I}}_k^{\text{D0-D0}} = \frac{1}{k!} \prod_{i \neq j}^k \text{sh}(\phi_i - \phi_j) \prod_{i,j}^k \frac{\text{sh}(\phi_i - \phi_j - \epsilon_{1,2,3} - \epsilon_4)}{\text{sh}(\phi_i - \phi_j - \epsilon_{1,2,3}) \text{sh}(\phi_i - \phi_j + \epsilon_4)} \quad (\text{C.39})$$

Therefore, the full partition function is:

$$\tilde{\mathcal{I}}_{N,k}^{\text{D0-D8-}\overline{\text{D8}}} = \tilde{\mathcal{I}}_k^{\text{D0-D0}} \times \prod_{i=1}^k \prod_{\alpha=1}^N \frac{\text{sh}(\phi_i - w_{\underline{4},\alpha})}{\text{sh}(\phi_i - v_{\underline{4},\alpha})}, \quad (\text{C.40})$$

For the case of $N = 1, k = 2$, there are four possible poles corresponding to four 4d Young diagrams, namely:

$$\begin{aligned} \rho_1 &= \{(1, 1, 1, 1), (2, 1, 1, 1)\}, & \rho_2 &= \{(1, 1, 1, 1), (1, 2, 1, 1)\}, \\ \rho_3 &= \{(1, 1, 1, 1), (1, 1, 2, 1)\}, & \rho_4 &= \{(1, 1, 1, 1), (1, 1, 1, 2)\} \end{aligned} \quad (\text{C.41})$$

Only the residue from the fourth Young diagram ρ_4 requires an additional minus sign, because according to the sign rule:

$$\text{Res}_{\mathcal{X}(\mathbf{x} \in \rho)} \left(\prod_{i=1}^k \frac{d\phi_i}{2\pi i} \right) \tilde{\mathcal{I}}_{N,k}^{\text{D0-D8-}\overline{\text{D8}}} = (-1)^{h(\rho)} \text{Res}_{\mathcal{X}(\mathbf{x} \in \rho)} \left(\prod_{i=1}^k \frac{d\phi_i}{2\pi i} \right) \mathcal{I}_{N,k}^{\text{D0-D8-}\overline{\text{D8}}} \quad (\text{C.42})$$

where:

$$h(\rho) = 1 + |\rho| + \#\{(a, d) \mid (a, a, a, d) \in \rho \text{ and } a \leq d\} \quad (\text{C.43})$$

Therefore, we have $h(\rho_1) = h(\rho_2) = h(\rho_3) = 4$ and $h(\rho_4) = 5$. In the residue computation of the partition function, the part that contributes to this extra sign is:

$$\begin{aligned} \tilde{\mathcal{I}}_{1,2}^{\text{D0-D8-}\overline{\text{D8}}} \supset \tilde{\mathcal{I}} &= \frac{1}{\text{sh}(\phi_{1,2} - v) \text{sh}(\phi_1 - \phi_2 + \epsilon_4) \text{sh}(\phi_2 - \phi_1 + \epsilon_4)} \\ \mathcal{I}_{1,2}^{\text{D0-D8-}\overline{\text{D8}}} \supset \mathcal{I} &= \frac{1}{\text{sh}(\phi_{1,2} - v) \text{sh}(\phi_1 - \phi_2 - \epsilon_4) \text{sh}(\phi_2 - \phi_1 - \epsilon_4)} \end{aligned} \quad (\text{C.44})$$

Then for the pole corresponding to ρ_4 : $(\phi_1, \phi_2) = (\mathcal{X}(1, 1, 1, 1), \mathcal{X}(1, 1, 1, 2))$, the residues of $\tilde{\mathcal{I}}$ and \mathcal{I} are:

$$\begin{aligned} \text{Res}_{\mathcal{X}(\mathbf{x} \in \rho_4)} \tilde{\mathcal{I}} &= \frac{1}{\text{sh}(\epsilon_4) \text{sh}(2\epsilon_4)} \\ \text{Res}_{\mathcal{X}(\mathbf{x} \in \rho_4)} \mathcal{I} &= \frac{1}{\text{sh}(\epsilon_4) \text{sh}(-2\epsilon_4)} = -\text{Res}_{\mathcal{X}(\mathbf{x} \in \rho_4)} \tilde{\mathcal{I}} \end{aligned} \quad (\text{C.45})$$

Since in this paper we adopt the definition of the partition function given in (4.3), and the shell formula is also formulated accordingly, no extra sign factor needs to be accounted for in our calculation.

References

[1] N.A. Nekrasov, *Seiberg-Witten prepotential from instanton counting*, *Adv. Theor. Math. Phys.* **7** (2003) 831 [[hep-th/0206161](#)].

[2] N. Nekrasov and A. Okounkov, *Seiberg-Witten theory and random partitions*, *Prog. Math.* **244** (2006) 525 [[hep-th/0306238](#)].

[3] N. Nekrasov, *BPS/CFT CORRESPONDENCE II: INSTANTONS AT CROSSROADS, MODULI AND COMPACTNESS THEOREM*, *Adv. Theor. Math. Phys.* **21** (2017) 503 [[1608.07272](#)].

[4] N. Nekrasov, *Magnificent four*, *Adv. Theor. Math. Phys.* **24** (2020) 1171 [[1712.08128](#)].

[5] E. Pomoni, W. Yan and X. Zhang, *Tetrahedron Instantons*, *Commun. Math. Phys.* **393** (2022) 781 [[2106.11611](#)].

[6] M. Aganagic, A. Klemm, M. Marino and C. Vafa, *The Topological vertex*, *Commun. Math. Phys.* **254** (2005) 425 [[hep-th/0305132](#)].

[7] S.H. Katz, A. Klemm and C. Vafa, *Geometric engineering of quantum field theories*, *Nucl. Phys. B* **497** (1997) 173 [[hep-th/9609239](#)].

[8] N.C. Leung and C. Vafa, *Branes and toric geometry*, *Adv. Theor. Math. Phys.* **2** (1998) 91 [[hep-th/9711013](#)].

[9] H. Hayashi and R.-D. Zhu, *More on topological vertex formalism for 5-brane webs with O5-plane*, *JHEP* **04** (2021) 292 [[2012.13303](#)].

[10] S. Nawata and R.-D. Zhu, *Instanton counting and O-vertex*, *JHEP* **09** (2021) 190 [[2107.03656](#)].

[11] V. Pestun et al., *Localization techniques in quantum field theories*, *J. Phys. A* **50** (2017) 440301 [[1608.02952](#)].

[12] N. Seiberg and E. Witten, *Electric - magnetic duality, monopole condensation, and confinement in $N=2$ supersymmetric Yang-Mills theory*, *Nucl. Phys. B* **426** (1994) 19 [[hep-th/9407087](#)].

[13] D. Gaiotto, *$N=2$ dualities*, *JHEP* **08** (2012) 034 [[0904.2715](#)].

[14] L.F. Alday, D. Gaiotto and Y. Tachikawa, *Liouville Correlation Functions from Four-dimensional Gauge Theories*, *Lett. Math. Phys.* **91** (2010) 167 [[0906.3219](#)].

[15] N. Nekrasov, *BPS/CFT correspondence: non-perturbative Dyson-Schwinger equations and qq -characters*, *JHEP* **03** (2016) 181 [[1512.05388](#)].

[16] N. Nekrasov, *BPS/CFT Correspondence III: Gauge Origami partition function and qq -characters*, *Commun. Math. Phys.* **358** (2018) 863 [[1701.00189](#)].

[17] N. Nekrasov, *BPS/CFT correspondence IV: sigma models and defects in gauge theory*, *Lett. Math. Phys.* **109** (2019) 579 [[1711.11011](#)].

[18] N. Nekrasov, *BPS/CFT correspondence V: BPZ and KZ equations from qq -characters*, [1711.11582](#).

[19] A. Iqbal, C. Kozcaz and C. Vafa, *The Refined topological vertex*, *JHEP* **10** (2009) 069 [[hep-th/0701156](#)].

[20] H. Awata and H. Kanno, *Refined BPS state counting from Nekrasov's formula and Macdonald functions*, *Int. J. Mod. Phys. A* **24** (2009) 2253 [[0805.0191](#)].

[21] T. Kimura and V. Pestun, *Quiver W -algebras*, *Lett. Math. Phys.* **108** (2018) 1351 [[1512.08533](#)].

[22] S. Nawata, K. Zhang and R.-D. Zhu, *ABCD of qq -characters*, *JHEP* **08** (2023) 200 [[2302.00525](#)].

[23] D. Maulik and A. Okounkov, *Quantum Groups and Quantum Cohomology*, [1211.1287](#).

[24] H. Awata, B. Feigin and J. Shiraishi, *Quantum Algebraic Approach to Refined Topological Vertex*, *JHEP* **03** (2012) 041 [[1112.6074](#)].

[25] D. Maulik, N. Nekrasov, A. Okounkov and R. Pandharipande, *Gromov-Witten theory and Donaldson-Thomas theory, I*, *Compos. Math.* **142** (2006) 1263 [[math/0312059](#)].

[26] D. Maulik, N. Nekrasov, A. Okounkov and R. Pandharipande, *Gromov-Witten theory and Donaldson-Thomas theory, II*, *Compos. Math.* **142** (2006) 1286 [[math/0406092](#)].

[27] A. Okounkov, N. Reshetikhin and C. Vafa, *Quantum Calabi-Yau and classical crystals*, *Prog. Math.* **244** (2006) 597 [[hep-th/0309208](#)].

[28] N. Nekrasov and N.S. Prabhakar, *Spiked Instantons from Intersecting D-branes*, *Nucl. Phys. B* **914** (2017) 257 [[1611.03478](#)].

[29] M. Rapcak, Y. Soibelman, Y. Yang and G. Zhao, *Cohomological Hall algebras, vertex algebras and instantons*, *Commun. Math. Phys.* **376** (2019) 1803 [[1810.10402](#)].

[30] E. Pomoni, W. Yan and X. Zhang, *Probing M-theory with tetrahedron instantons*, *JHEP* **11** (2023) 177 [[2306.06005](#)].

[31] N. Fasola and S. Monavari, *Tetrahedron instantons in Donaldson-Thomas theory*, *Adv. Math.* **462** (2025) 110099 [[2306.07145](#)].

[32] N. Nekrasov and N. Piazzalunga, *Magnificent Four with Colors*, *Commun. Math. Phys.* **372** (2019) 573 [[1808.05206](#)].

[33] M. Billò, M. Frau, F. Fucito, L. Gallot, A. Lerda and J.F. Morales, *On the $D(-1)/D7$ -brane systems*, *JHEP* **04** (2021) 096 [[2101.01732](#)].

[34] M. Kool and J.V. Rennemo, *Proof of a magnificent conjecture*, [2507.02852](#).

[35] S.-S. Kim, X. Li, S. Nawata and F. Yagi, *Freezing and BPS jumping*, *JHEP* **05** (2024) 340 [[2403.12525](#)].

[36] B. Feigin, M. Jimbo, T. Miwa and E. Mukhin, *Quantum toroidal gl_1 -algebra: Plane partitions*, *Kyoto Journal of Mathematics* **52** (2012) .

[37] S. Shadchin, *On certain aspects of string theory/gauge theory correspondence*, other thesis, 2, 2005, [[hep-th/0502180](#)].

[38] N. Nekrasov and S. Shadchin, *ABCD of instantons*, *Commun. Math. Phys.* **252** (2004) 359 [[hep-th/0404225](#)].

[39] M.F. Atiyah, N.J. Hitchin, V.G. Drinfeld and Y.I. Manin, *Construction of Instantons*, *Phys. Lett. A* **65** (1978) 185.

[40] A. Lossev, N. Nekrasov and S.L. Shatashvili, *Testing Seiberg-Witten solution*, *NATO Sci. Ser. C* **520** (1999) 359 [[hep-th/9801061](#)].

[41] J.-E. Bourgine, M. Fukuda, K. Harada, Y. Matsuo and R.-D. Zhu, *(p, q) -webs of DIM representations, 5d $\mathcal{N} = 1$ instanton partition functions and qq -characters*, *JHEP* **11** (2017) 034 [[1703.10759](#)].

[42] T. Kimura and G. Noshita, *Gauge origami and quiver W -algebras*, *JHEP* **05** (2024) 208 [[2310.08545](#)].

[43] O. Aharony and A. Hanany, *Branes, Superpotentials and Superconformal Fixed Points*, *Nucl. Phys. B* **504** (1997) 239 [[hep-th/9704170](#)].

[44] O. Aharony, A. Hanany and B. Kol, *Webs of (p, q) 5-branes, Five Dimensional Field Theories and Grid Diagrams*, *JHEP* **9801** (1998) 002 [[hep-th/9710116](#)].

[45] G. Zafrir, *Brane webs and $O5$ -planes*, *JHEP* **03** (2016) 109 [[1512.08114](#)].

[46] C. Hwang, J. Kim, S. Kim and J. Park, *General instanton counting and 5d SCFT*, *JHEP* **07** (2015) 063 [[1406.6793](#)].

[47] H.-C. Kim, S.-S. Kim and K. Lee, *5-dim Superconformal Index with Enhanced En Global Symmetry*, *JHEP* **10** (2012) 142 [[1206.6781](#)].

[48] S.-S. Kim, X. Li, F. Yagi and R.-D. Zhu, *O -vertex, $O7^+$ -plane, and topological vertex*, *JHEP* **04** (2025) 182 [[2412.19655](#)].

[49] G. Noshita, *Gauge Origami and BPS/CFT correspondence*, other thesis, 2, 2025, [[2502.07573](#)].

[50] R.P. Thomas, *A Holomorphic Casson invariant for Calabi-Yau three folds, and bundles on K3 fibrations*, *J. Diff. Geom.* **54** (2000) 367 [[math/9806111](#)].

[51] T. Kimura and G. Noshita, *Gauge origami and quiver W-algebras IV: Pandharipande-Thomas qq-characters*, [2508.12125](#).

[52] E. Witten, *BPS Bound states of D0 - D6 and D0 - D8 systems in a B field*, *JHEP* **04** (2002) 012 [[hep-th/0012054](#)].

[53] R.J. Szabo and M. Tirelli, *Noncommutative instantons in diverse dimensions*, *Eur. Phys. J. ST* **232** (2023) 3661 [[2207.12862](#)].

[54] C. Vafa, *Brane / anti-brane systems and $U(N/M)$ supergroup*, [hep-th/0101218](#).

[55] N. Berkovits, A. Sen and B. Zwiebach, *Tachyon condensation in superstring field theory*, *Nucl. Phys. B* **587** (2000) 147 [[hep-th/0002211](#)].

[56] E.T. Akhmedov, *D-brane annihilation, renorm group flow and nonlinear sigma model for the ADHM construction*, *Nucl. Phys. B* **592** (2001) 234 [[hep-th/0005105](#)].

[57] T. Kimura and G. Noshita, *Gauge origami and quiver W-algebras. Part III. Donaldson-Thomas qq-characters*, *JHEP* **03** (2025) 050 [[2411.01987](#)].

[58] N. Nekrasov and A. Okounkov, *Membranes and sheaves.*, *Algebr. Geom.* **3** (2016) 320 [[1404.2323](#)].

[59] D. Galakhov, W. Li and M. Yamazaki, *Shifted quiver Yangians and representations from BPS crystals*, *JHEP* **08** (2021) 146 [[2106.01230](#)].

[60] Y. Chen, J. Jiang, S. Nawata and Y. Shao, *Instantons on Young diagrams with matters*, *JHEP* **03** (2023) 120 [[2301.02342](#)].

[61] H.-C. Kim, M. Kim, S.-S. Kim and G. Zafrir, *Superconformal indices for non-Lagrangian theories in five dimensions*, *JHEP* **03** (2024) 164 [[2307.03231](#)].

[62] H. Ooguri and M. Yamazaki, *Crystal Melting and Toric Calabi-Yau Manifolds*, *Commun. Math. Phys.* **292** (2009) 179 [[0811.2801](#)].

[63] N. Nekrasov and N. Piazzalunga, *Global Magnificence, or: 4G Networks*, *SIGMA* **20** (2024) 106 [[2306.12995](#)].

[64] R. Pandharipande and R.P. Thomas, *Curve counting via stable pairs in the derived category*, *Invent. Math.* **178** (2009) 407 [[0707.2348](#)].

[65] Y. Cao and M. Kool, *Curve counting and DT/PT correspondence for Calabi-Yau 4-folds*, *Adv. Math.* **375** (2020) 107371 [[1903.12171](#)].

[66] T. Kimura and G. Noshita, *The 4-fold Pandharipande-Thomas vertex and Jeffrey-Kirwan residue*, [2508.12128](#).

[67] L.C. Jeffrey and F.C. Kirwan, *Localization for nonabelian group actions*, [alg-geom/9307001](#).

[68] A. Szendrői and M. Vergne, *Toric reduction and a conjecture of batyrev and matrosov*, *Inventiones mathematicae* **158** (2004) 453–495.

[69] F. Benini, R. Eager, K. Hori and Y. Tachikawa, *Elliptic genera of two-dimensional $N=2$ gauge theories with rank-one gauge groups*, *Lett. Math. Phys.* **104** (2014) 465 [[1305.0533](#)].

[70] F. Benini, R. Eager, K. Hori and Y. Tachikawa, *Elliptic Genera of 2d $\mathcal{N} = 2$ Gauge Theories*, *Commun. Math. Phys.* **333** (2015) 1241 [[1308.4896](#)].

[71] S. Nawata, Y. Pan and J. Zheng, *Class S theories on S^2* , *Phys. Rev. D* **109** (2024) 105015 [[2310.07965](#)].

[72] M. Cirafici, A. Sinkovics and R.J. Szabo, *Cohomological gauge theory, quiver matrix models and donaldson-thomas theory*, *Nuclear Physics B* **809** (2009) 452–518.